NASA/CR-2004-213025

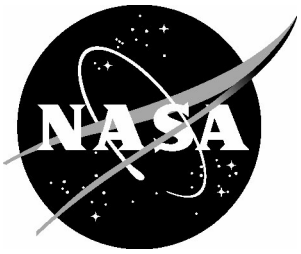

Characterizing the Severe Turbulence Environments Associated With Commercial Aviation Accidents

A Real-Time Turbulence Model (RTTM) Designed for the Operational Prediction of Hazardous Aviation Turbulence Environments

Michael L. Kaplan, Kevin M. Lux, Jeffrey D. Cetola, Allan W. Huffman, Allen J. Riordan, Sarah W. Slusser, and Yuh-Lang Lin
North Carolina State University, Raleigh, North Carolina

Joseph J. Charney
USDA/Forest Service, North Central Research Station, East Lansing, Michigan

Kenneth T. Waight
MESO, Inc., Raleigh, North Carolina

August 2004

The NASA STI Program Office . . . in Profile

Since its founding, NASA has been dedicated to the advancement of aeronautics and space science. The NASA Scientific and Technical Information (STI) Program Office plays a key part in helping NASA maintain this important role.

The NASA STI Program Office is operated by Langley Research Center, the lead center for NASA's scientific and technical information. The NASA STI Program Office provides access to the NASA STI Database, the largest collection of aeronautical and space science STI in the world. The Program Office is also NASA's institutional mechanism for disseminating the results of its research and development activities. These results are published by NASA in the NASA STI Report Series, which includes the following report types:

- TECHNICAL PUBLICATION. Reports of completed research or a major significant phase of research that present the results of NASA programs and include extensive data or theoretical analysis. Includes compilations of significant scientific and technical data and information deemed to be of continuing reference value. NASA counterpart of peer-reviewed formal professional papers, but having less stringent limitations on manuscript length and extent of graphic presentations.

- TECHNICAL MEMORANDUM. Scientific and technical findings that are preliminary or of specialized interest, e.g., quick release reports, working papers, and bibliographies that contain minimal annotation. Does not contain extensive analysis.

- CONTRACTOR REPORT. Scientific and technical findings by NASA-sponsored contractors and grantees.

- CONFERENCE PUBLICATION. Collected papers from scientific and technical conferences, symposia, seminars, or other meetings sponsored or co-sponsored by NASA.

- SPECIAL PUBLICATION. Scientific, technical, or historical information from NASA programs, projects, and missions, often concerned with subjects having substantial public interest.

- TECHNICAL TRANSLATION. English-language translations of foreign scientific and technical material pertinent to NASA's mission.

Specialized services that complement the STI Program Office's diverse offerings include creating custom thesauri, building customized databases, organizing and publishing research results ... even providing videos.

For more information about the NASA STI Program Office, see the following:

- Access the NASA STI Program Home Page at ***http://www.sti.nasa.gov***

- E-mail your question via the Internet to help@sti.nasa.gov

- Fax your question to the NASA STI Help Desk at (301) 621-0134

- Phone the NASA STI Help Desk at (301) 621-0390

- Write to:
  NASA STI Help Desk
  NASA Center for AeroSpace Information
  7121 Standard Drive
  Hanover, MD 21076-1320

NASA/CR-2004-213025

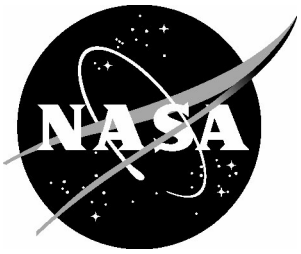

Characterizing the Severe Turbulence Environments Associated With Commercial Aviation Accidents

A Real-Time Turbulence Model (RTTM) Designed for the Operational Prediction of Hazardous Aviation Turbulence Environments

Michael L. Kaplan, Kevin M. Lux, Jeffrey D. Cetola, Allan W. Huffman, Allen J. Riordan, Sarah W. Slusser, and Yuh-Lang Lin
North Carolina State University, Raleigh, North Carolina

Joseph J. Charney
USDA/Forest Service, North Central Research Station, East Lansing, Michigan

Kenneth T. Waight
MESO, Inc., Raleigh, North Carolina

National Aeronautics and
Space Administration

Langley Research Center
Hampton, Virginia 23681-2199

Prepared for Langley Research Center
under Contract NAS1-02007

August 2004

Acknowledgments

This research has been funded under the Turbulence Prediction and Warning System element of NASA's Aviation Safety Program. The authors wish to acknowledge the support of Dr. Fred H. Proctor, the NASA Langley Research Center Technical Contract Monitor.

Available from:

NASA Center for AeroSpace Information (CASI)
7121 Standard Drive
Hanover, MD 21076-1320
(301) 621-0390

National Technical Information Service (NTIS)
5285 Port Royal Road
Springfield, VA 22161-2171
(703) 605-6000

Abstract

Real-time prediction of environments predisposed to producing moderate-severe aviation turbulence is studied. We describe the numerical model and its postprocessing system designed for said prediction of environments predisposed to severe aviation turbulence as well as presenting numerous examples of its utility. The numerical model is MASS version 5.13, which is integrated over three different grid matrices in real time on a university work station in support of NASA Langley Research Center's B-757 turbulence research flight missions. The postprocessing system includes several turbulence-related products, including four turbulence forecasting indices, winds, streamlines, turbulence kinetic energy, and Richardson numbers. Additionally, there are convective products including precipitation, cloud height, cloud mass fluxes, lifted index, and K-index. Furthermore, soundings, sounding parameters, and Froude number plots are also provided. The horizontal cross-section plot products are provided from 16 000 to 46 000 ft in 2000-ft intervals. Products are available every 3 hours at the 60- and 30-km grid interval and every 1.5 hours at the 15-km grid interval. The model is initialized from the NWS ETA analyses and integrated two times a day.

1. Introduction

The operational forecasting of turbulence potential has been ongoing for several years. Many indices are generated daily from operational numerical weather prediction models. The National Weather Service (NWS) has employed the Ellrod Index (Ellrod and Knapp 1992), the NOAA Forecasting Systems Laboratory has employed indices developed by Marroquin (1998) based on turbulence kinetic energy and eddy dissipation rate, and the Research Applications Program of the National Center for Atmospheric Research employs the Integrated Turbulence Forecasting Algorithm (ITFA) index as part of the suite of products from the NWS RUC II model (Sharman, Wiener, and Brown 2000). The Ellrod index is by far the simplest based solely on deformation and vertical wind shear. The Marroquin index is based on a formulation of turbulence kinetic energy. ITFA is, by far, the most comprehensive and sophisticated index that is used operationally, employing a weighted set of nearly 20 individual component terms as well as contemporary observations of turbulence pireps into a turbulence probability index. Despite the sophistication of ITFA, it is designed primarily for nonconvective turbulence, that is, clear air turbulence (CAT) and mountain wave-induced turbulence. It is not exclusively designed to denote regions of severe turbulence but a broad cross section of turbulence intensities including light, moderate, and severe. As noted in Kaplan et al. (2003a), most severe aviation turbulence encounters that result in damage to aircraft or onboard injuries are closely associated with moist convection. Hence, a turbulence predictive index, to be employed on an operational basis, needs to have the capacity to predict not only light-moderate turbulence, which typically occurs in clear air, but the more severe turbulence most often found in association with moist convection, that is, convectively induced turbulence (CIT), which is most often associated with aviation accidents. Additionally, one negative aspect of ITFA is that it is an amalgamation of so many different specific dynamical terms and empirical weighting factors that it is unclear what physical or dynamical processes are most relevant in organizing the environment that is favorable for turbulence in a given case study, particularly

severe accident-producing turbulence. Therefore, one is dependent upon statistical validation rather than dynamical understanding when the inevitable improvement of said index is undertaken.

In the remainder of this paper we demonstrate the utility of the index described in Kaplan et al. (2003a–b) in delimiting, in real time, areas of moderate-severe turbulence potential. Additionally, we demonstrate that said index has the capacity to denote all three forms of turbulence, including CAT, CIT, and mountain wave-induced turbulence. We describe the numerical modeling system and postprocessor employed in the Real-Time Turbulence Model (RTTM) run operationally at North Carolina State University in support of NASA's B-757 turbulence research missions. We focus on a description of the key turbulence forecasting index in this section of the paper. Next we focus on several real-time examples of the model, its index, and simulated precipitation and wind fields associated with case studies of observed turbulence as reported by pireps. The ability of the model to denote CIT will be diagnosed, in particular, although its versatility in defining regions of both CAT and mountain wave-induced turbulence will also be described. Finally, we focus on summarizing the modeling system and its application to the problem of the real-time forecasting of turbulence potential.

2. Numerical Model and Postprocessor

The numerical model is MASS version 5.13 (Kaplan et al. 2000). The MASS model is a hydrostatic terrain-following sigma coordinate system with comprehensive boundary layer and convective parameterizations (note table 1). The model is integrated over three different horizontal resolutions, that is, 60 km, 30 km, and 15 km for the coarse, fine1, and fine2 grids with the finest two meshes employing one-way nested-grid lateral boundary conditions (note fig. 1). The grid matrix size is 70×60×50 points for the coarse mesh grid, 90×100×50 points for the 30-km grid, and 90×100×50 points for the 15-km grid. The vertical sigma spacing is such that there are 15 levels below 850 mb, between 850 and 400 mb there are levels every 20 mb, and above 400 mb they are spaced every 40 mb. The initial state for the coarse mesh employs the NWS ETA analyses at 0000 UTC and 1200 UTC as well as reanalyzed rawinsonde and aviation surface observations employing an optimum interpolation scheme. Time-dependent lateral boundary conditions are derived from the NWS ETA model 40-km data set and are updated every 3 hours at the 60-km scale. Hourly coarser mesh simulated fields serve as the time-dependent lateral boundary conditions for the 30- and 15-km grid meshes. The 30-km simulation is initialized at 3 hours past 0000 UTC and 1200 UTC from the coarse mesh simulation and the 15-km simulation is initialized at 3 hours past 0300 UTC and 1500 UTC from the fine1 simulation. The three grids are located in a manner that enables them to produce simulations covering the entire 24-hour period, that is, 24 hours at the coarse mesh, 21 hours at the fine1 mesh, and 18 hours at the fine2 mesh from the NWS ETA analysis data cycles consistent with the range of typical operational NASA Langley B-757 turbulence research flights. The modeling system is designed solely to support the NASA turbulence research flight missions.

The postprocessing system is designed to support real-time forecasts of turbulence potential for use in directing the NASA B-757 research aircraft to locations of turbulence. There are four components to the postprocessor (note table 2). The most important component is the suite of turbulence products listed in table 2. These include: winds, streamlines, Richardson numbers, turbulence kinetic energy, and four turbulence prediction indices. They are depicted on horizontal surfaces from 16000 to 46000 ft in 2000-ft intervals because mid-upper tropospheric turbulence is the focus of the B-757 turbulence research flights.

The four indices are mathematically depicted in equations (1)–(4).

$$\frac{V - V_t}{\left[0.1 + 1000\left(\frac{d\theta}{dz}\right)\right]^2} \qquad (1)$$

$V =$ Wind speed
$V_t = 35$ m/s
$\theta =$ Potential temperature if RH $<$ 95 percent
$\theta =$ Equivalent potential temperature if RH $\geq$ 95 percent

$$\mathrm{KTI} = f\left[f\left(1 - \frac{1}{Ri}\right) + \zeta\right] \qquad (2)$$

$f =$ Coriolis parameter
$Ri =$ Bulk Richardson number
$\zeta =$ Relative vorticity

$$\mathrm{NCSU1} = \left[U \bullet \nabla(U)\right]\frac{\left|\nabla(\zeta)\right|}{\left|Ri\right|} \qquad (3)$$

$U =$ Wind vector
$Ri =$ Bulk Richardson number
$\zeta =$ Relative vorticity

$$\mathrm{NCSU2} = \left|\nabla\psi \times \nabla\zeta\right| \qquad (4)$$

$\nabla\psi =$ Montgomery stream function
$\nabla\zeta =$ Relative vorticity

Index 1 (eq. (1)) is the NASA turbulence index developed by Proctor (2000) that is primarily designed to determine layers of neutral static stability. Index 2 (eq. (2)) is the inertial instability parameter from Knox (1997) based on Stone's (1966) representation. According to Knox (1997), it should be useful in cases of strong anticyclonic shear juxtaposed with low Richardson numbers indicative of environments favorable for CAT. Index 3 (eq. (3)), is the NCSU1 index. Index 3 is designed to be responsive to inertial-advective forcing indicative of highly curved and accelerative jet stream flows. Finally, the index that we demonstrate in section 3 is the NCSU2 index (eq. (4)). This index, which was described in Kaplan et al. (2003a–b), represents the cross product of the Montgomery stream function and relative vertical vorticity on an isentropic surface passing through the specific height surface. It represents our most versatile and fundamental index, which is designed to be applied to all three types of turbulence, that is, CAT, CIT, and mountain. It is based on the concept that streamwise ageostrophically forced frontogenesis is favored during unbalanced supergradient flow regimes. As fronts form in confluent curved flows, the streamwise gradient of temperature and relative vertical vorticity become superimposed as the geostrophic and total relative vertical vorticity become displaced in space. Hence, a folded isentrope represents a region of convergence of streamwise-oriented maxima of vertical vorticity. The cross-product of the pressure gradient and relative vertical vorticity gradient maximizes where the pressure gradient force vector and streamwise vorticity maxima become orthogonal in contradistinction to geostrophic flow where the pressure gradient force and vorticity gradient vectors are parallel.

The second most important component of the postprocessor is the convective product suite. As indicated by the results presented in Kaplan et al. (2003a), CIT is a highly ubiquitous form of severe turbulence. Furthermore, the fundamental goal of the NASA B-757 research flights is to collect data for the certification of onboard turbulence-detecting radars. Hence, it is very important to be able to forecast convection and convectively induced turbulence. This group of products is listed in table 2. The products include: convective precipitation, total precipitation, cloud heights and cloud mass fluxes as diagnosed from the Kain-Fritsch (1990) convective parameterization scheme, the lifted index, and the K-index for all three grids.

The final two components of the product suite include skew-T/log-p soundings and accompanying convective forecasting parameters at all rawinsonde and most aviation surface station locations within each of the three grid matrices as well as vertical Froude number profiles at select locations along the Colorado Front Range of the Rocky Mountains for the coarse mesh grid only (table 2).

The temporal frequency of the turbulence, convective, sounding, and Froude number products is as follows: coarse mesh—turbulence, sounding, and Froude number products at initial time and every 3 hours; convective products at initial time plus 3 hours and every 3 hours thereafter; fine1 mesh—the same except starting at 3 hours after 0000 UTC and 1200 UTC for turbulence and sounding products; convective products starting 6 hours after 0000 UTC and 1200 UTC; fine2 mesh—the same for turbulence and sounding products except starting at 6 hours after 0000 UTC and 1200 UTC and every 90 minutes; convective products starting at 7.5 hours after 0000 UTC and 1200 UTC and every 90 minutes. All horizontal plot products are available ≈5 hours after observed data time for the coarse mesh, ≈6 hours for the fine1 mesh, and ≈7 hours for the fine2 mesh with sounding and Froude number products delayed ≈2 hours after the horizontal plots for each grid. The computing is performed on a DEC-ALPHA workstation at the Department of Marine, Earth, and Atmospheric Sciences at North Carolina State University. All of these products are displayed at the following web site: <http://shear.meas.ncsu.edu/>.

3. Case Study Examples of RTTM Simulations

In this section of the paper we heuristically compare some of the RTTM products to the turbulence pireps as well as observations of winds, temperatures, and clouds for several case studies of moderate-severe turbulence. These case studies were simulated in real time with the RTTM and all products generated in real time during the May 2001 to April 2002 time frame. Most are associated with convective precipitation and jet entrance regions consistent with the findings in Kaplan et al. (2003a–b). The NCSU2 index fields to be displayed for the following case studies range in magnitude from <1 to >200 $\times 10^{-12}$ units of the time tendency of enstrophy, that is, s^{-3}. A case study was assumed to lie in the moderate-severe range of turbulence potential if any of the following criteria applied: (1) the RTTM coarse mesh values exceeded 10×10^{-12} units, (2) the RTTM fine1 values exceeded 50×10^{-12} units, and/or (3) the RTTM fine2 values exceeded 150×10^{-12} units of enstrophy. These thresholds were based on daily comparisons of index maxima to moderate-severe turbulence pireps. A total of eight moderate-severe case studies will be described including six moderate-severe convective turbulence, one very intense day of combined convective and clear air sequence of turbulence reports, and one moderate-severe day of combined clear air and mountain turbulence case studies. It should be emphasized that all the RTTM NCSU2 turbulence potential index fields represent forecasts of 6 hours or more ranging upward of 18 hours.

3.1. Convective Turbulence Case Studies

3.1.1. Case 1: September 18, 2001

On September 18, 2001, the 25000- to 40000-ft pireps depicted in figure 2(a) shift abruptly southeastward during the 1326 UTC to 1508 UTC time period from the northern Mississippi River Valley, including Iowa and northern Missouri, to southern Missouri, Illinois, and the Ohio River Valley region. A moderate-severe turbulence pilot report at 15000 ft is apparent near St. Louis, Missouri (STL), highlighting this southeastward shift. The 1415 UTC water vapor imagery in figure 2(b) indicates a massive area of convection across the northern Mississippi River Valley and eastern sections of Kansas and Oklahoma. Apparent in this satellite imagery are streaks of outflow oriented in an anticyclonically curved manner across Arkansas, southern Missouri, and southern Illinois that are close to the aforementioned rapid shift in dense

pirep coverage. This anticyclonic outflow and relatively short-radii turning flow structure are typical of a convective outflow jet-induced entrance region (Kaplan et al. 2003b). Observed 1200 UTC soundings at Topeka, Kansas (TOP), Springfield, Missouri (SGF), and Peoria, Illinois (ILX), all indicate near neutral layers from ≈350 to 250 mb with the ILX balloon (only sounding depicted in fig. 3(a)) indicating a major anticyclonic shear zone within this near neutral layer. The neutral layer is indicative of a downstream cold pool aloft formed ahead of the lifting and accompanying a convective outflow jetlet (Kaplan et al. 2003b). Consistent with this is the RUC-II model 1500 UTC simulated 200-mb wind fields depicted in figure 3(b) and superimposed upon the 1200 UTC rawinsonde observations. This shows a classic outflow jet covering eastern Iowa, eastern Missouri, as well as Illinois and western Indiana and Kentucky. These fields strongly suggest that the upstream convection is producing an anticyclonically configured outflow jet in response to convective heating with the strongest accelerations located well downstream near the 2-hour shift in turbulence pireps over eastern Missouri and southern Illinois and Indiana.

Figures 4(a) to (c) depict the RTTM fine1 15-hour simulated 40000-ft winds, NCSU2 index, and total precipitation valid at 1500 UTC, 1500 UTC, and from 1200 UTC to 1500 UTC, respectively, from the 0000 UTC September 18, 2001, simulation. Evident is the shift in outflow jet and index maxima ahead of the convective precipitation, thus forcing the maxima of the NCSU2 index >150 units of enstrophy tendency at 40000 ft from central Missouri southeastward into Illinois. This NCSU2 index maxima location is more consistent with the pireps depicted in figure 2(a). The NCSU2 index at 36000 and 30000 ft is very similar to the 40000-ft values (not shown) indicating that the layer from just below 300 mb to just above 200 mb was accelerating under the influence of convective heating upstream and that the convectively accelerated entrance region over Missouri was close to the index maxima and therefore likely contributing to the favorable environment for turbulence. This is consistent with the inferences drawn from the satellite and rawinsonde observations.

3.1.2. Case 2: October 16, 2001

Pilot reports from 1631 UTC to 1850 UTC indicate several moderate to severe turbulence encounters over southwestern Pennsylvania and western Maryland between 15000 and 27000 ft (fig. 5(a)). The water vapor satellite imagery indicates a sharp comma cloud with convection over westcentral Pennsylvania at 1915 UTC (fig. 5(b)). The turbulence maximum is close to the strong 500-mb front as noted in the RUC analyses in figure 5(c).

The RTTM fine1 6-hour simulated 26000-ft NCSU2 index as well as winds and total precipitation for the period from 1500 UTC to 1800 UTC are depicted in figures 6(a) through (c). The NCSU2 index shows a comma-shaped maximum and bull's-eye >150 units over southwestern Pennsylvania and precipitation is simulated to fall just upstream near Pittsburgh (PIT), indicating that the maximum index values were just downstream from the convection. The 1500 UTC to 1800 UTC convection in the RTTM shifts the 1800 UTC NCSU2 index maximum slightly downstream from the 500-mb front in figure 5(c), thus reflecting the effect of convective forcing. Additionally, the simulated sounding at Buffalo, New York (BUF) (not shown), indicates a strong signal of the neutral layer and vertical shear maximum near the 26000-ft level and in proximity to the height of the observed turbulence. However, it is fair to say that the strong 500-mb front allows the NCSU2 index maxima to be relatively closely juxtaposed to the midtropospheric baroclinic zone, unlike the previous case study where the NCSU2 index maxima were more substantially detached from the background jet or front system and more closely coupled to the convective maxima, that is, the confluence maximum within the jet or front system is just as important for substantial index values in the RTTM, indicating the significant role of adiabatic forcing in organizing an environment predisposed to turbulence in this case study.

3.1.3. Case 3: October 5, 2001

This case study, illustrated in figures 7(a) through (d), strongly suggests major differences from the previous case study in that the RTTM index maxima are based on the development of a convective outflow jet, not unlike case study 1, in particular. The turbulence pireps during the 1126 UTC to 1320 UTC time frame depicted in figure 7(a) indicate a swath of almost unbroken moderate intensity activity from Kansas through Missouri, Illinois, Indiana, and Ohio. This belt of observed turbulence is nearly coincident with the split structure in the convection in the 1215 UTC water vapor imagery depicted in figure 7(b) and is closely aligned, actually just northwest of, the anticyclonic turning flow in the rawinsondes at 1200 UTC superimposed on the 1500 UTC RUC 200-mb winds in figure 7(d). Soundings at Peoria, Illinois (ILX), and Columbus, Ohio (ILN), at 0000 UTC and 1200 UTC, respectively, indicated a deep neutral layer above 350 mb (ILN sounding is depicted in fig. 7(c)). Hence, there is some proof supporting a convectively enhanced jet that acts to split the flow and produce conditions not unlike that shown in case study 1, above.

The 36000-ft winds and NCSU2 index at 1200 UTC on October 5, 2001, as well as 3-hour precipitation valid at 1200 UTC from the 0000 UTC on October 5, 2001, and RTTM fine1 simulation depicted in figures 8(a) through (c) nicely show how the RTTM is developing a separate convectively enhanced anticyclonic outflow jet from Missouri to northern Ohio. This outflow jet lies south of the main (large-scale) jet entrance region, producing a swath of high turbulence probability >150 units near the observed turbulence. The heavy convective precipitation simulated to occur over Missouri accelerates the flow downstream over northern Illinois, Indiana, and Ohio and provides the vorticity gradients necessary to trigger large index values south of the large-scale jet entrance region.

3.1.4. Case 4: January 5, 2002

This case study represents yet another example of severe convective turbulence. Figure 9(a) depicts the turbulence pireps between 1511 UTC and 1710 UTC. An examination of these fields indicates that several moderate to severe reports occur early in the day over central and northeastern Arkansas with an abrupt shift in the moderate activity toward the lower Ohio River Valley region later in the day (not shown). Additionally, the airmets (not shown) do not anticipate turbulence in the region where it occurs; therefore, the strongest warning area occurs south of the Louisiana coastal region.

Visible satellite imagery valid at 1702 UTC, the rawinsonde sounding at Fort Worth, Texas (FWD), valid at 1200 UTC, and the RUC 300-mb analyses valid at 1500 UTC in figures 9(b) through (d) all strongly indicate a subsynoptic jet stream that is, in part, likely the result of convection extending through northcentral Texas and turning eastward across Arkansas concurrent with the moderate-severe turbulence pireps over Arkansas. This strong jet with its short radius of curvature is representative of the jet features in previous case studies, particularly 1 and 3, where convective heating has contracted the scale of the jet stream and its strong streamwise shear fields. The imagery and rawinsondes strongly indicate a tight radius of curvature across western Arkansas as the wind flow observed over northern Texas and Oklahoma is highly ageostrophic and directed to the left of the height field. The FWD rawinsonde also indicates a neutral layer just below 300 mb, that is, near 30000 ft, within the layer of the most ageostrophic flow regime. As noted earlier in case studies 1 and 3, this neutral layer is close to both the convective jet and the level of pirep-reported turbulence.

The RTTM fine1 winds, NCSU2 index, precipitation, and sounding from the simulation initialized at 0000 UTC January 5, 2002, and depicted in figures 10(a) through (d), indicate that at 1800 UTC January 5, 2002, a strong convectively forced jet, similar to the one observed, is located over eastern Texas, northwestern Louisiana, and southwestern Arkansas at 32000 ft. At 1800 UTC, this jet is located just north and east of a region of heavy simulated precipitation during the 1200 UTC to 1500 UTC period over eastcentral

Texas, and the NCSU2 index indicates two regions of moderate to strong turbulence, that is, one near and encompassing the borders of Louisiana, Arkansas, and Texas with a second developing near southern Illinois and Indiana at 32000 ft. The simulated 1500 UTC FWD sounding is located just northwest of a large region of simulated precipitation between 1200 UTC and 1500 UTC. It is interesting that the 1500 UTC FWD simulated sounding captures some of the observed deep neutral layer structure, that is, below 500 mb, as well as the strong vertical variation of wind velocity and directional shear, particularly from southwest to south back to southwest in the vertical near the level of observed shear at 1200 UTC. The RTTM fine1 simulated fields initialized at 0000 UTC January 5, 2002, indicate the tendency toward a shift of the turbulence potential >150 units from Louisiana and Arkansas at 1800 UTC to over the lower Ohio River Valley by 2100 UTC (not shown) analogous to the newly developing pireps over this region (not shown) as well as the growth of the convectively forced jet northeastward. Hence, the RTTM favors highest turbulence potential over Louisiana and Arkansas with a jump in the maxima similar to where it is observed to occur.

3.1.5. Case 5: October 11, 2001

This case study is very similar to case studies 1, 3, and 4 in terms of strong convective outflow jet formation. During the early morning hours of October 11, 2001, the focus of pireps shifts eastward into the Ohio River Valley from the overnight maxima in the eastern Great Plains and Mississippi River Valley. Figure 11(a) depicts these pireps from 1028 UTC to 1157 UTC. Water vapor satellite imagery at ≈1145 UTC, the observed sounding at Columbus, Ohio (ILN), valid at 1200 UTC, and 200-mb RUC analyses winds valid at 0900 UTC with superimposed 0000 UTC October 11, 2001, rawinsondes depicted in figures 11(b) through (d) all are similar to a pattern seen in case studies 1, 3, and 4. Convection in the lower Mississippi River Valley amplifies a jet stream over the upper Missisippi River Valley and western Ohio River Valley during the overnight period. This results in a split anticyclonic structure to the downstream water vapor imagery accompanying a secondary anticyclonic wind maximum over Indiana by 1100 UTC. The 1200 UTC rawinsonde at ILN has a strong anticyclonic shear forced by the strong westerly component increase with height in the upper troposphere between 300 and 250 mb with near neutral layers just below the region of strongest anticyclonic shear.

The RTTM fine1, 12-hour simulation initialized at 0000 UTC October 11, 2001, and depicted in figures 12(a) through (c), of 1200 UTC 34000-ft winds, 1200 UTC 36000-ft NCSU2 index, and total precipitation during the 0900 UTC to 1200 UTC period, indicates a region of heavy precipitation over the lower Mississippi River Valley from northeastern Texas to southern Indiana, strong anticyclonic outflow downstream over Indiana and Ohio, and significant turbulence potential along the Ohio River and closely mimicks in location most of the pireps in the 30000- to 35000-ft layer. Again, as in the previous case studies, the maximum of turbulence potential >150 units reflects the eastward shift of three-dimensional wind shears accompanying the convectively forced outflow jet as the NCSU2 index maximizes well downstream which is consistent with the RTTM simulated precipitation fields and newly developing pireps.

3.1.6. Case 6: February 17, 2002

Unlike four of the previous five case studies that occurred primarily in the middle part of the United States, the case study illustrated in figures 13(a) through (c) is of an isolated but severe turbulence pirep on about 1800 UTC near Boston, Massachusetts (BOS). The pirep, which occurred between 1650 UTC and 1843 UTC, is depicted in figure 13(a). The pirep indicates that the severe turbulence was occurring at 20000 ft. The observed 500-mb winds at 1200 UTC superimposed on the RUC 1800 UTC fields in figure 13(c) valid at 1800 UTC indicate that this was a region of curved flow rich in cyclonic vorticity on the northwestern side of an upper level frontal system. The accompanying 1846 UTC infrared

satellite imagery depicted in figure 13(b) supports the fact that the report occurred on the northwestern fringe of a region of cold cloud tops likely associated with significant precipitation. Hence, this is likely a region favored for latent heating-induced outflow that is consistent with the radar (not shown).

The RTTM fine1 simulation initialized at 1200 UTC February 17, 2002, did an excellent job of focusing a bull's-eye on the locations near BOS (figs. 14(a) through (f)). Not only did the 1800 UTC 18000-ft NCSU2 index from the fine1 simulation nicely locate a significant magnitude maximum >50 units near the turbulence encounter, but all the indices including the 20000-ft NCSU1 index and 20000-ft Richardson number produced maxima at 1800 UTC very close to the turbulence location (note figs. 14(b), (e), and (f)). Figures 14(a) and (d) depict the RTTM fine1 simulated 20000-ft winds and skew-t sounding at Hyannisport, Massachusetts (HYA), for the 1800 UTC period. Also depicted in figure 14(c) is the total precipitation for the preceding 3-hour period. Evident is a small scale wind maximum just east-southeast of the turbulence pirep location and just ahead of the local precipitation maximum embedded within the highly curved cyclonic vorticity maximum over southeastern New England inferred from the RTTM wind fields and RUC analyses. The location of the simulated precipitation maximum is consistent with the coldest cloud tops in the infrared imagery off the southern New England coast. The simulated HYA 1800 UTC sounding indicates a near neutral layer between 500 and 400 mb, which corresponds with the region of maximum vertical wind shear.

3.2. Combined (Convective and Clear Air) Case Study

3.2.1. Case 7: February 23, 2002

This case study is an example of both convectively induced and clear air turbulence occurring on the same day and at the same time. Additionally, it is the most active severe turbulence case study in the more than 2-year period that the RTTM has been operational. Figures 15(a) and (b) depict the pireps at two different time periods, that is, 1641 UTC to 1836 UTC and 1947 UTC to 2140 UTC over the southeastern and northeastern United States, respectively. Evident are two pockets of numerous severe turbulence reports. The early pocket occurs predominantly over southeastern Georgia and northcentral Florida whereas later pocket occurs over central and western Virginia with numerous moderate reports over North Carolina.

The reasons for the double severe turbulence episodes can be inferred from the observed data depicted in figure 16. The visible and infrared satellite imagery depicted in figures 16(a) and (b) and RUC/rawinsonde 300- and 500-mb winds, temperatures, and heights in figures 16(c) and (d) indicate that at around 1800 UTC a long trough of low pressure extends from western New England to the eastern Gulf of Mexico with active convection over much of the Florida peninsula and the offshore waters of the southeastern coast. Additionally, a well-defined cirrus shield extends up over most of the Atlantic coastal plain. There is both a very strong jet entrance region over New England and the middle Atlantic region and a secondary narrow jet entrance region at 300 mb extending southward along the Atlantic coast to northeastern Florida. Both orthogonal to and parallel to these jet entrance regions are strong temperature gradients at 500 mb, particularly north of South Carolina, indicating two cold pools: one over the central Appalachians across West Virginia and another over the eastern Gulf of Mexico northeastward to the Georgia coast. Warmer air at 300 mb above the coldest pool at 500 mb over the central Appalachians indicates a possible tropopause fold. A cyclonic structure and dry air signal in the water vapor imagery over this region as well as over the eastern Gulf indicates strong descent of air on the immediate rearward side of the two cyclonic circulations. Thus, one could reasonably infer a double region of intense frontogenesis, that is, one to the north with the larger scale jet or front system accompanying the tropopause fold and one to the south with the secondary jet entrance region in proximity to convection. Observed rawinsondes at Charleston, South Carolina (CHS), and Roanoke, Virginia

(RNK), at 0000 UTC February 24, 2002, in figures 16(e) and 16(f) strongly indicate that a midtropospheric zone of intense vertical wind shear and nearly dry adiabatic lapse conditions exist reinforcing the fact the dual jet entrance regions are accompanying extremely strong frontal structures. These shears indicate an environment covering a large region that is conducive for severe turbulence.

The RTTM fine1 simulations valid from 1800 UTC to 2100 UTC and initialized from the 1200 UTC February 23, 2002, database strongly support the concept of a double frontal zone creating a favorable environment for severe turbulence. The simulated 2100 UTC wind field at 22000 ft depicted in figure 17(a) indicates a double entrance region structure with one maximum along the southeast Atlantic coast and a second one over the northern part of the middle Atlantic coast. The strong perturbation in the wind fields accompanying the southern entrance region indicates the role in convective heating in organizing this jet. Consistent with this wind field are the NCSU2 turbulence potential indices at 1800 UTC and 2100 UTC and 22000 to 24000 ft depicted in figures 17(b) and (c). The NCSU2 indicates that the region from northern Florida through coastal Georgia is preferred for high turbulence potential whereas later on this potential shifts northward and westward into interior North Carolina, Virginia, and even into southern New Jersey where additional severe reports of turbulence are observed. The total precipitation simulated by the RTTM in figure 17(d) during the 1500 UTC to 1800 UTC period maximizes over Florida and off the southeast Atlantic coast consistent with observations and the concept of strong convective outflow supporting the early turbulence-producing vertical wind shears in the more southern jet entrance region. This is also consistent with the 2100 UTC simulated Richardson number and 0000 UTC simulated CHS sounding depicted in figures 17(e) and (f). These clearly indicate a double frontal zone and extreme vertical wind shear scenario over the southeastern and middle Atlantic coastal and piedmont regions consistent with the observations of atmospheric variables and severe turbulence.

3.3. Combined (Clear Air and Mountain) Case Study

3.3.1. Case 8: February 9, 2002

In contradistinction to the preceding case studies, this was a clear air turbulence case and mountain turbulence case with little or no moist convection, and is, in many ways, a classic example of a tropopause fold case study (figs. 18(a) through (e)). Figures 18(c) and (d) depict the RUC analysis 500- and 300-mb wind and temperature fields which indicated that a highly curved jet stream entrance region and very strong frontal system were approaching the region of observed severe turbulence (northcentral Oklahoma) reported in the pireps depicted in figure 18(a) shortly before 1900 UTC. Also, a second maximum in the jet stream was rotating across eastern Utah near additional severe pireps over New Mexico and Colorado. The Amarillo, Texas (AMA), 1200 UTC observed sounding in figure 18(e) indicated a dry adiabatic layer at the same level of the severe turbulence report, that is, at 23000 ft, and the water vapor infrared satellite imagery depicted in figure 18(b) confirmed the absence of deep convection and very highly curved and sheared flow over northern Texas and northwestern Oklahoma at 1900 UTC. Despite these strong signals of three-dimensional shear and frontal structure, the airmets (not shown) do not highlight this region over Oklahoma as the most favored for very strong turbulence; the focus is farther westward in the mountainous regions.

The RTTM coarse simulations from February 9, 2002, are depicted in figures 19(a) through (c). The 1800 UTC RTTM coarse NCSU2 index values initialized at 1200 UTC February 9, 2002, and depicted in figure 19(b) unambiguously depict maxima over north central Oklahoma and the mountains of the intermountain west. The RTTM coarse NCSU2 index recorded the highest index value for the coarse mesh simulation of any of these case studies by exceeding 50 units. The simulated winds in figure 19(a) show the significant curvature and horizontal shear from which one can infer the strong gradients of vertical vorticity as well as the low

Richardson numbers inferred from the vertical wind shear and neutral layer in the observed Amarillo, Texas (AMA), sounding depicted in figure 18(e) and the simulated Oklahoma City, Oklahoma (OKC), sounding depicted in figure 19(c). This case study indicates that the RTTM has the potential to diagnose nonconvective turbulence as accurately as convective turbulence.

4. Summary and Discussion

A Real-Time Turbulence Model (RTTM) and its postprocessing system are described and several examples of its use in predicting the organizing environment for moderate and severe turbulence are presented. The doubly nested-grid modeling system is designed to predict the potential for atmospheric turbulence in clear air, convection, and in proximity to mountains. The system produces four turbulence indices, numerous convective products, winds, streamlines, Richardson numbers, soundings, and Froude number profiles at 60-, 30-, and 15-km horizontal resolutions and 2000-ft vertical resolutions over much of the continental United States in support of NASA Langley Research Center's B-757 operational turbulence research flights.

Several case studies of observed moderate-severe turbulence are described wherein 6- to 18-hour forecasts of turbulence potential from the RTTM NCSU2 index are compared to pireps and observations. The RTTM NCSU2 index is compared to observed winds, temperatures, and satellite imagery in an effort to heuristically diagnose its utility as a forecasting tool. Select case study analyses indicate that the RTTM index tends to perform well in the prediction of regions of both convective and clear air turbulence potential 6 to 18 hours prior to an observed report of an aircraft's encounter with moderate-severe turbulence. These results are for select individual case study comparisons, however, and are not as rigorously convincing of the utility of the RTTM as an in-depth statistical evaluation of a large number of case studies. Such an evaluation will be performed in the future.

References

Ellrod, G. P.; and Knapp, D. I. 1992: An Objective Clear-Air Turbulence Forecasting Technique: Verification and Operational Use. *Wea. Forecasting*, **7**, 150–165.

Kain, J. S.; and Fritsch, J. M. 1990: A One-Dimensional Entraining-Detraining Plume Model. *J. Atmos. Sci.*, **47**, 2784–2802.

Kaplan, M. L.; Lin, Y.-L.; Charney, J. J.; Pfeiffer, K. D.; Ensley, D. B.; DeCroix, D. S.; and Weglarz, R. P. 2000: A Terminal Area PBL Prediction System at Dallas-Fort Worth and Its Application in Simulating Diurnal PBL Jets. *Bull. Amer. Meteor. Soc.*, **81**, 2179–2204.

Kaplan, M. L.; Huffman, A. W.; Lux, K. M.; Charney, J. J.; Riordan, A. J.; and Lin, Y.-L. 2003a: Characterizing the severe turbulence environments associated with commercial aviation accidents. A 44 case study synoptic observational analyses. In press, *Meteor. Atmos. Phys.*

Kaplan, M. L.; Huffman, A. W.; Lux, K. M.; Cetola, J. D., Charney, J. J., Riordan, A. J., Lin, Y.-L., and Waight III, K. T. 2003b: Characterizing the severe turbulence environments associated with commercial aviation accidents. Hydrostatic mesoscale numerical simulations of supergradient wind flow and ageostrophic along-stream frontogenesis. In press, *Meteor. Atmos. Phys.*

Knox, J. A. 1997: Possible Mechanisms of Clear-Air Turbulence in Strongly Anticyclonic Flows. *Mon. Wea. Rev.*, **125**, 1251–1259.

Marroquin, A. 1998: An Advanced Algorithm To Diagnose Atmospheric Turbulence Using Numerical Model Output. Preprints, *16th AMS Conference on Weather Analysis and Forecasting*, 11–16 January, 79–81.

Proctor, F. H. 2000: Personal communication.

Sharman, R.; Wiener, G.; and Brown, B. 2000: Description and Integration of the NCAR Integrated Turbulence Forecasting Algorithm (ITFA). AIAA 00-0493.

Stone, P. H. 1966: On Non-Geostrophic Baroclinic Stability. *J. Atmos. Sci.*, **23**, 390–400.

.

Table 1. MASS Model (Version 5.13) Characteristics

Model numerics	Hydrostatic primitive equation model 3-D equations for u, v, T, q, and p Cartesian grid on polar stereographic map Sigma-p terrain-following vertical coordinate Vertical coverage from ≈10 m to ≈16 000 m Energy-absorbing sponge layer near model top Fourth-order horizontal space differencing on unstaggered grid Split-explicit time integration schemes: (a) forward backward for gravity mode (b) Adams-Bashforth for advective mode Time-dependent lateral boundary conditions Positive-definite advection scheme for scalar variables Massless tracer equations for ozone and aerosol transport
Initialization	First guess from large-scale gridded analyses Reanalysis with rawinsonde and surface data using a 3-D optimum interpolation scheme High-resolution terrain database derived from observations High-resolution satellite or climatological sea surface temperature database High-resolution land use classification scheme High-resolution climatological subsoil moisture database derived from antecedent precipitation High resolution normalized difference vegetation index
PBL specification	Blackadar PBL scheme Surface energy budget Soil hydrology scheme Atmospheric radiation attenuation scheme
Moisture physics	Grid-scale prognostic equations for cloud water and ice, rainwater, and snow Kain-Fritsch convective parameterization

Table 2. List of RTTM Products

Turbulence products	Horizontal winds Horizontal streamlines Richardson number NASA turbulence parameter NCSU turbulence parameter NCSU2 turbulence parameter Stone turbulence parameter (Knox parameter) Turbulent kinetic energy
Convective products	Convective precipitation Total precipitation Cloud heights Cloud mass fluxes Lifted index K-index Skew-t/log-p soundings Froude number profiles

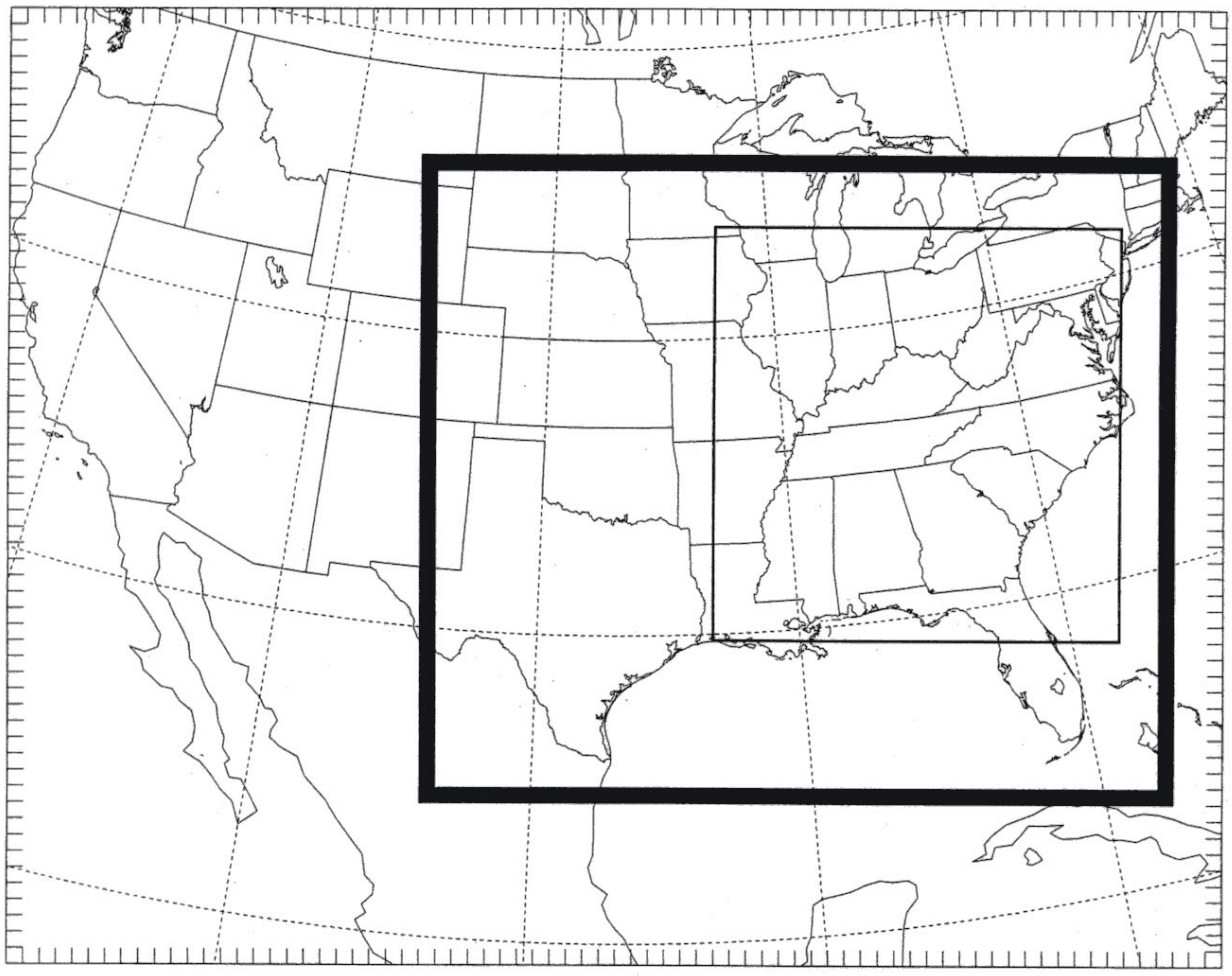

Figure 1. RTTM coarse, fine1, and fine2 grid locations.

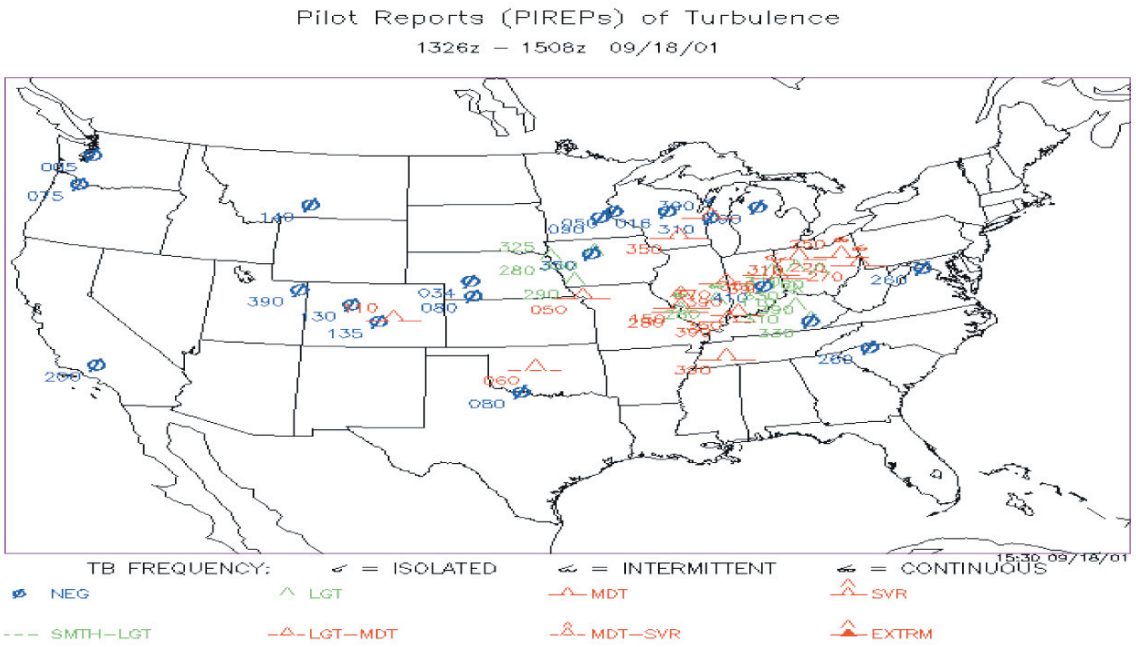

(a) Pireps from NOAA Aviation Digital Data source valid from 1326 UTC to 1508 UTC.

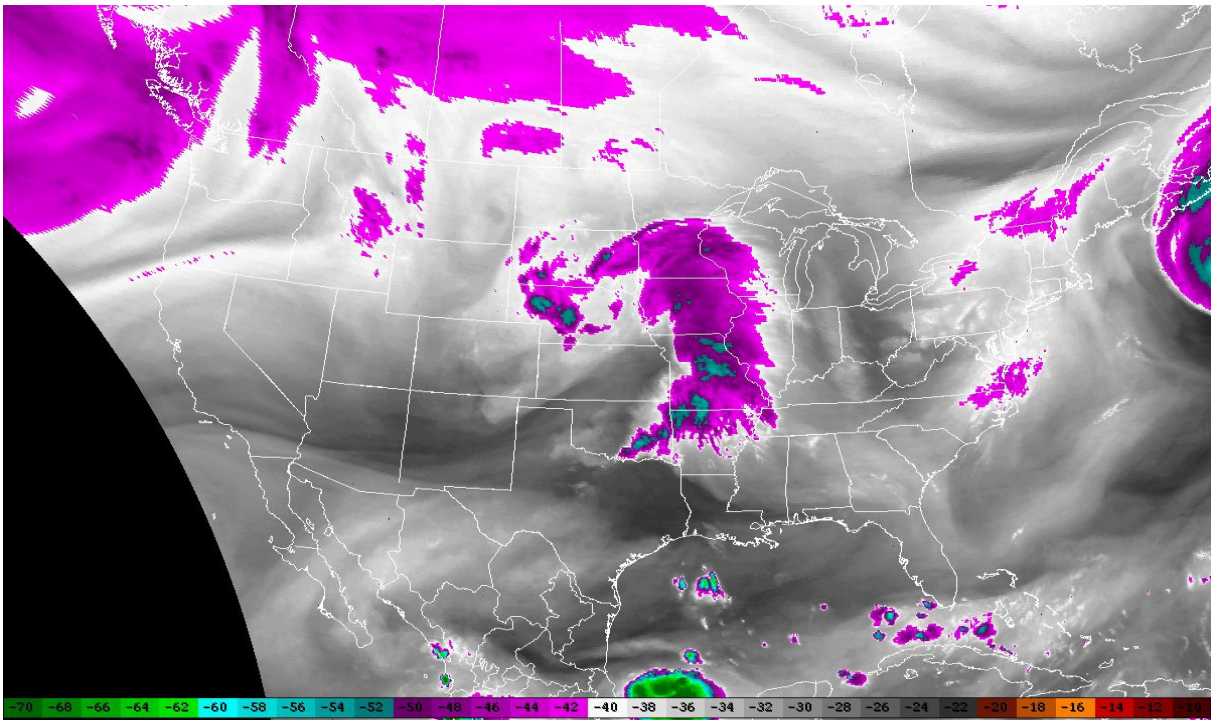

(b) Water vapor infrared satellite imagery valid at 1415 UTC.

Figure 2. September 18, 2001, pireps and water vapor imagery.

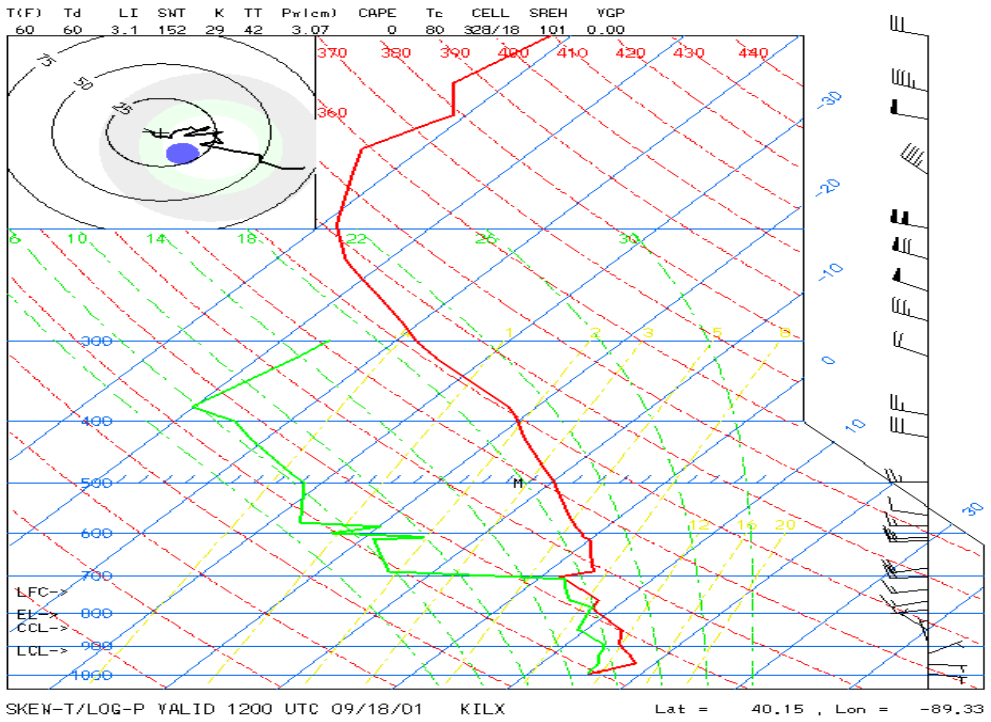

(a) Peoria, IL (ILX), rawinsonde sounding valid at 1200 UTC.

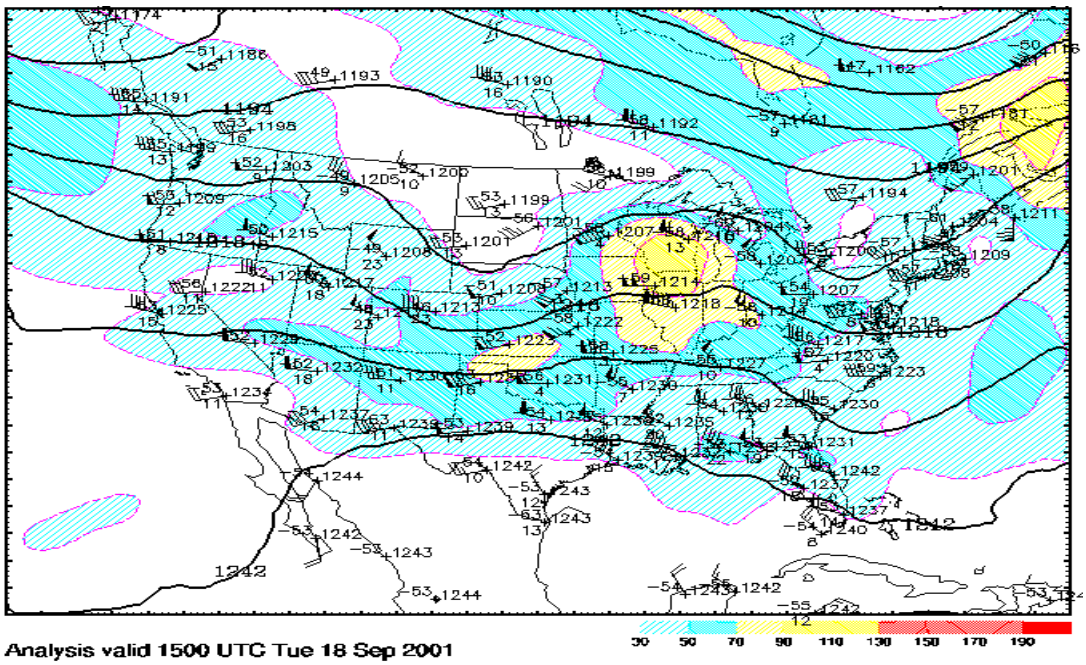

(b) RUC II simulated 200-mb wind isotachs (ms^{-1}) valid at 1500 UTC with superimposed observed 1200 UTC rawinsonde wind barbs (ms^{-1}), temperatures (C), and heights (m).

Figure 3. September 18, 2001, rawinsonde and RUC analysis.

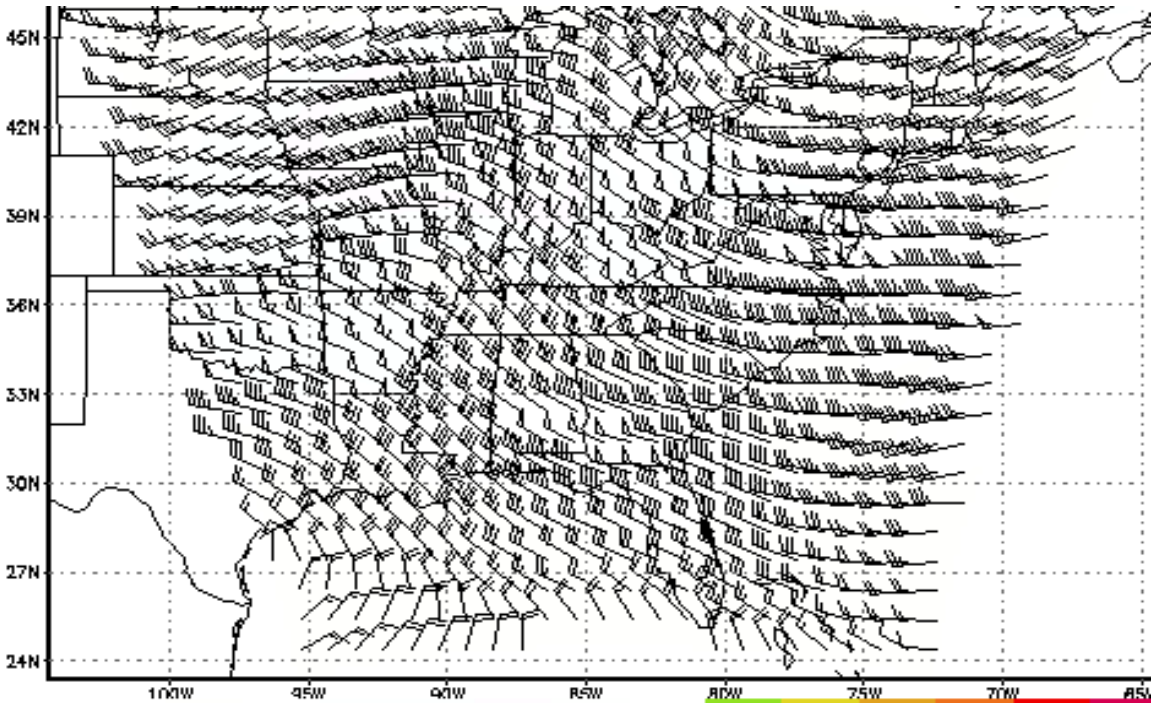

(a) RTTM fine1 simulated 40 000-ft wind isotachs and barbs (kn) valid at 1500 UTC.

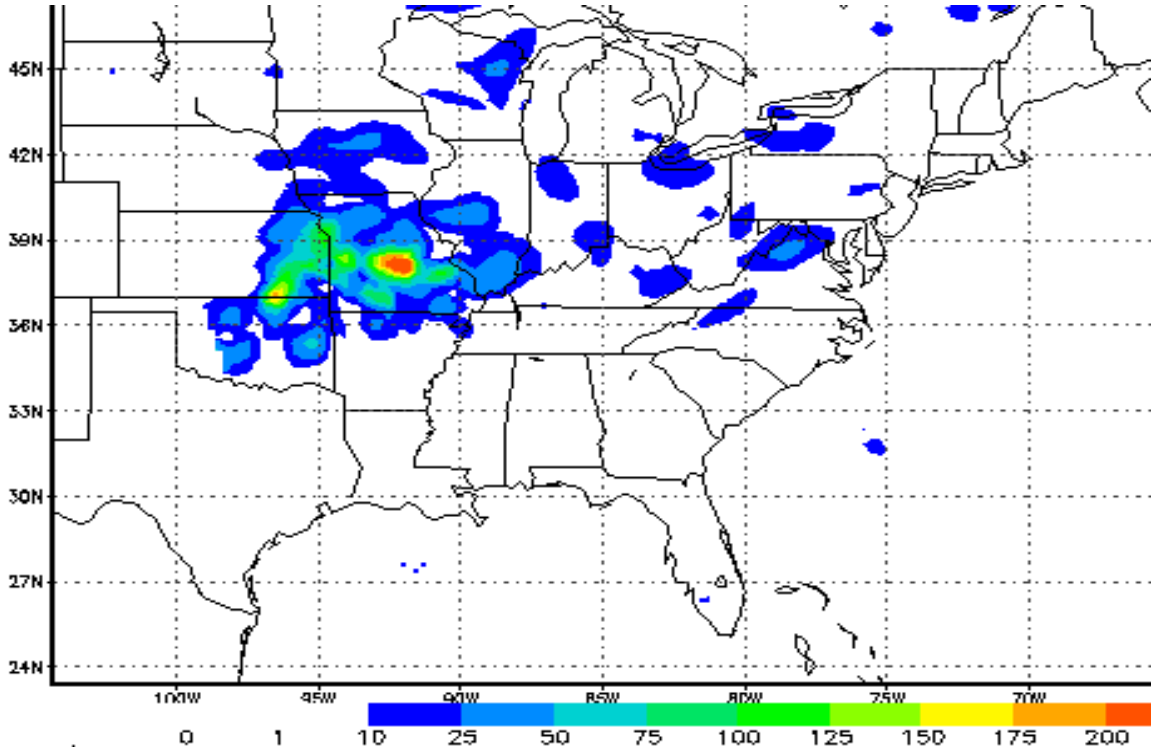

(b) RTTM fine1 simulated 40 000-ft NCSU2 index (s^{-3}) valid at 1500 UTC.

Figure 4. September 18, 2001, fine1 simulation winds, index, and precipitation.

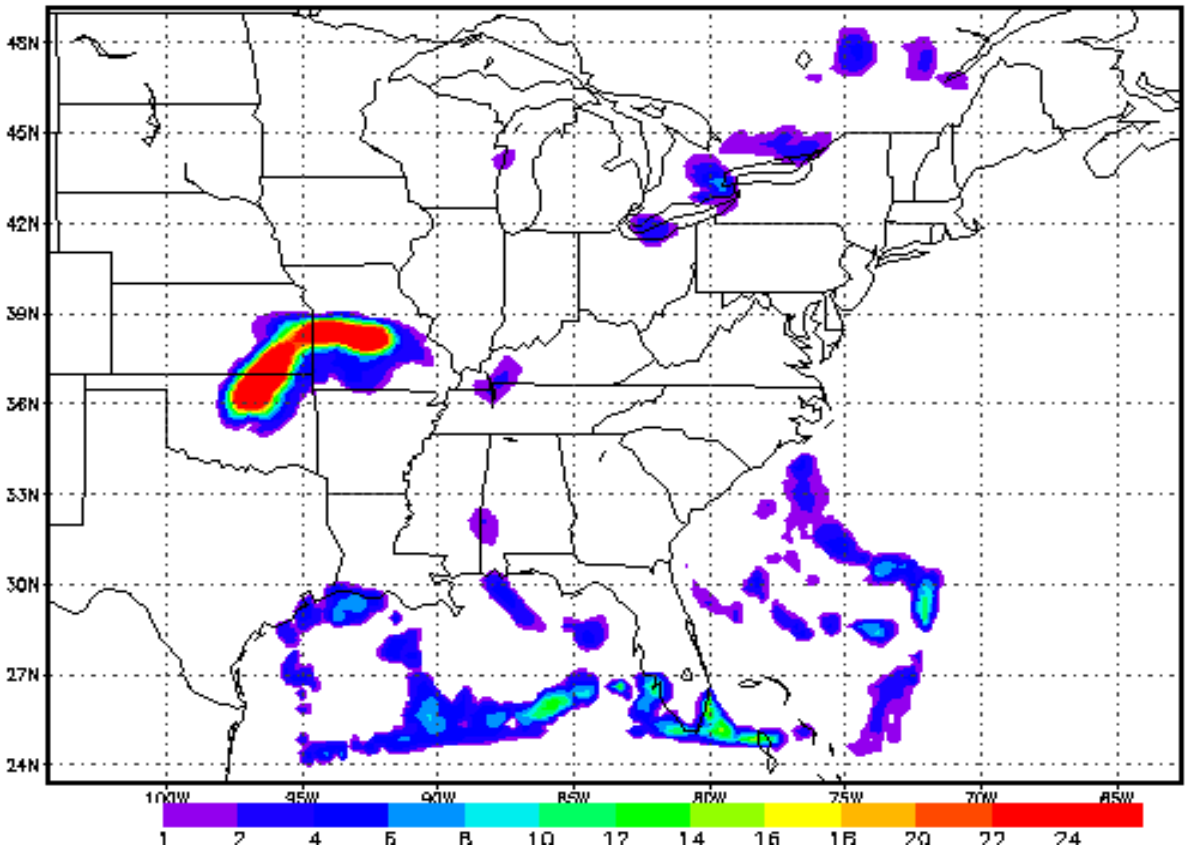

(c) RTTM fine1 3-hour total precipitation (mm) valid from 1200 UTC to 1500 UTC.

Figure 4. Concluded.

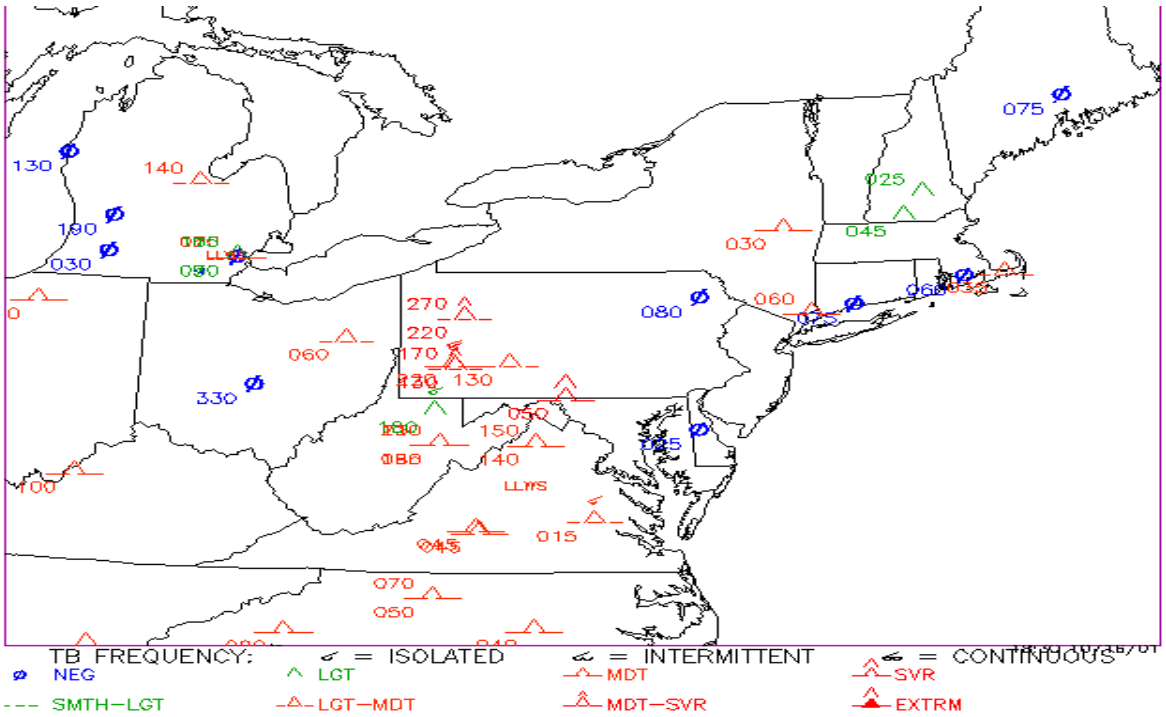

(a) Pireps from NOAA Aviation Digital Data source valid from 1631 UTC to 1850 UTC.

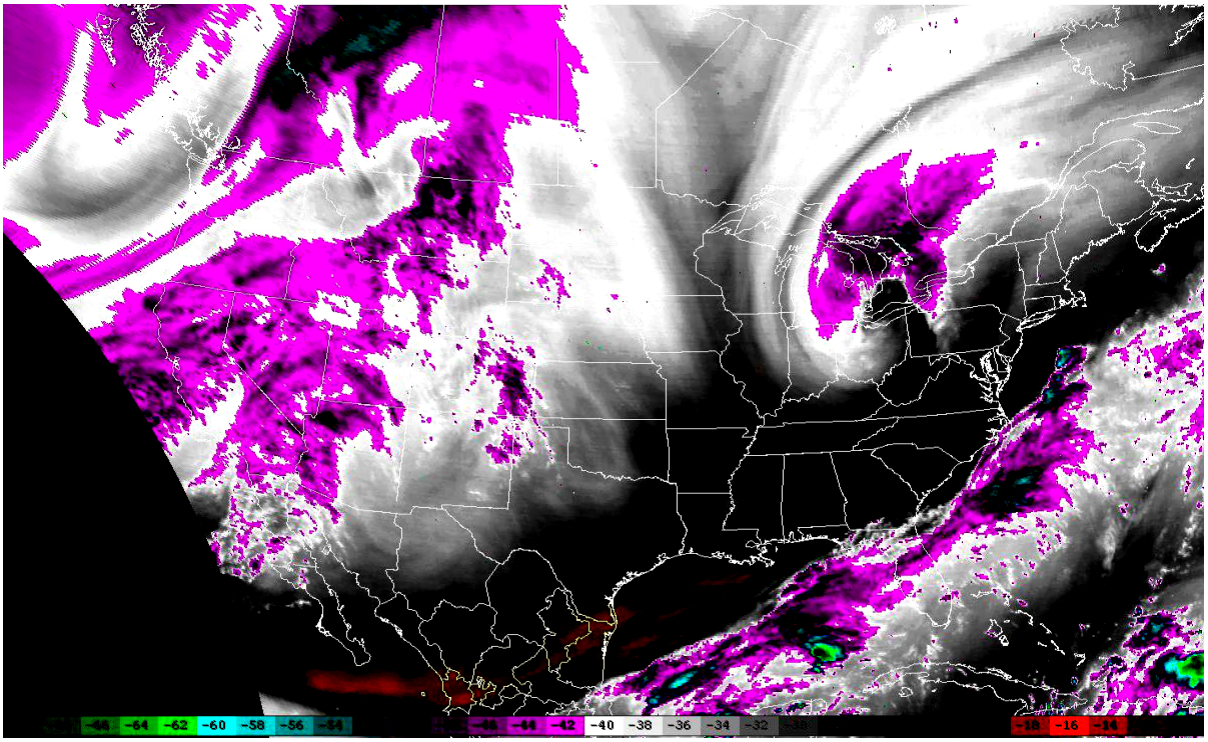

(b) Water vapor infrared satellite imagery valid at 1915 UTC.

Figure 5. October 16, 2001, pireps, water vapor imagery, and RUC analysis.

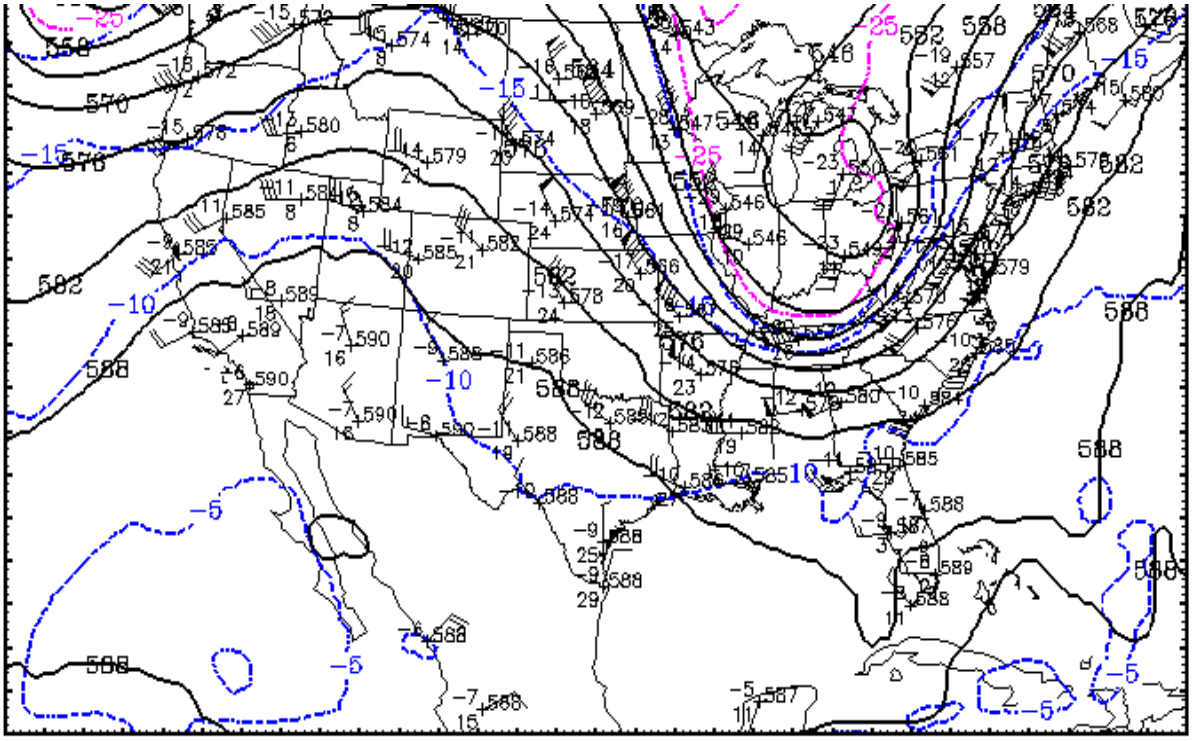

(c) RUC II simulated 500-mb temperatures (C) valid at 1800 UTC with superimposed observed 1200 UTC rawinsonde wind barbs (ms^{-1}), temperatures (C), and heights (m).

Figure 5. Concluded.

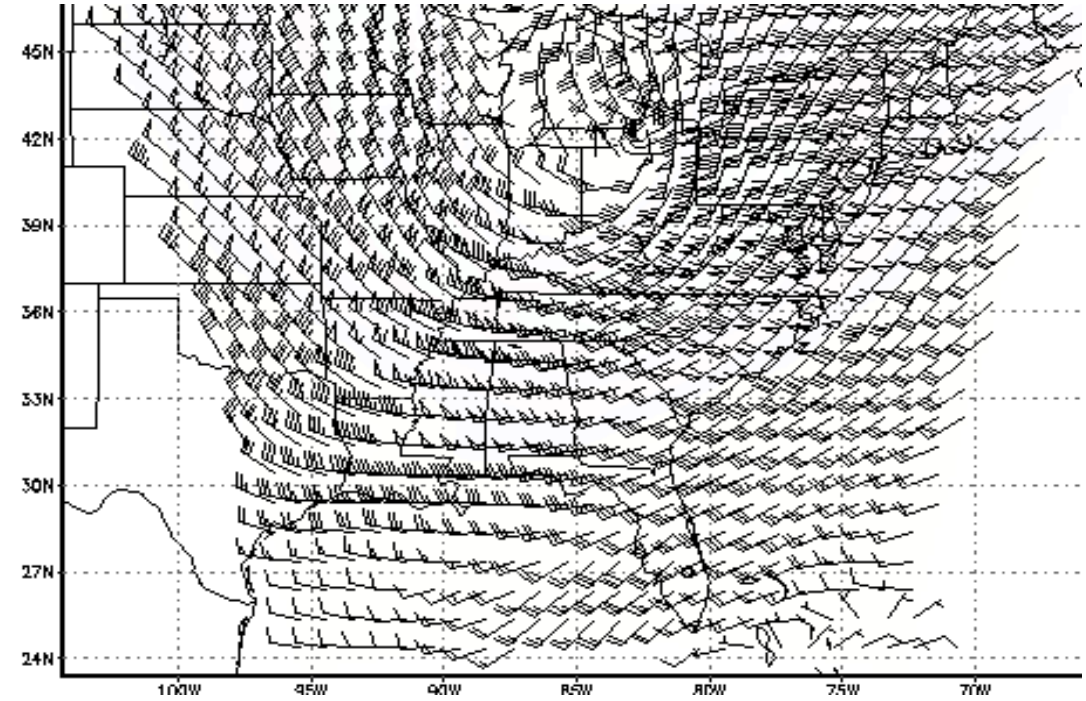

(a) RTTM fine1 simulated 26000-ft wind isotachs and barbs (kn) valid at 1800 UTC.

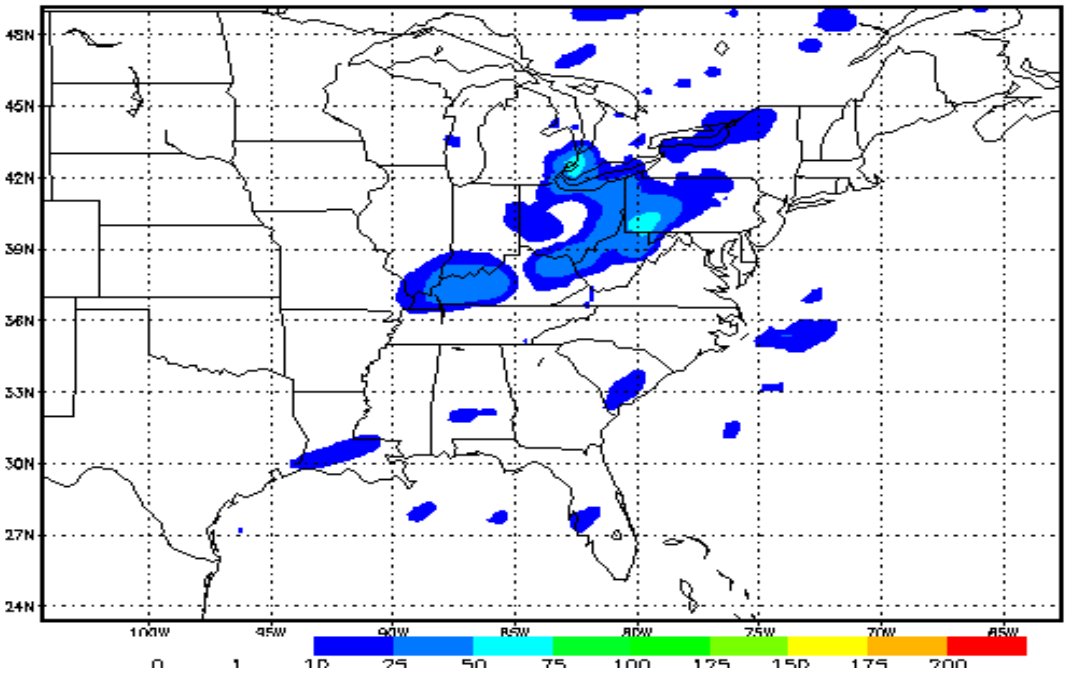

(b) RTTM fine1 simulated 26000-ft NCSU2 index (s^{-3}) valid at 1800 UTC.

Figure 6. October 16, 2001, fine1 simulation winds, index, and precipitation.

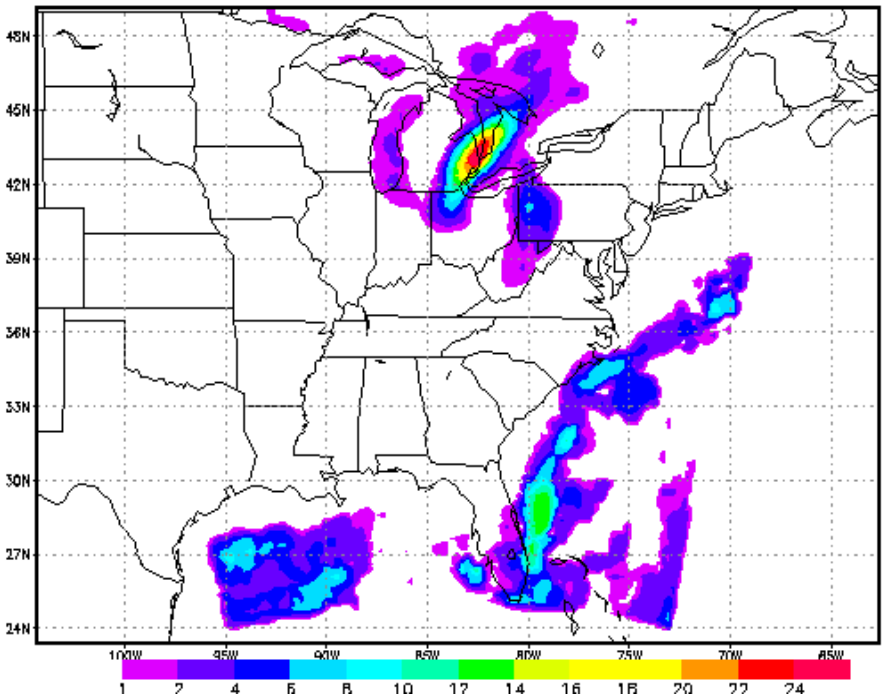

(c) RTTM fine1 simulated 3-hour total precipitation (mm) valid from 1500 UTC to 1800 UTC.

Figure 6. Concluded.

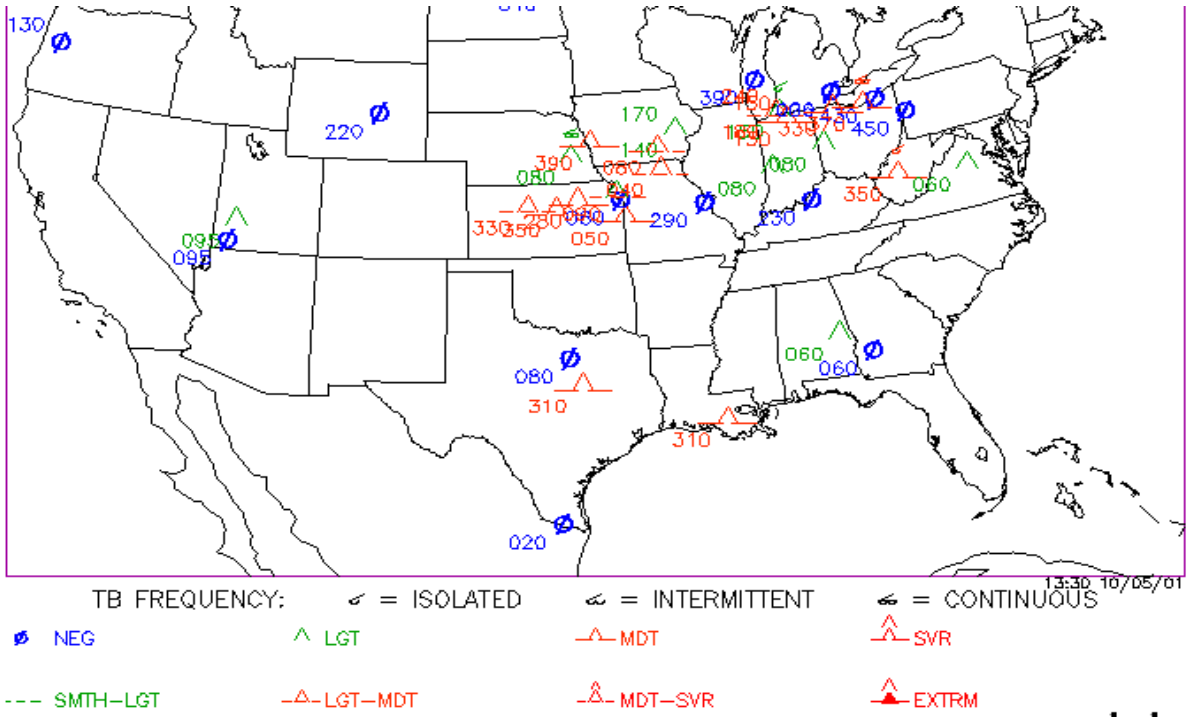

(a) Pireps from NOAA Aviation Digital Data source valid from 1126 UTC to 1320 UTC.

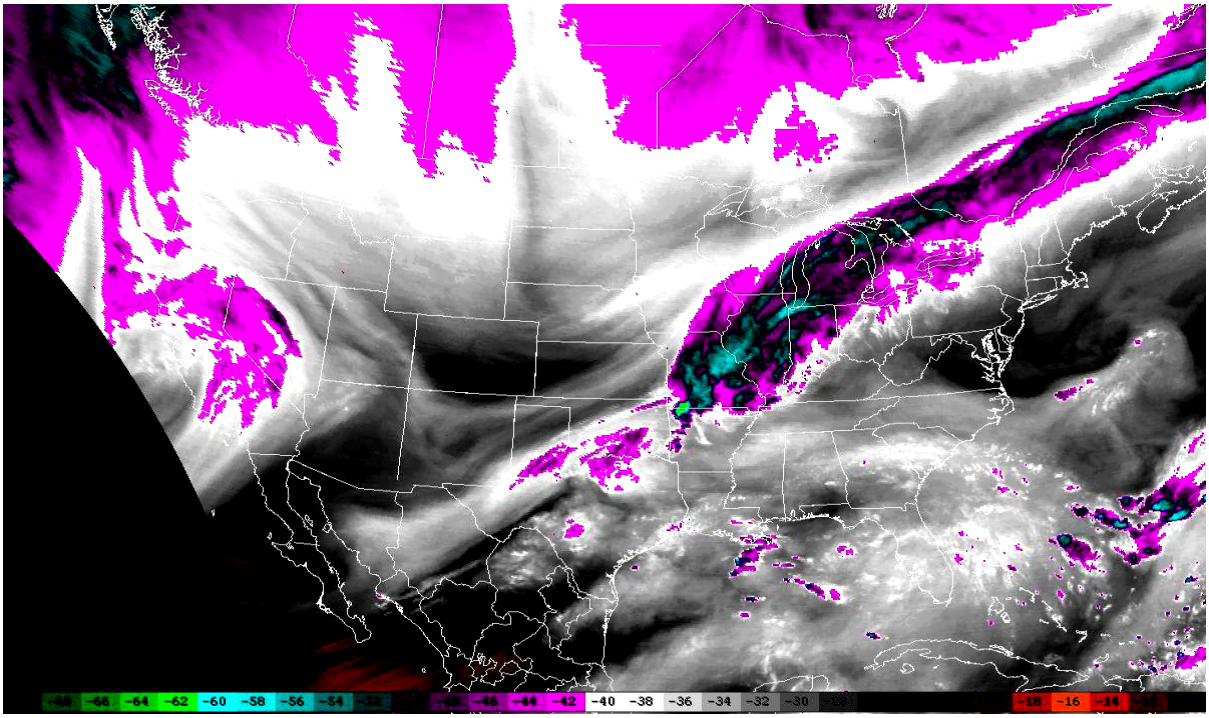

(b) Water vapor infrared satellite imagery valid at 1215 UTC.

Figure 7. October 5, 2001, pireps, water vapor imagery, rawinsonde, and RUC analysis.

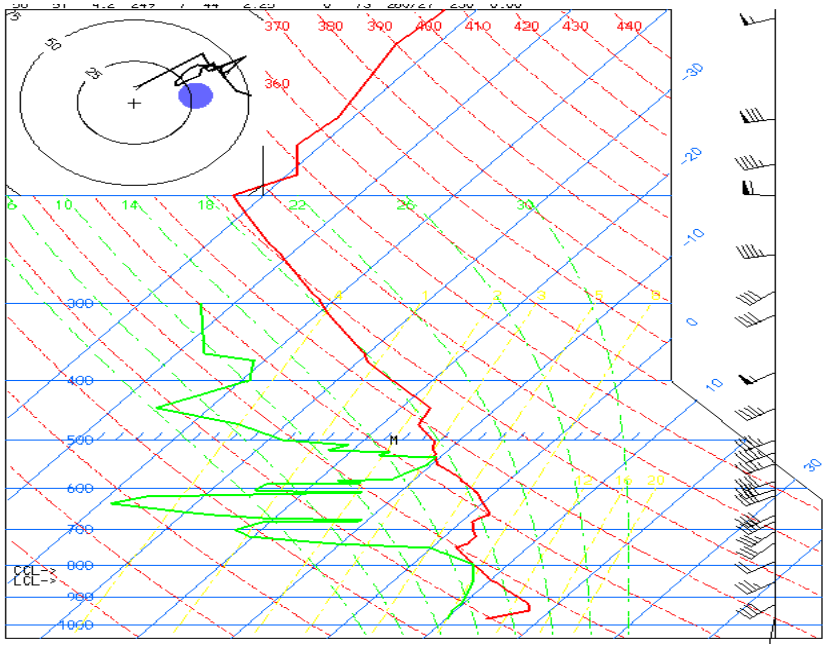

(c) Rawinsonde sounding valid at 1200 UTC.

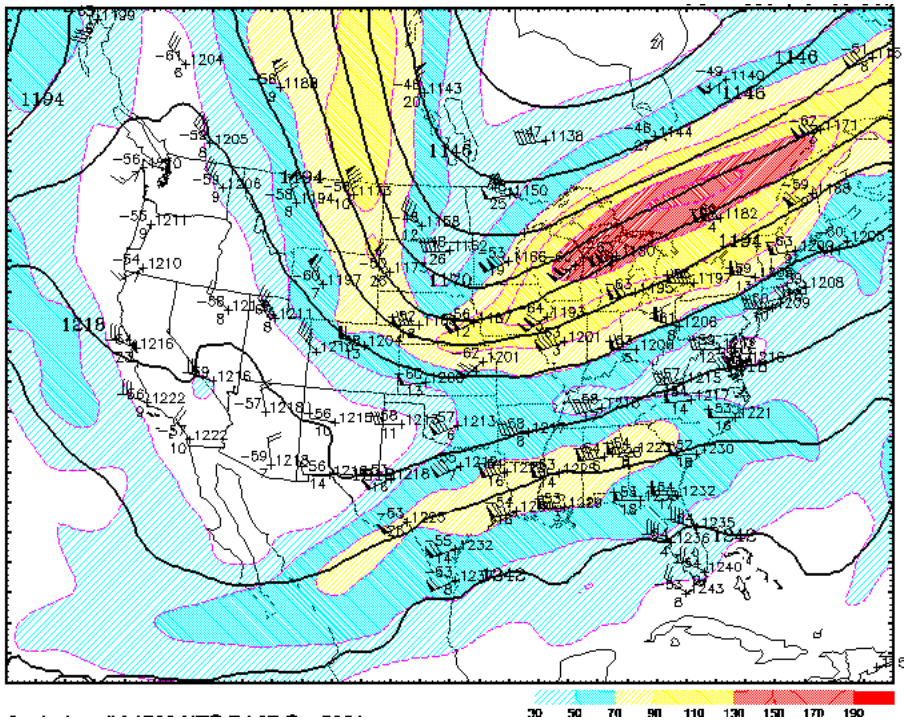

(d) RUC II simulated 200-mb wind isotachs (ms^{-1}) valid at 1500 UTC with superimposed observed 1200 UTC rawinsonde wind barbs (ms^{-1}), temperatures (C), and heights (m).

Figure 7. Concluded.

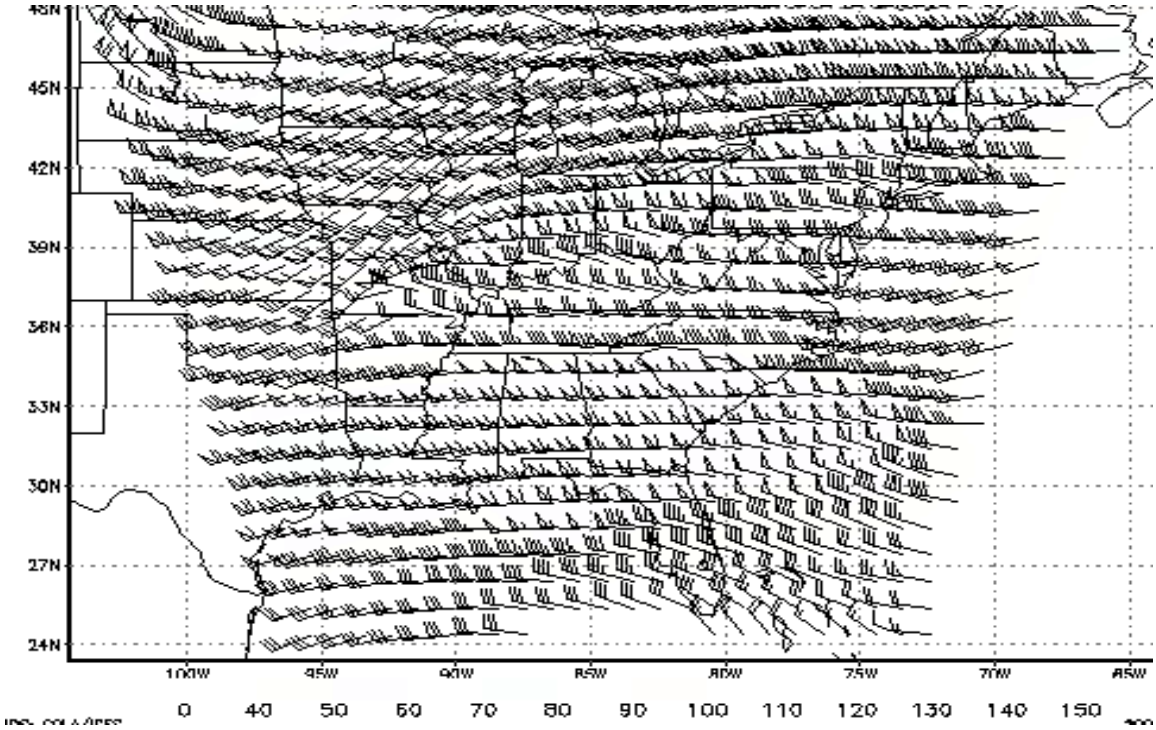

(a) RTTM fine1 36000-ft wind isotachs and barbs (kn) valid at 1200 UTC.

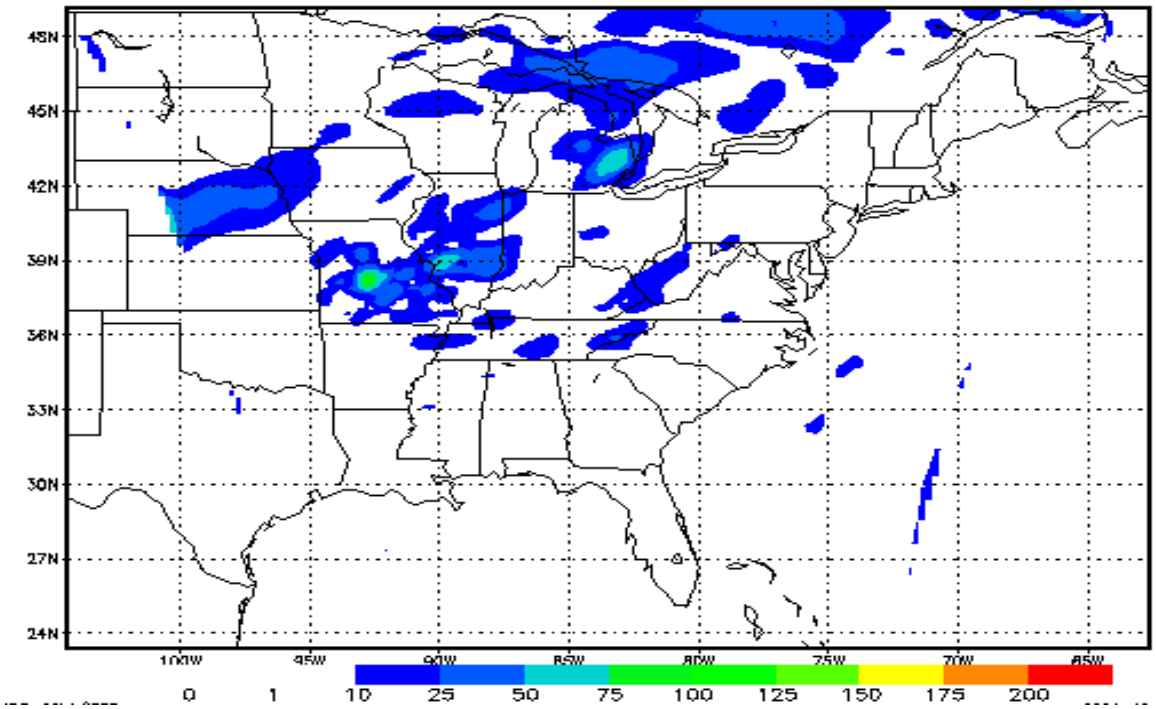

(b) RTTM fine1 36000-ft NCSU2 index (s^{-3}) valid at 1200 UTC.

Figure 8. October 5, 2001, fine1 simulation winds, index, and precipitation.

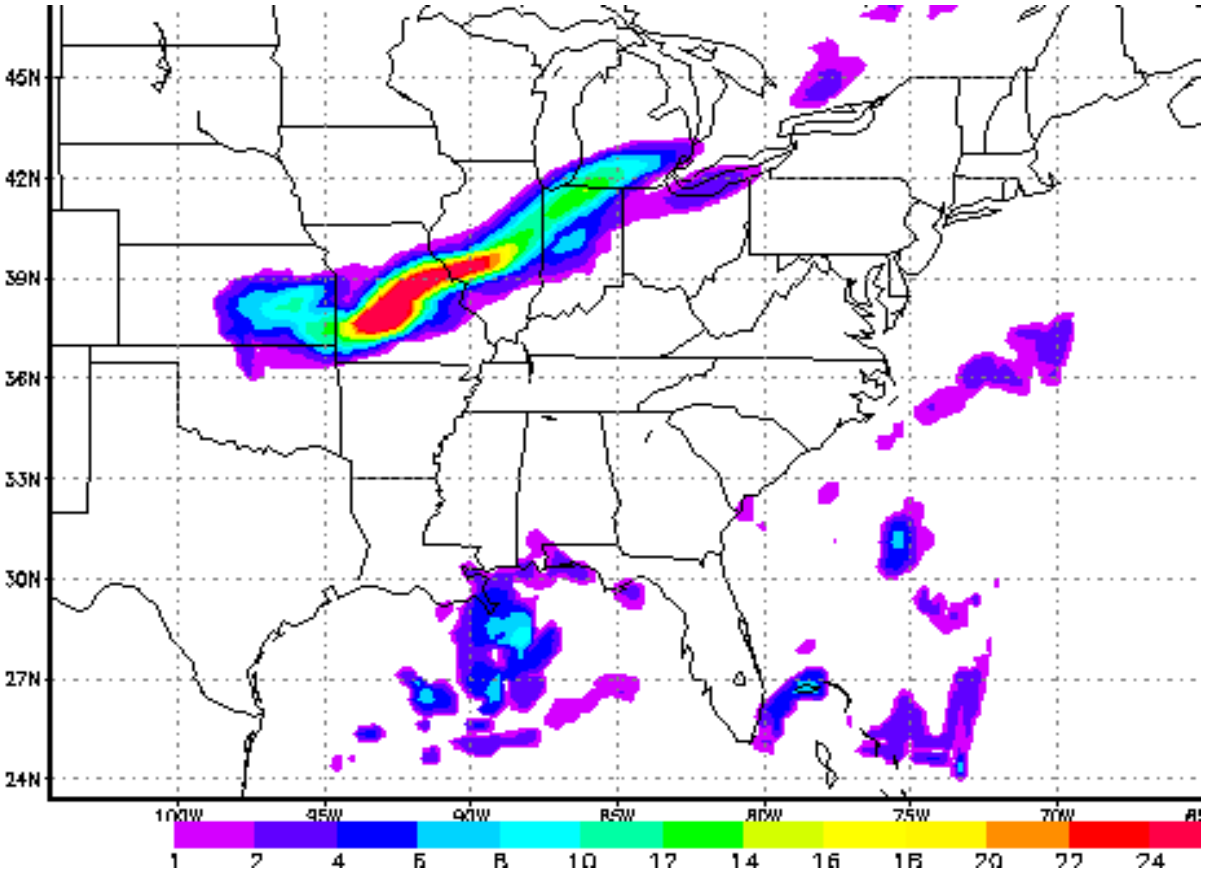

(c) RTTM fine1 simulated 3-hour precipitation (mm) valid from 0900 UTC to 1200 UTC.

Figure 8. Concluded.

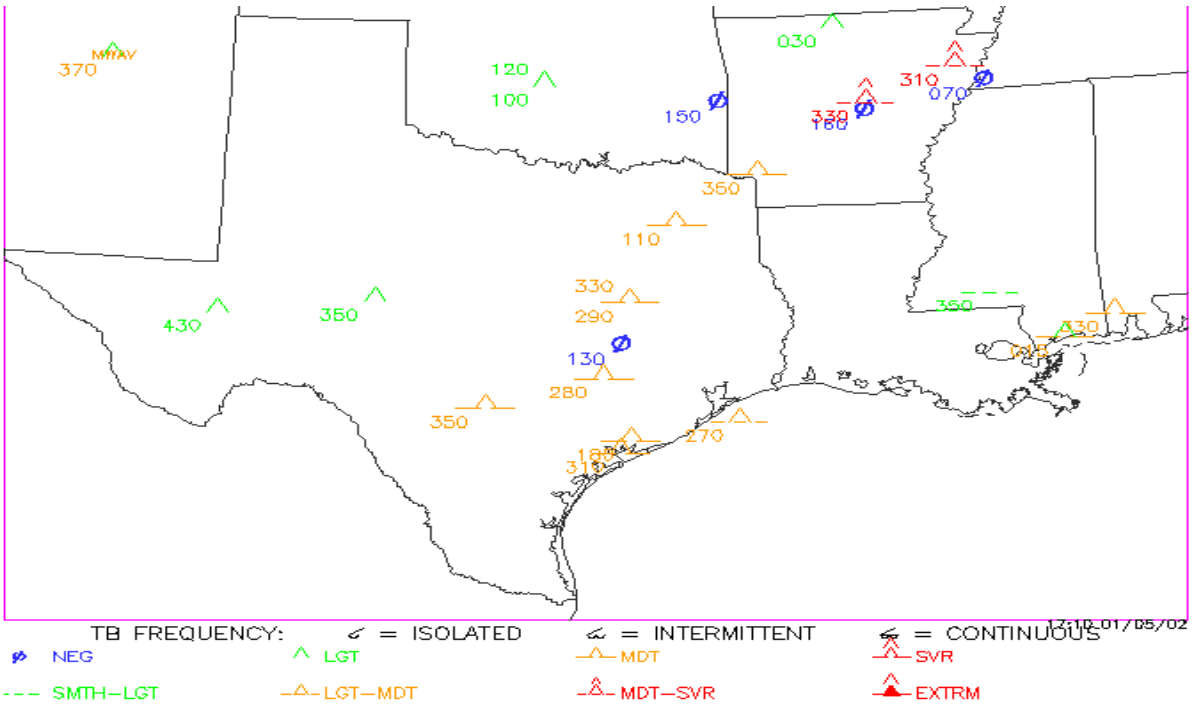

(a) Pireps from NOAA Aviation Digital Data source valid from 1511 UTC to 1703 UTC.

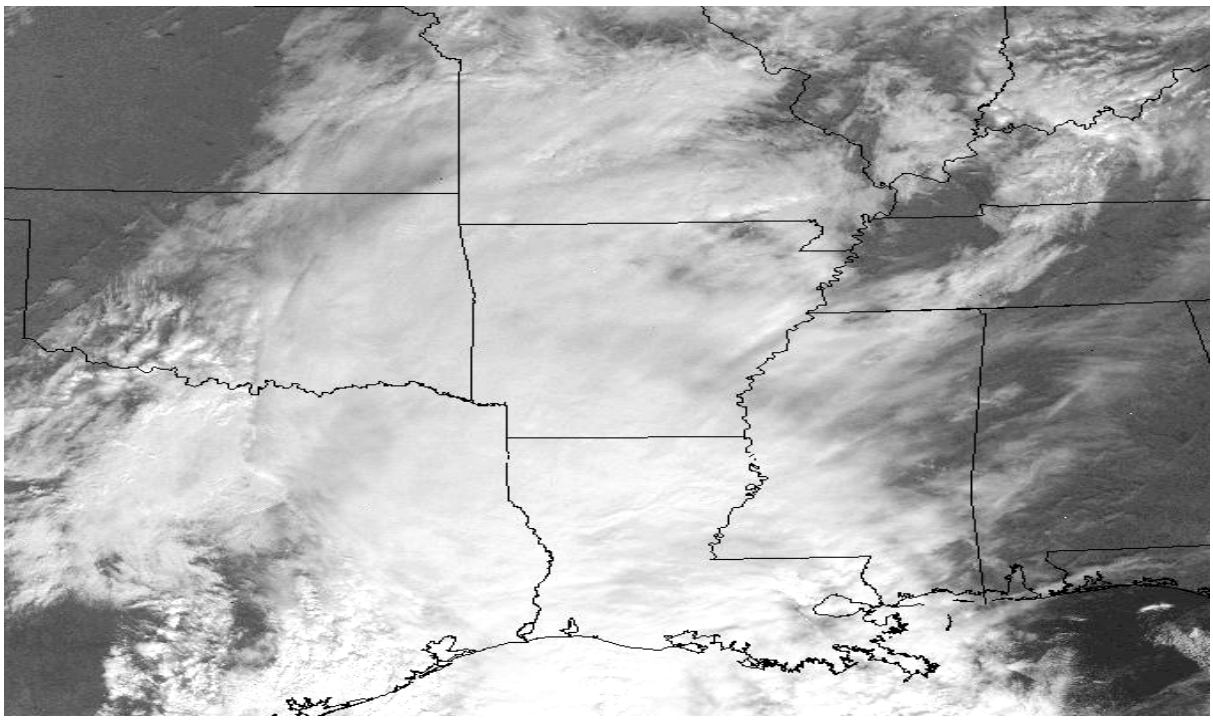

(b) Visible satellite imagery valid at 1702 UTC.

Figure 9. January 5, 2002, pireps, visible imagery, rawinsonde, and RUC analysis.

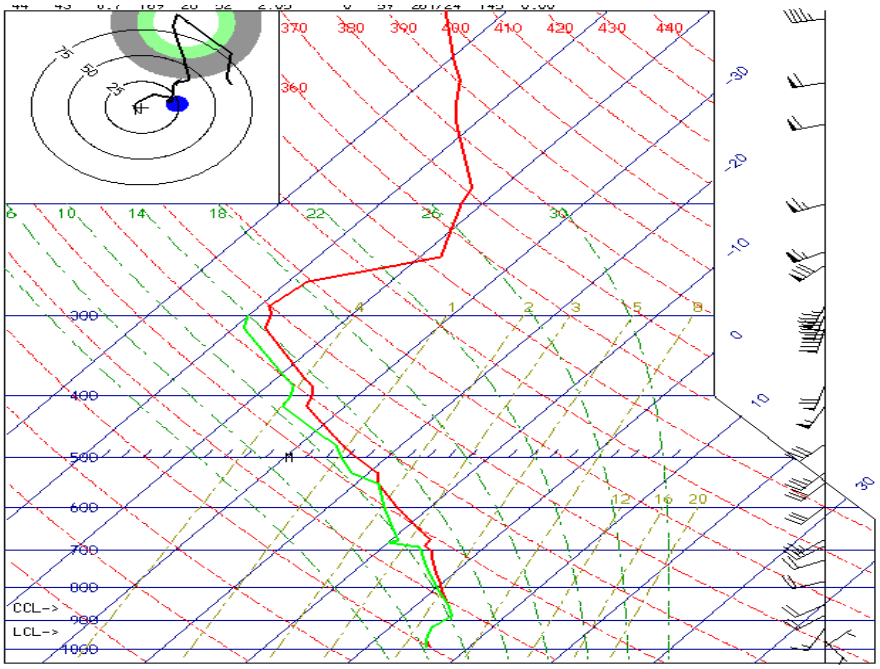

(c) Fort Worth, Texas, rawinsonde sounding valid at 1200 UTC.

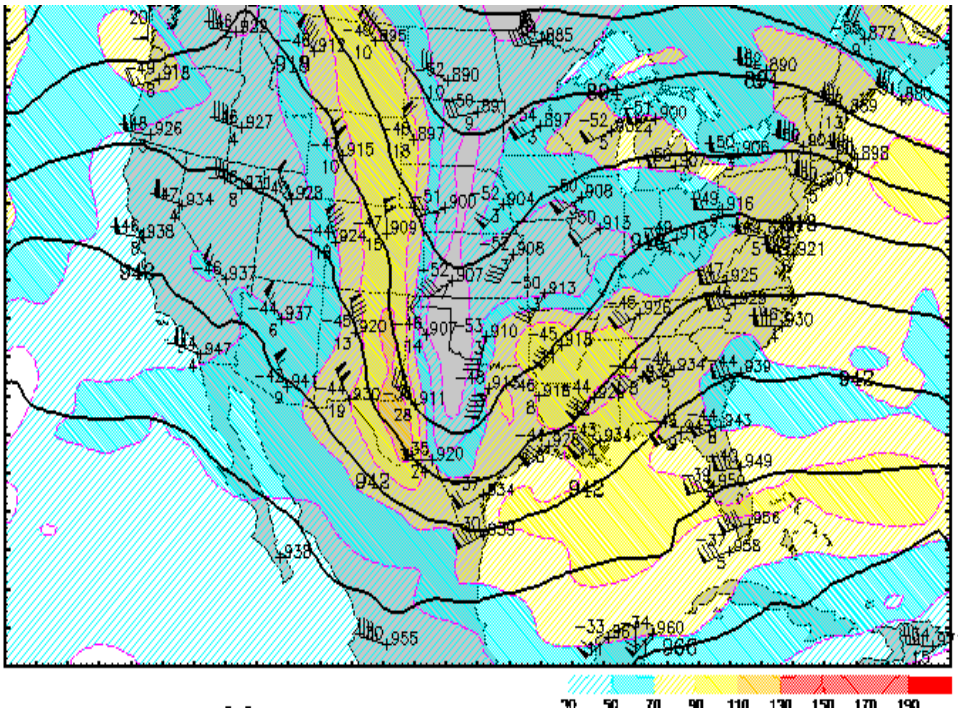

(d) RUC II simulated 300-mb wind isotachs (ms^{-1}) valid at 1500 UTC with superimposed observed 1200 UTC rawinsonde wind barbs (ms^{-1}), temperatures (C), and heights (m).

Figure 9. Concluded.

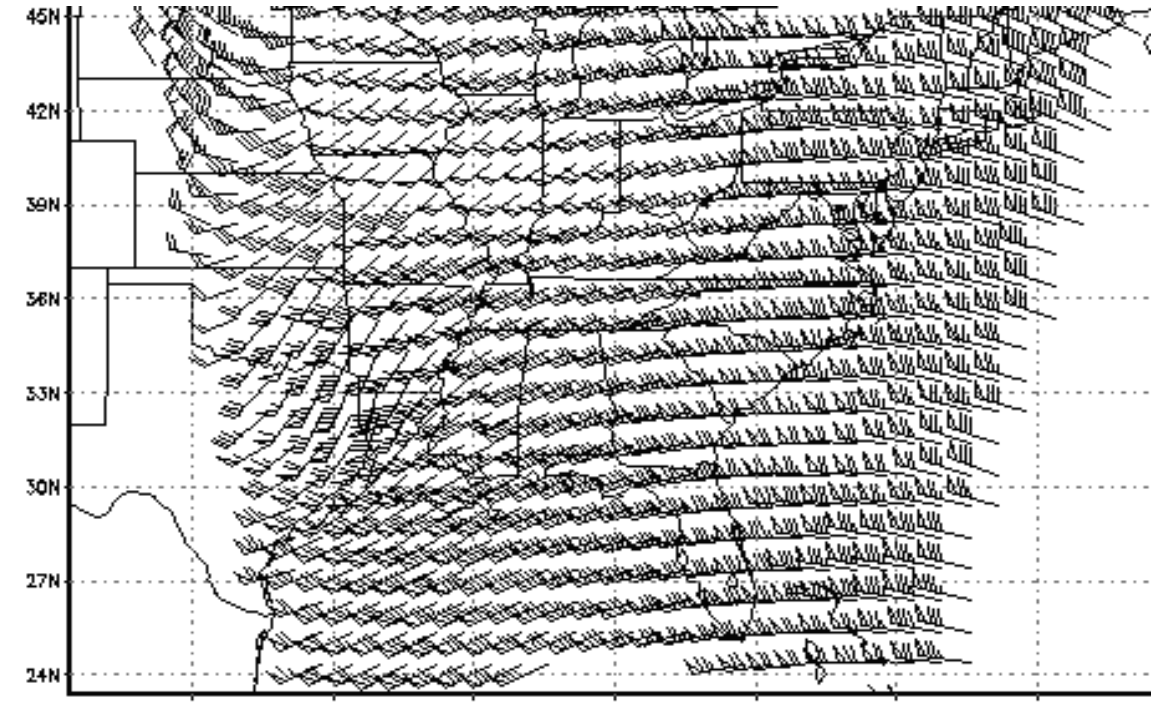

(a) RTTM fine1 simulated 32 000-ft wind isotachs and barbs (kn) valid at 1800 UTC.

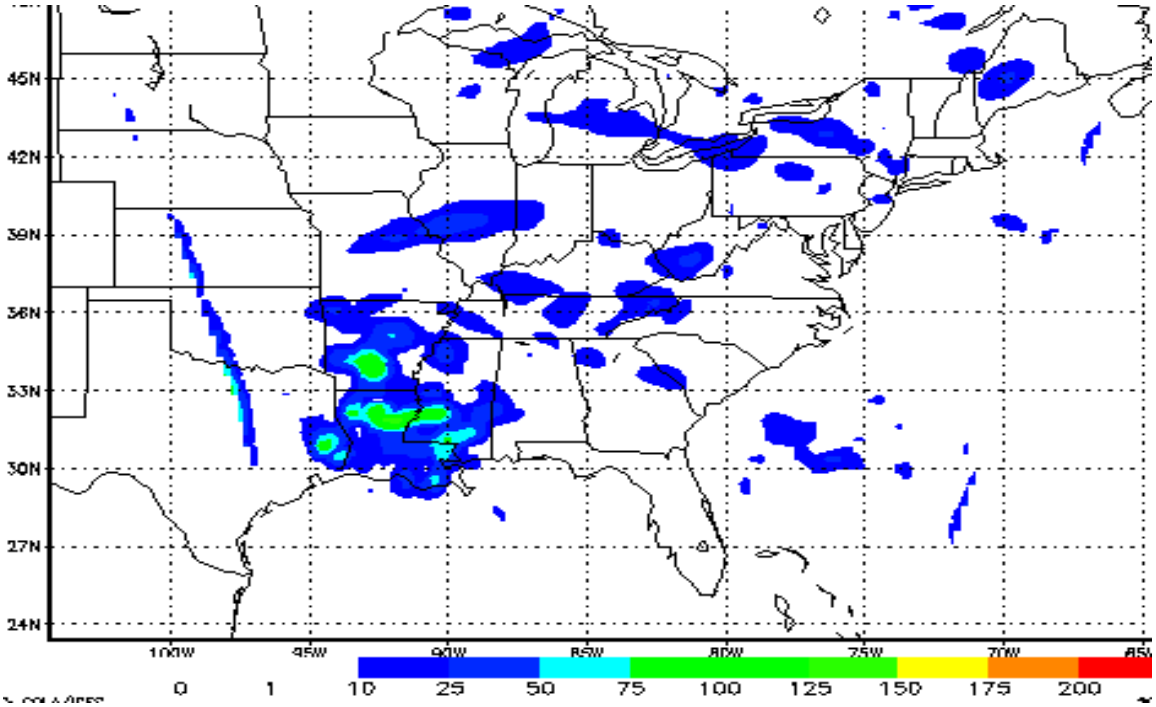

(b) RTTM fine1 simulated 32 000-ft NCSU2 index (s^{-3}) valid at 1800 UTC.

Figure 10. January 5, 2002, fine1 simulation winds, index, precipitation, and sounding.

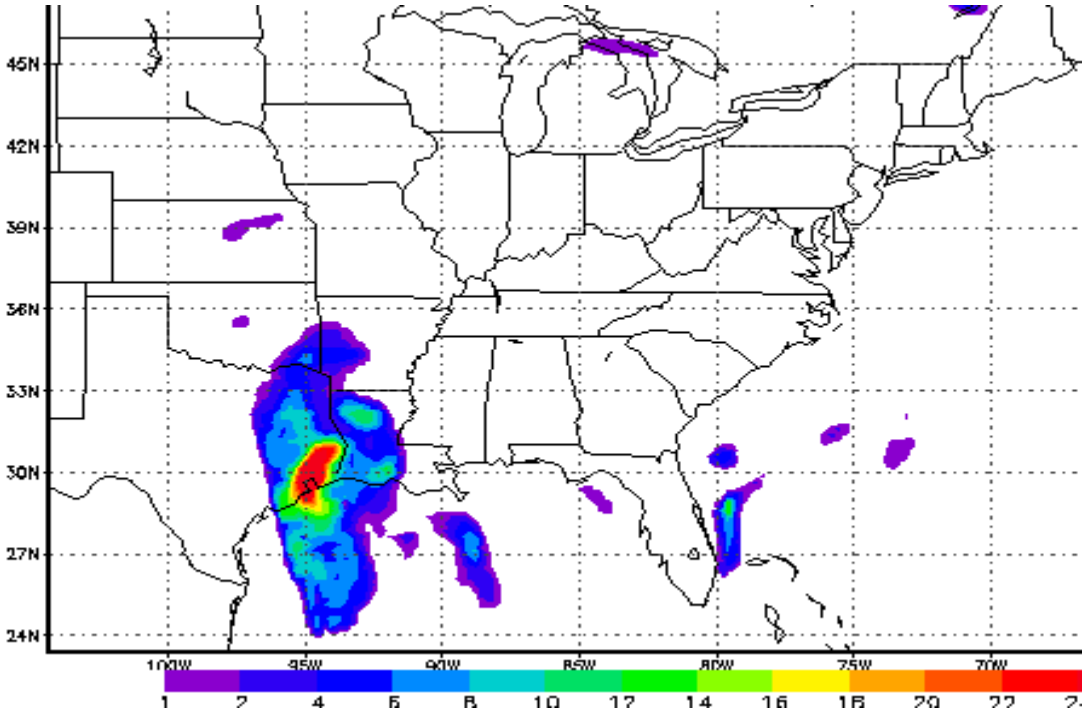

(c) RTTM fine1 simulated total precipitation (mm) valid from 1200 UTC to 1500 UTC.

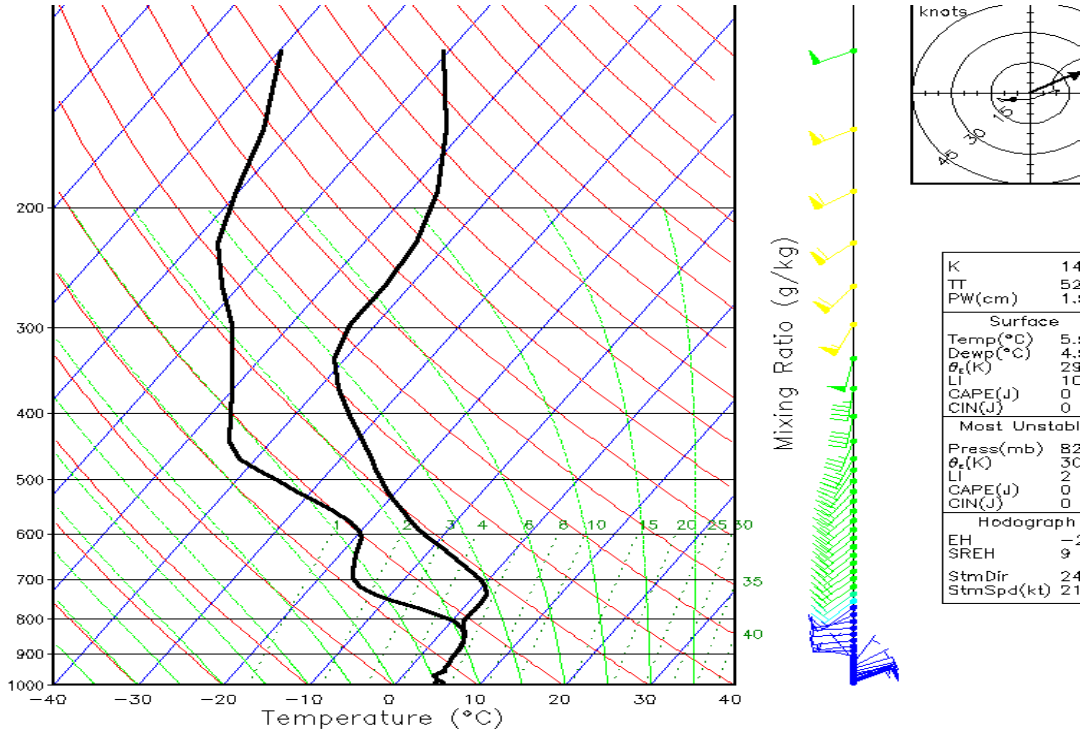

(d) RTTM fine1 simulated skew-t sounding located at Fort Worth, Texas, and valid at 1800 UTC.

Figure 10. Concluded.

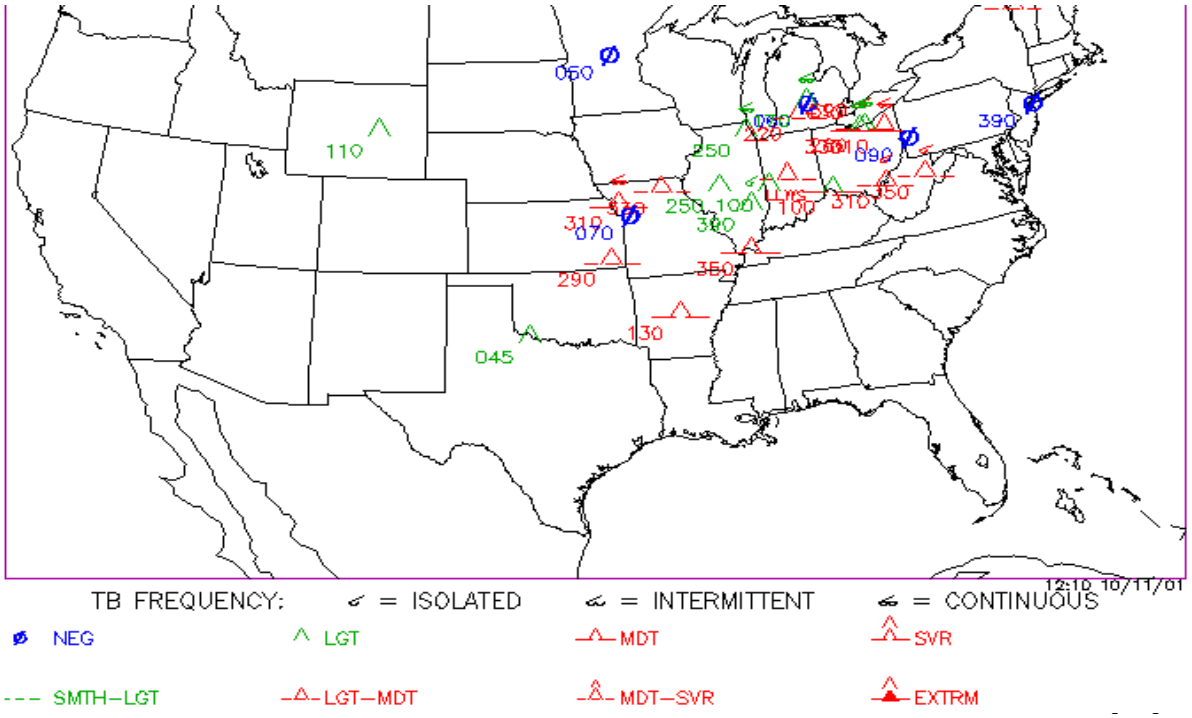

(a) Pireps from NOAA Aviation Digital Data source valid from 1028 UTC to 1157 UTC.

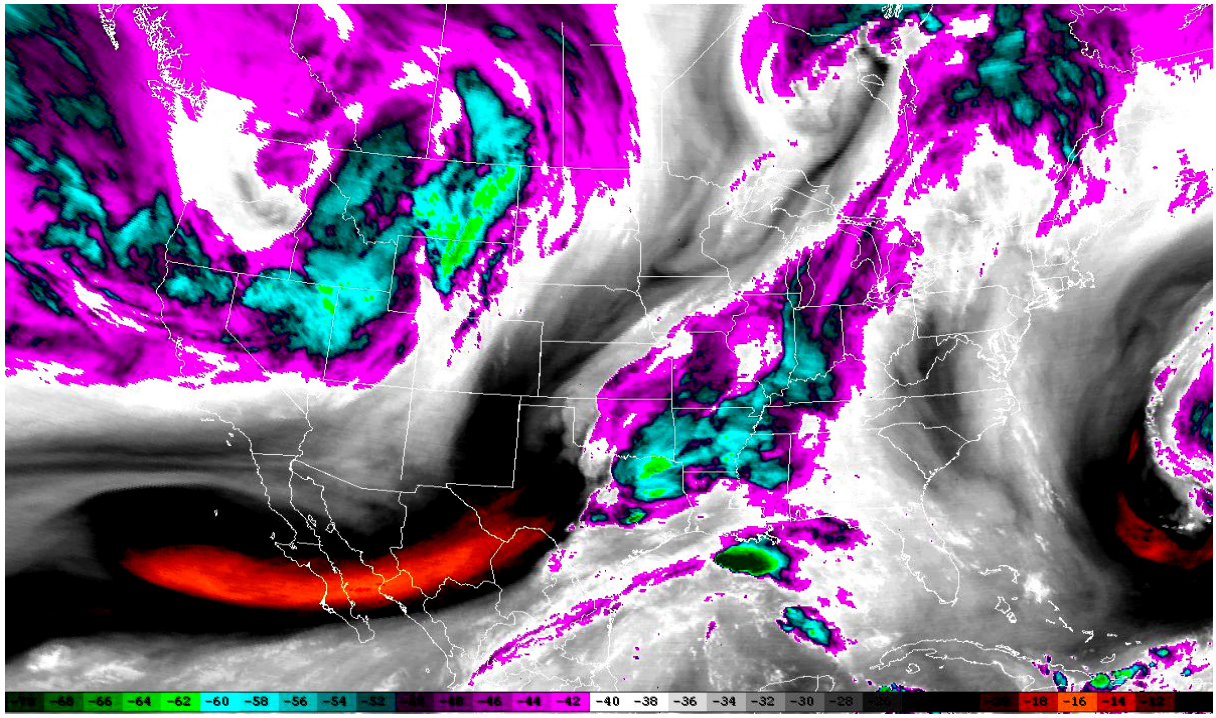

(b) Water vapor infrared satellite imagery valid at 1145 UTC.

Figure 11. October 11, 2001, pireps, water vapor imagery, rawinsonde, and RUC analysis.

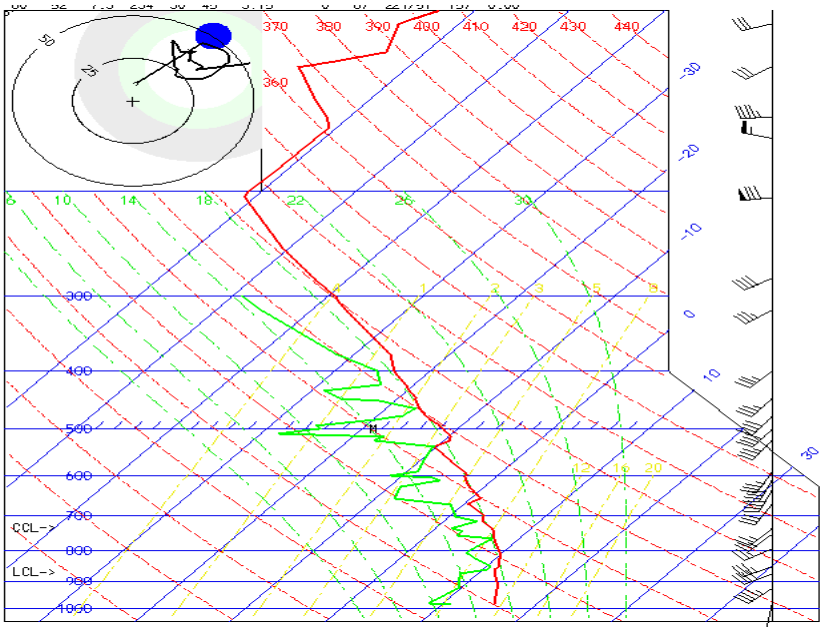

(c) Columbus, Ohio, rawinsonde sounding valid at 1200 UTC.

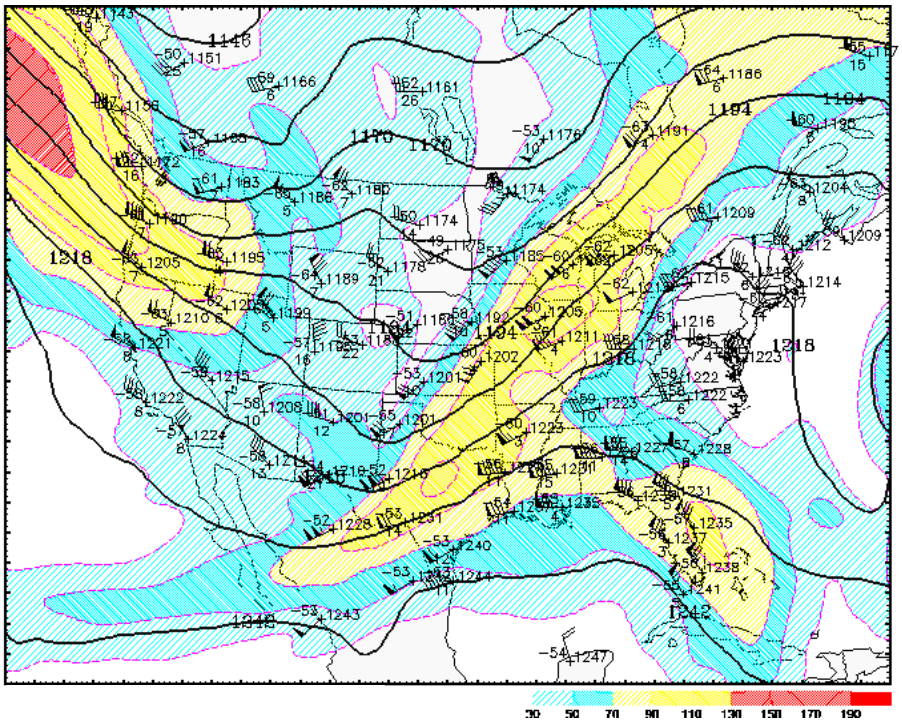

(d) RUC II simulated 200-mb wind isotachs (ms^{-1}) valid at 0900 UTC with superimposed observed 0000 UTC rawinsonde wind barbs (ms^{-1}), temperatures (C), and heights (m).

Figure 11. Concluded.

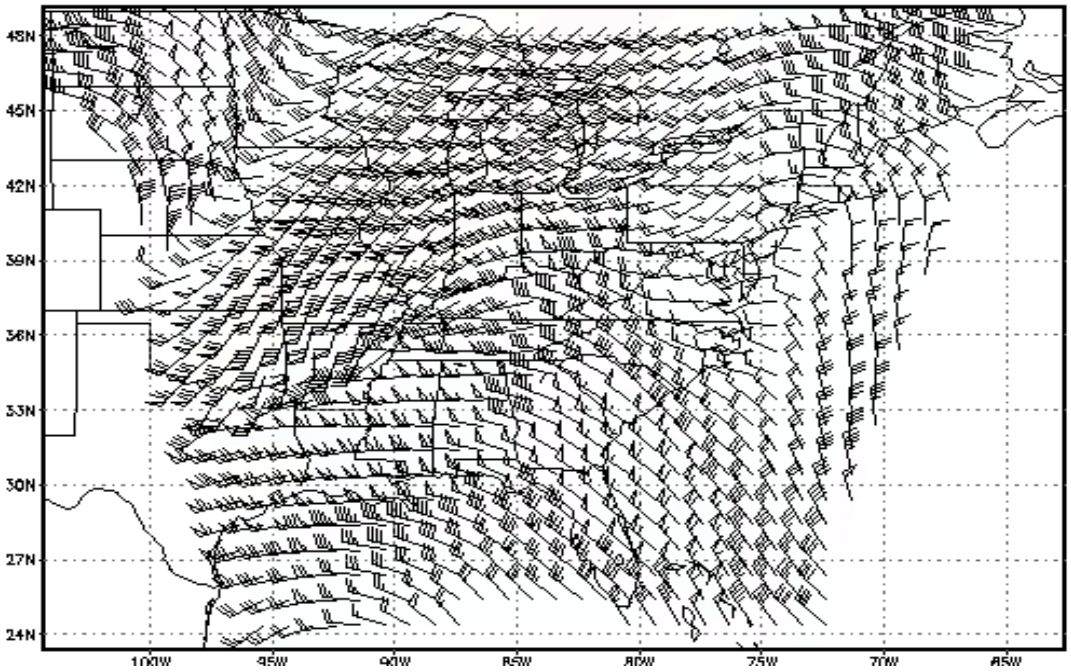

(a) RTTM fine1 simulated 34 000-ft wind isotachs and barbs (kn) valid at 1200 UTC.

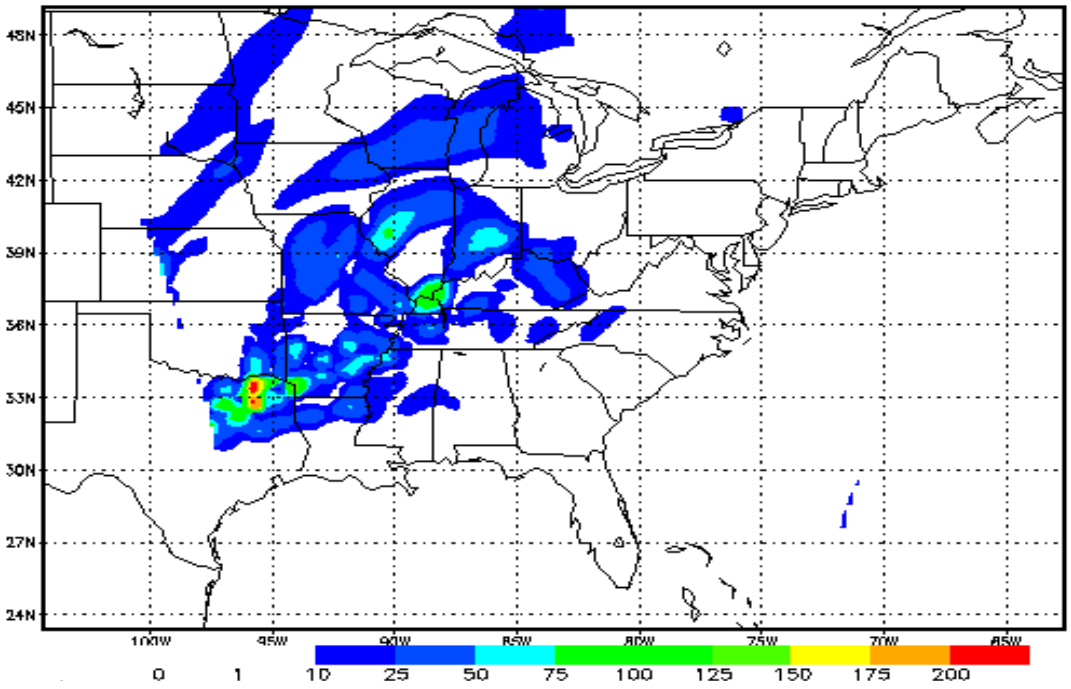

(b) RTTM fine1 simulated 36 000-ft NCSU2 index (s^{-3}) valid at 1200 UTC.

Figure 12. October 11, 2001, fine1 simulation winds, index, and precipitation.

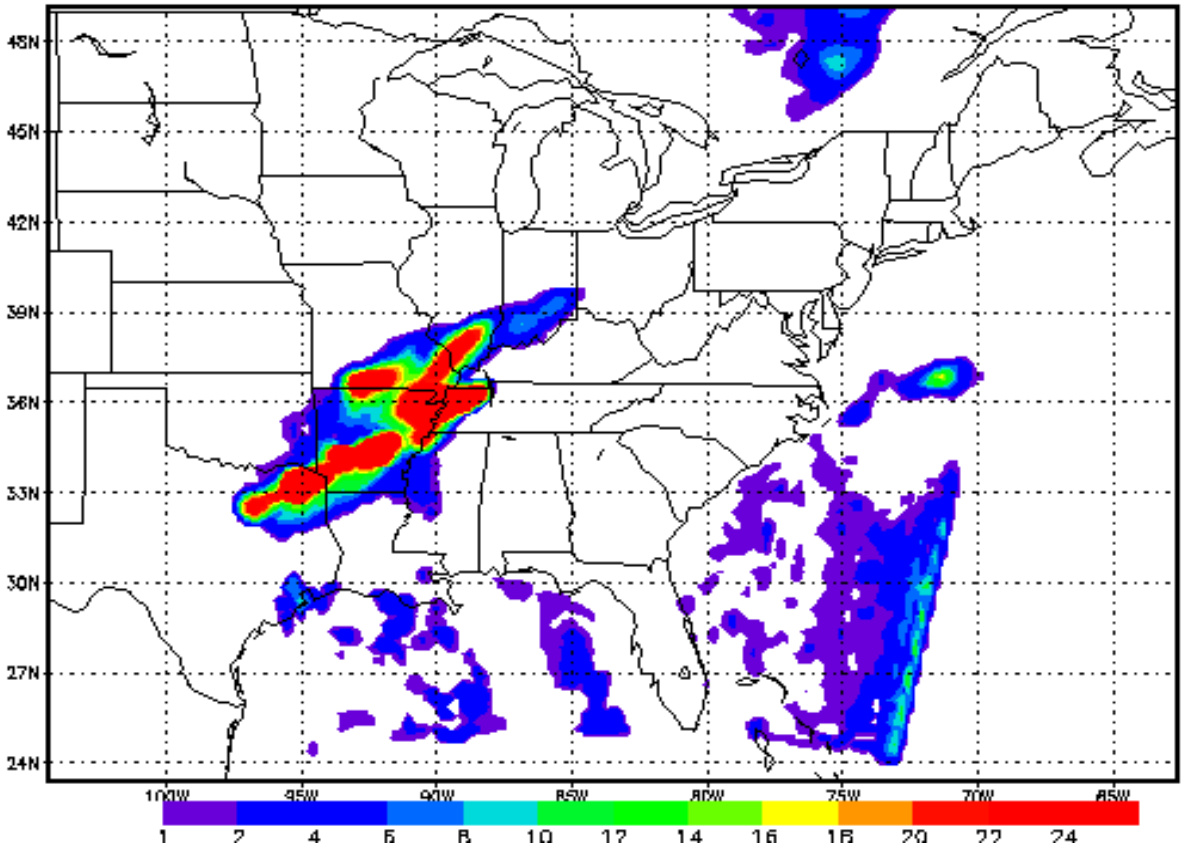

(c) RTTM fine1 simulated total precipitation (mm) valid from 0900 UTC to 1200 UTC.

Figure 12. Concluded.

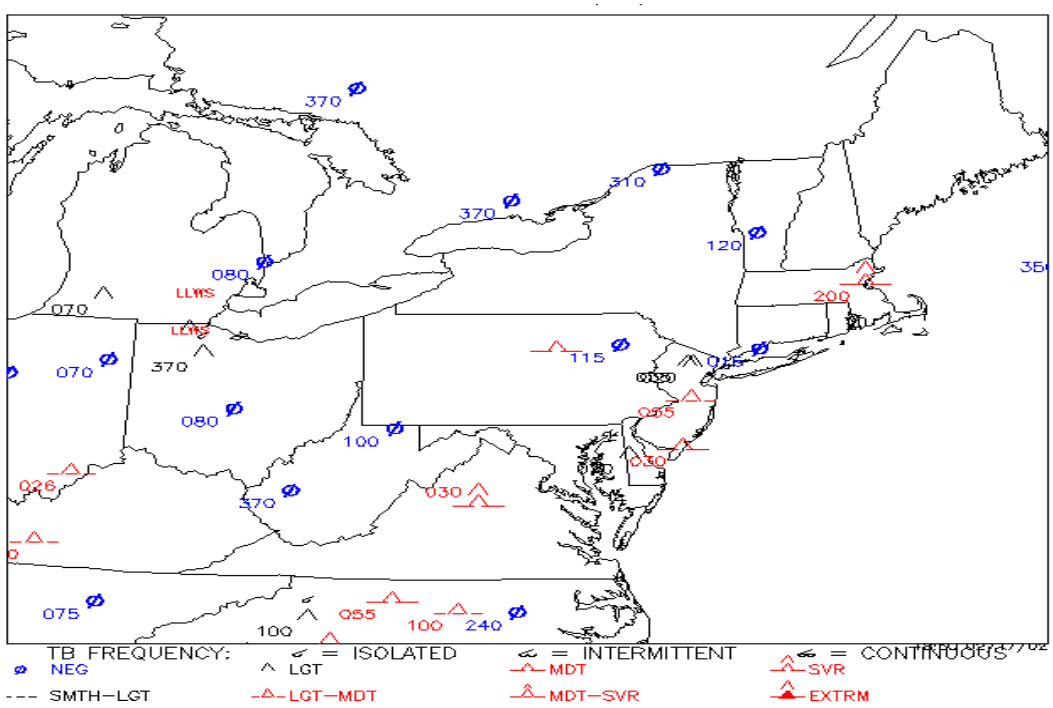

(a) Pireps from NOAA Aviation Digital Data source valid from 1650 UTC to 1843 UTC.

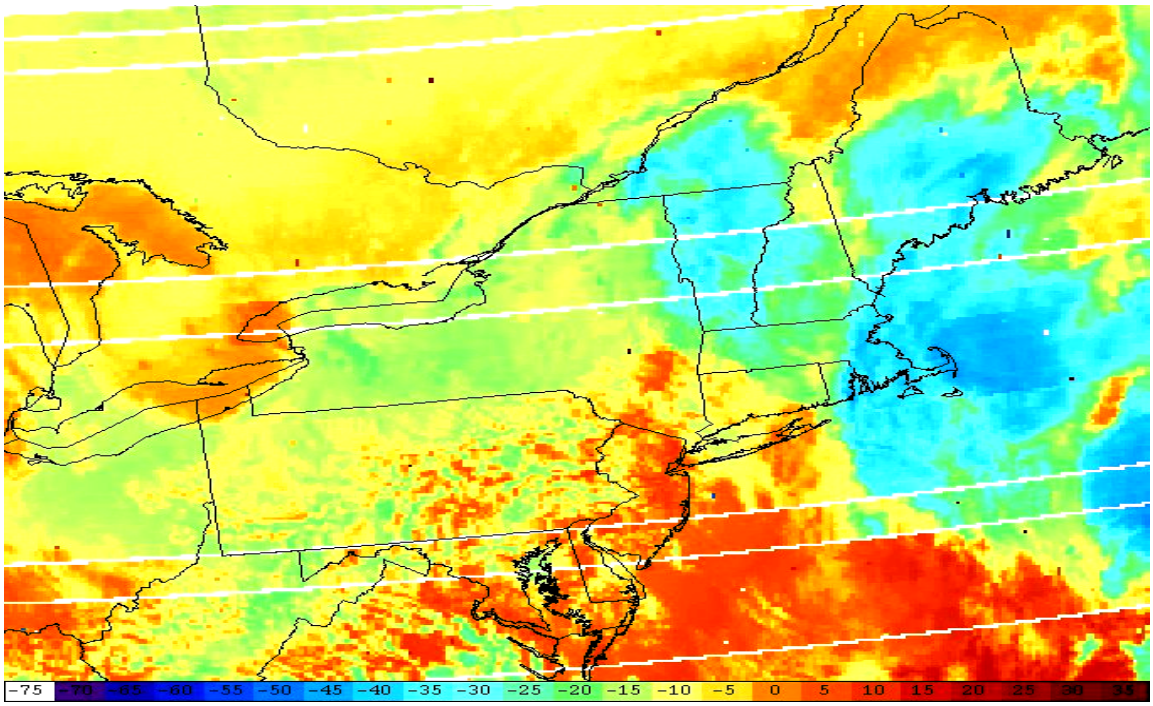

(b) Infrared satellite imagery valid at 1846 UTC.

Figure 13. February 17, 2002, pireps, infrared imagery, and RUC analysis.

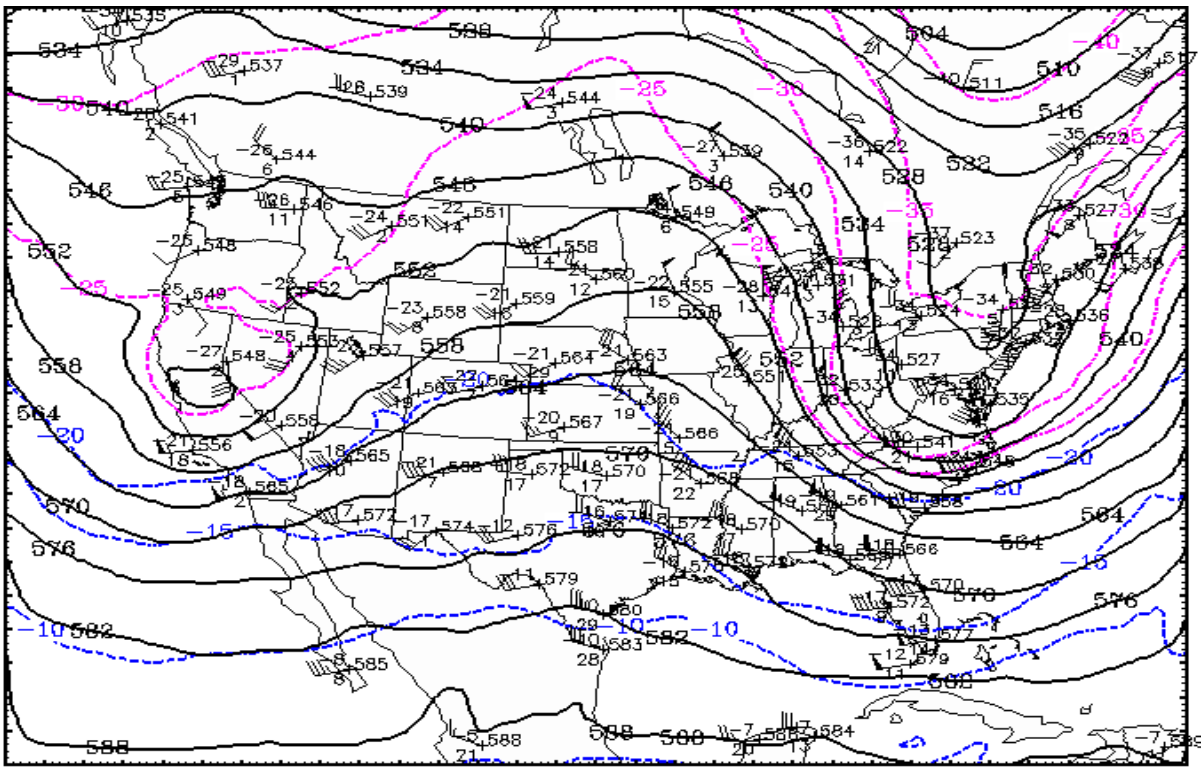

(c) RUC II simulated 500-mb temperatures (C) valid at 1800 UTC with superimposed observed 1200 UTC rawinsonde wind barbs (ms^{-1}), temperatures (C), and heights (m).

Figure 13. Concluded.

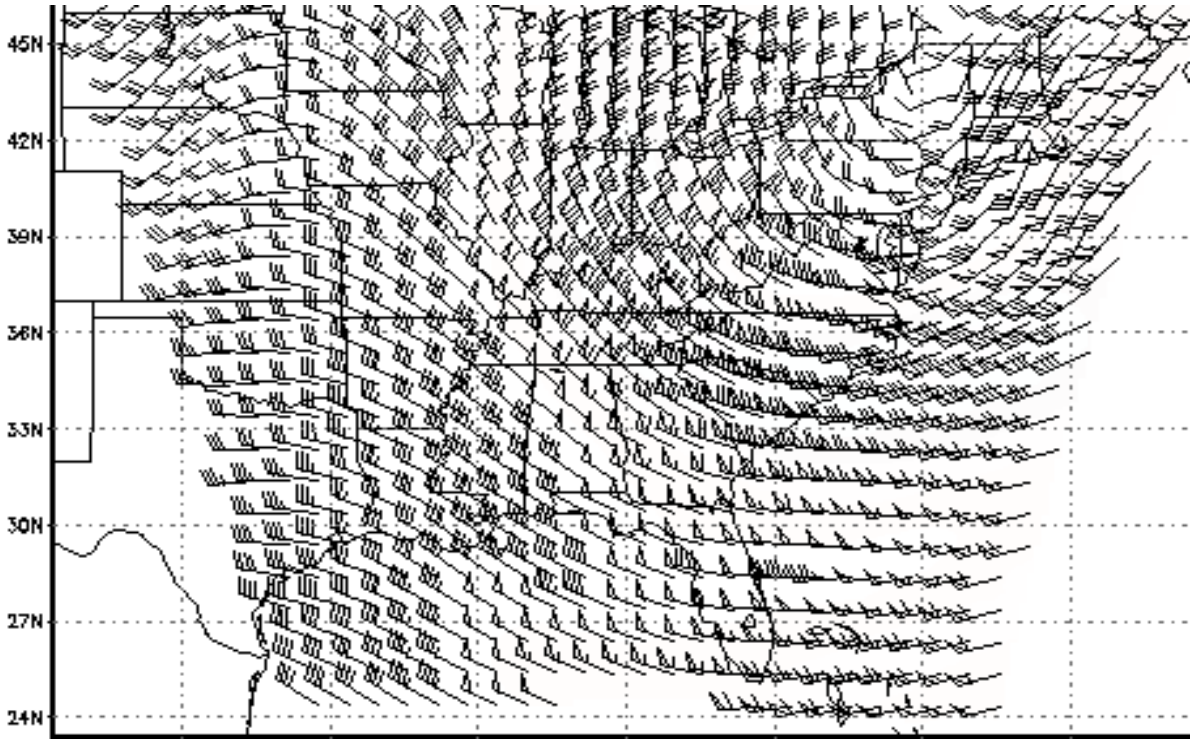

(a) RTTM fine1 simulated 20 000-ft wind isotachs and barbs (kn) valid at 1800 UTC.

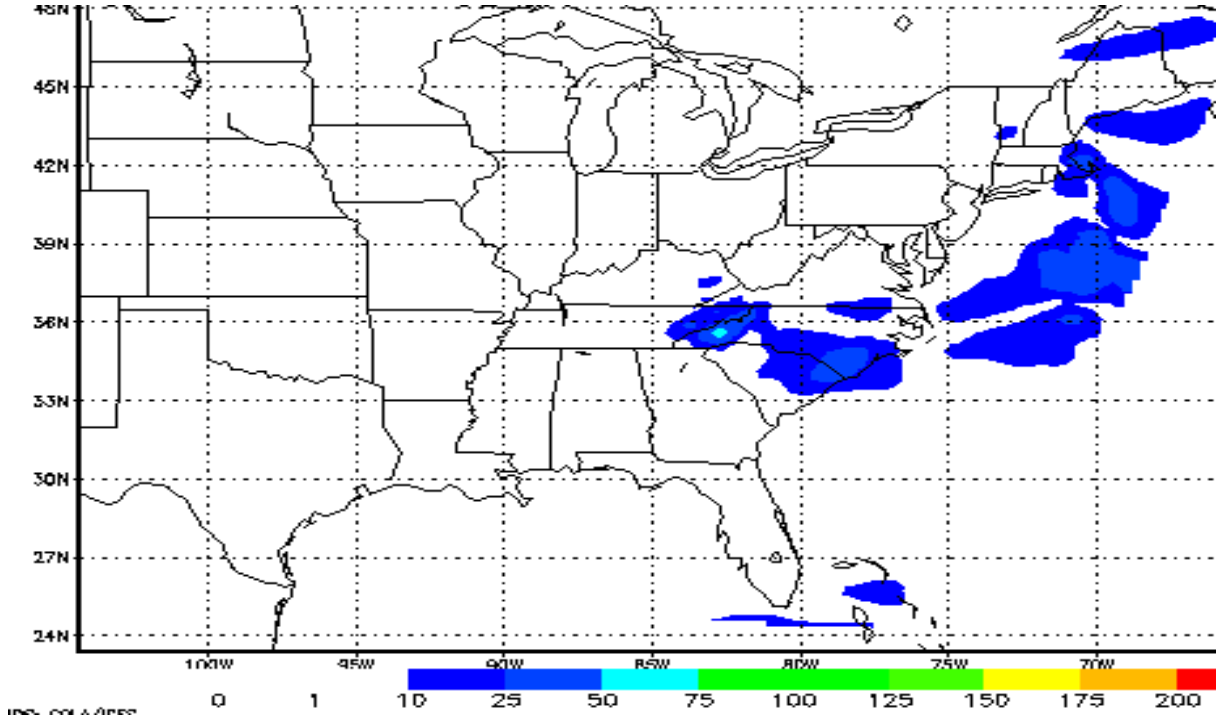

(b) RTTM fine1 simulated 18 000-ft NCSU2 index (s^{-3}) valid at 1800 UTC.

Figure 14. February 17, 2002, fine1 simulation winds, indices, precipitation, sounding, and Richardson number.

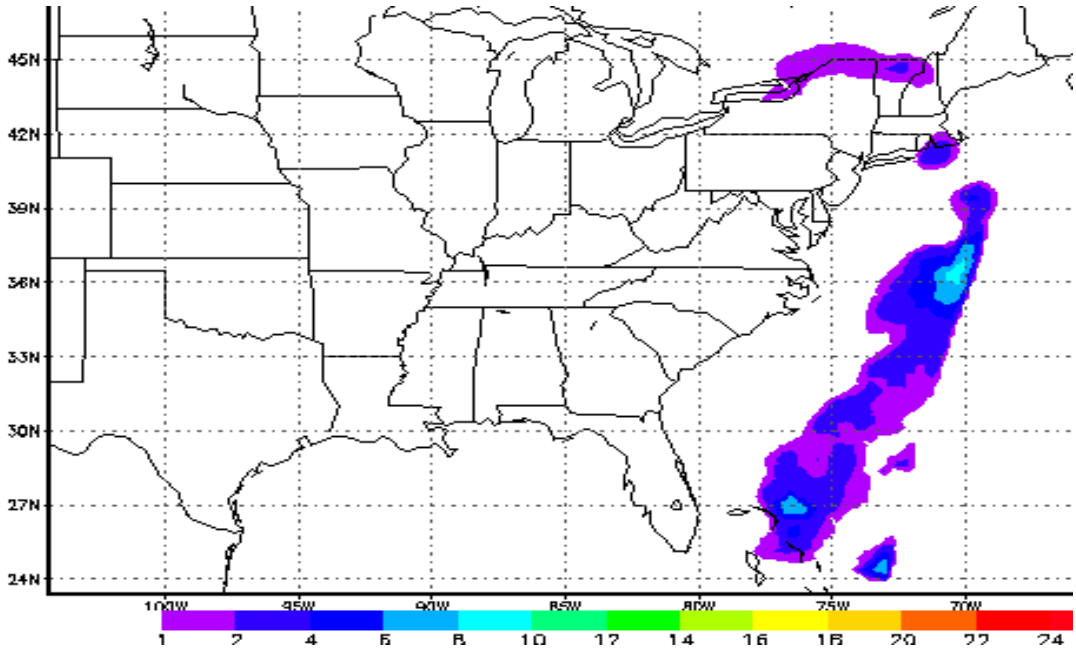

(c) RTTM fine1 simulated total precipitation (mm) valid from 1500 UTC to 1800 UTC.

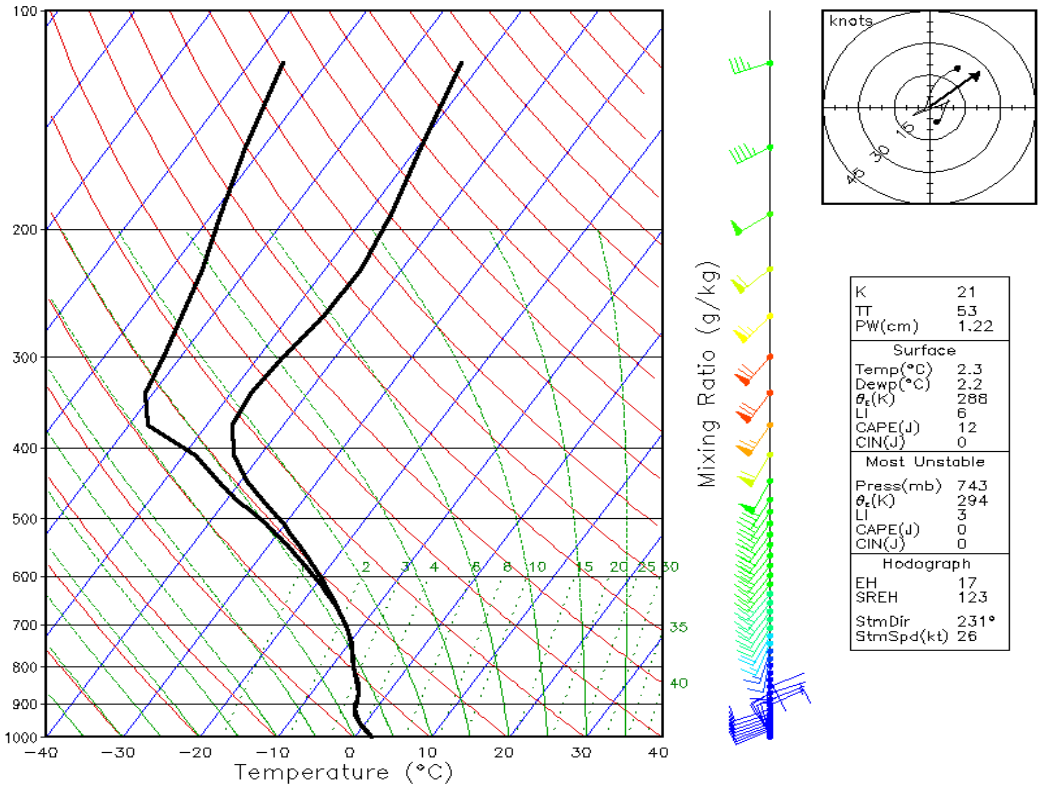

(d) RTTM fine1 simulated skew-t sounding located at Hyannisport, Massachusetts, and valid at 1800 UTC.

Figure 14. Continued.

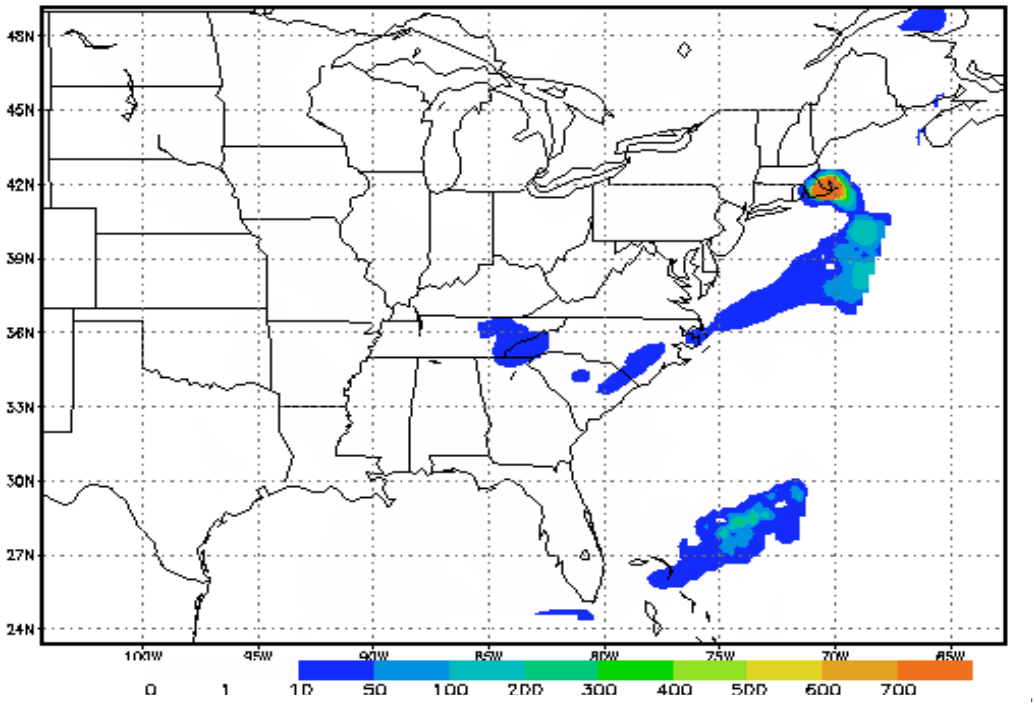

(e) RTTM fine1 simulated 20 000-ft NCSU1 index (s^{-3}) valid at 1800 UTC.

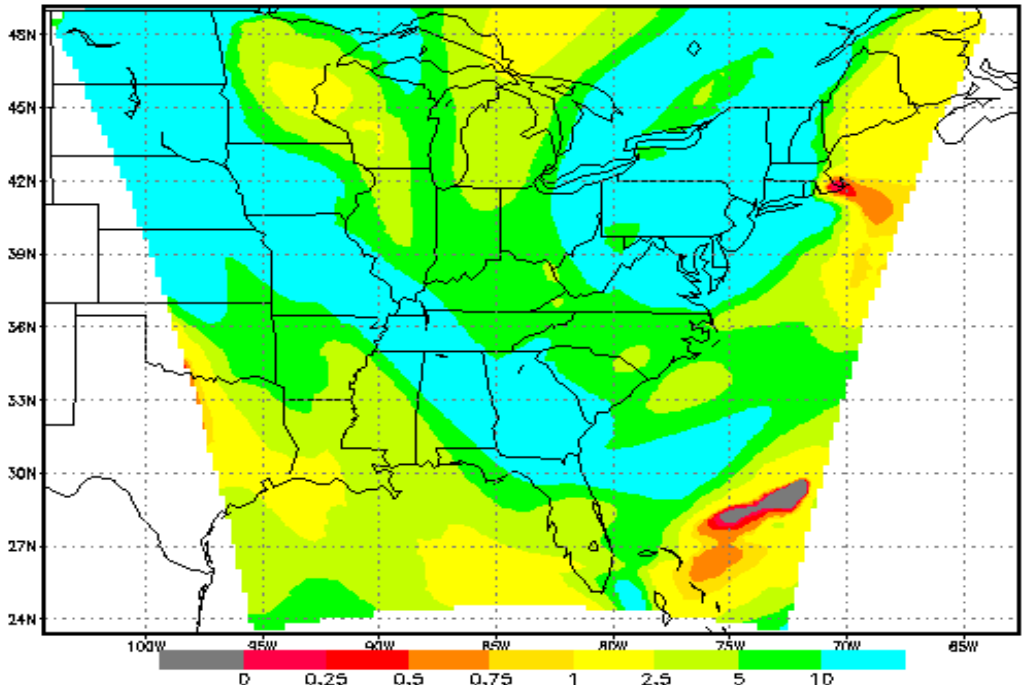

(f) RTTM fine1 simulated 20 000-ft Richardson number valid at 1800 UTC.

Figure 14. Concluded.

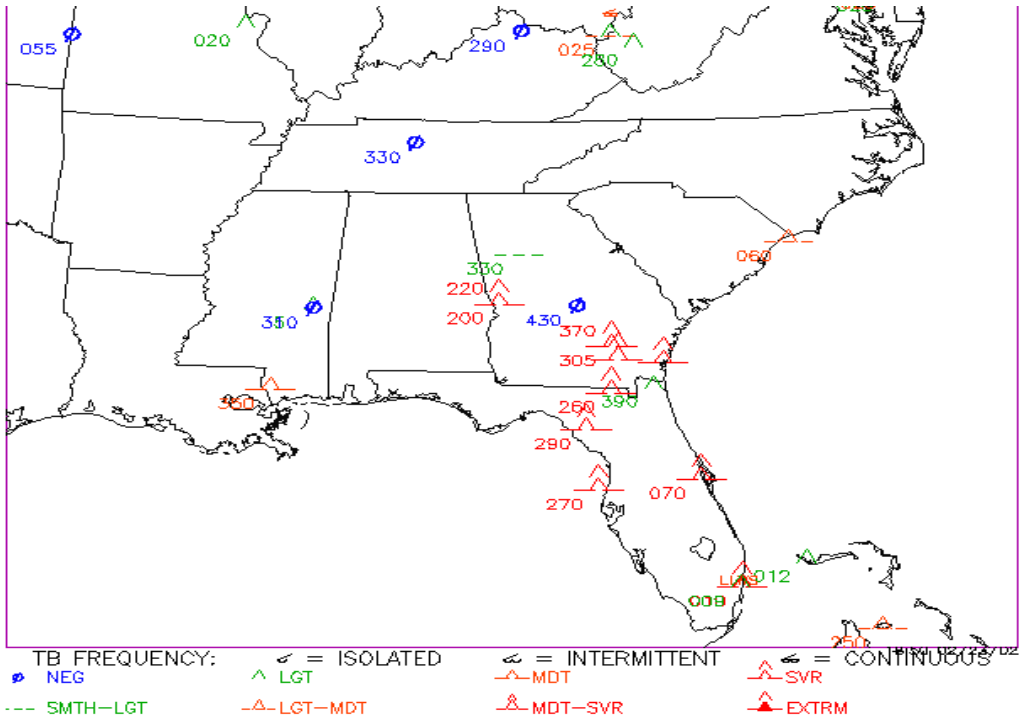

(a) Pireps from NOAA Aviation Digital Data source valid from 1641 UTC to 1836 UTC.

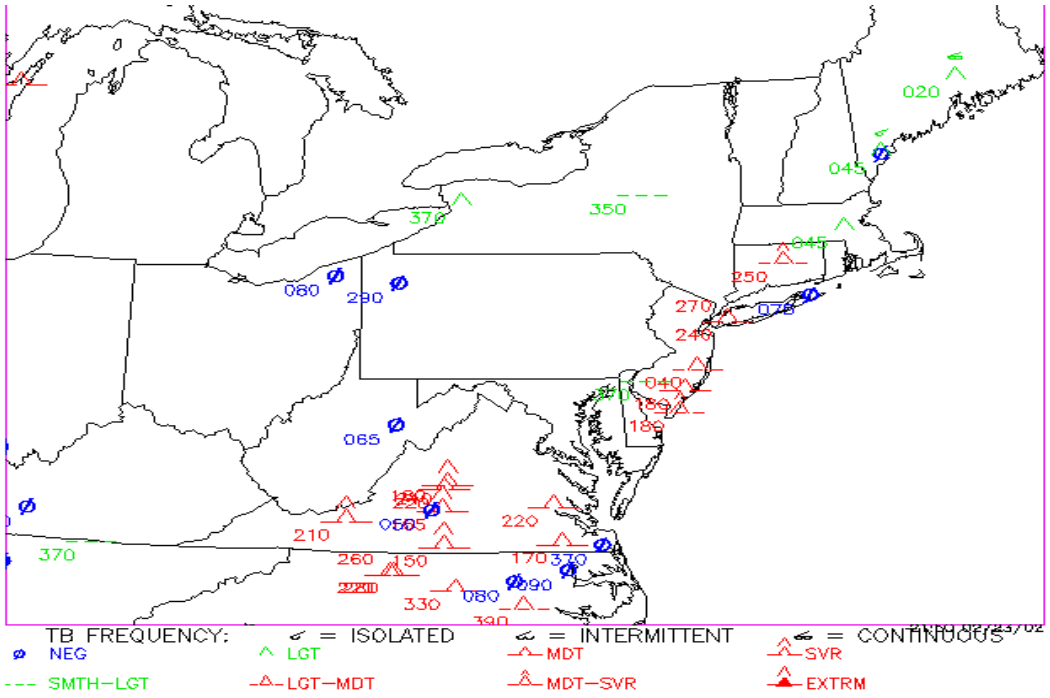

(b) Pireps from NOAA Aviation Digital Data source valid from 1947 UTC to 2140 UTC.

Figure 15. February 23, 2002, pireps.

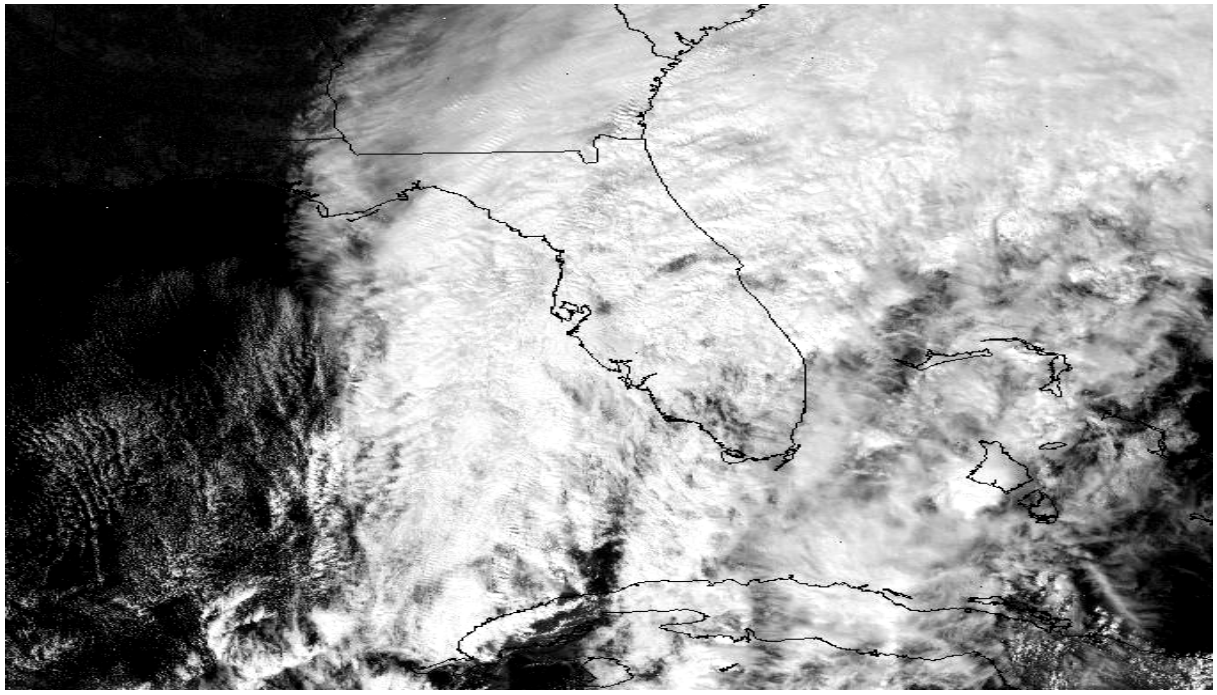

(a) Visible satellite imagery valid at 1845 UTC.

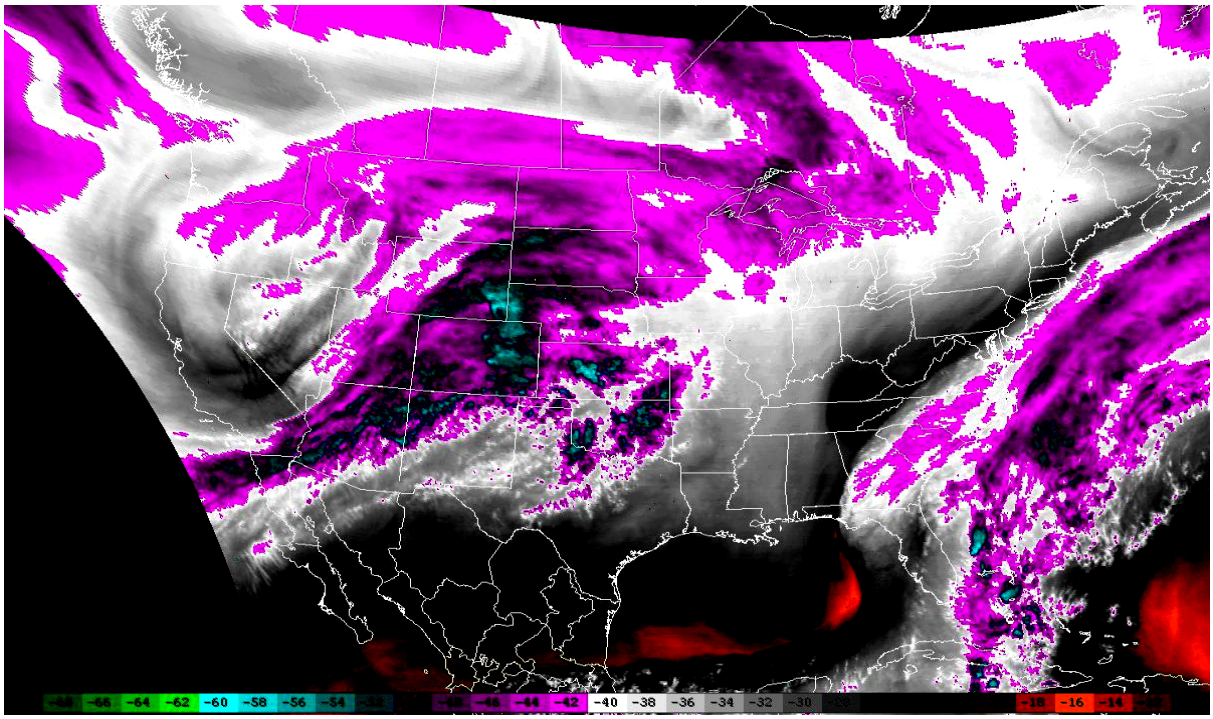

(b) Water vapor infrared satellite imagery valid at 2015 UTC.

Figure 16. February 23, 2002, visible and water vapor imagery, RUC analyses, and rawinsondes.

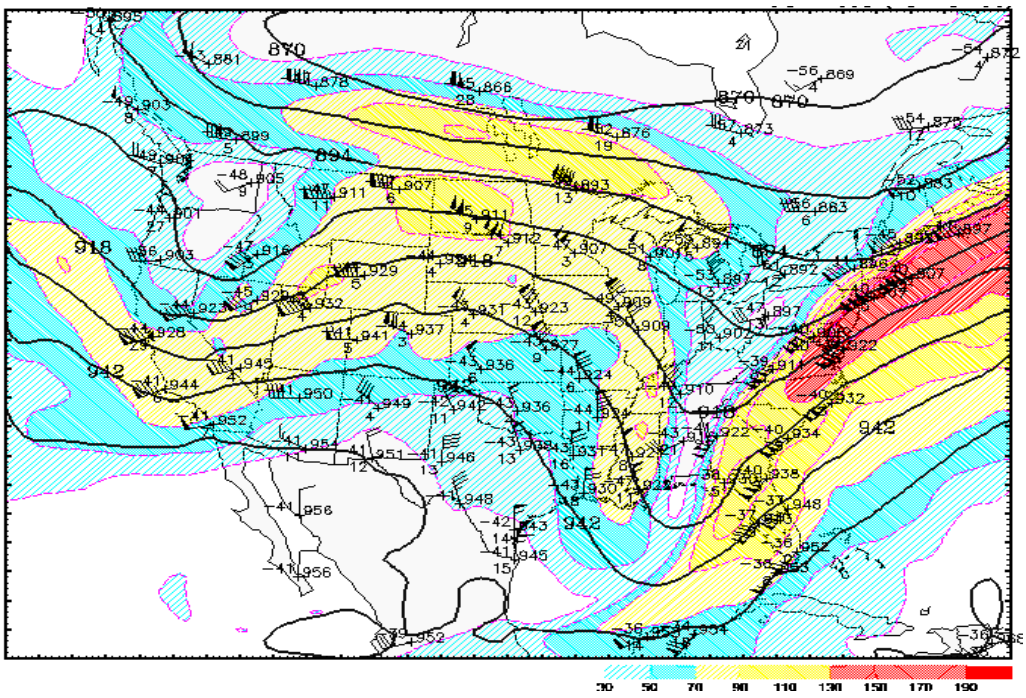

(c) RUC II simulated 300-mb winds (ms^{-1}) valid at 1800 UTC with superimposed observed 1200 UTC winds (ms^{-1}), temperatures (C), and heights (m).

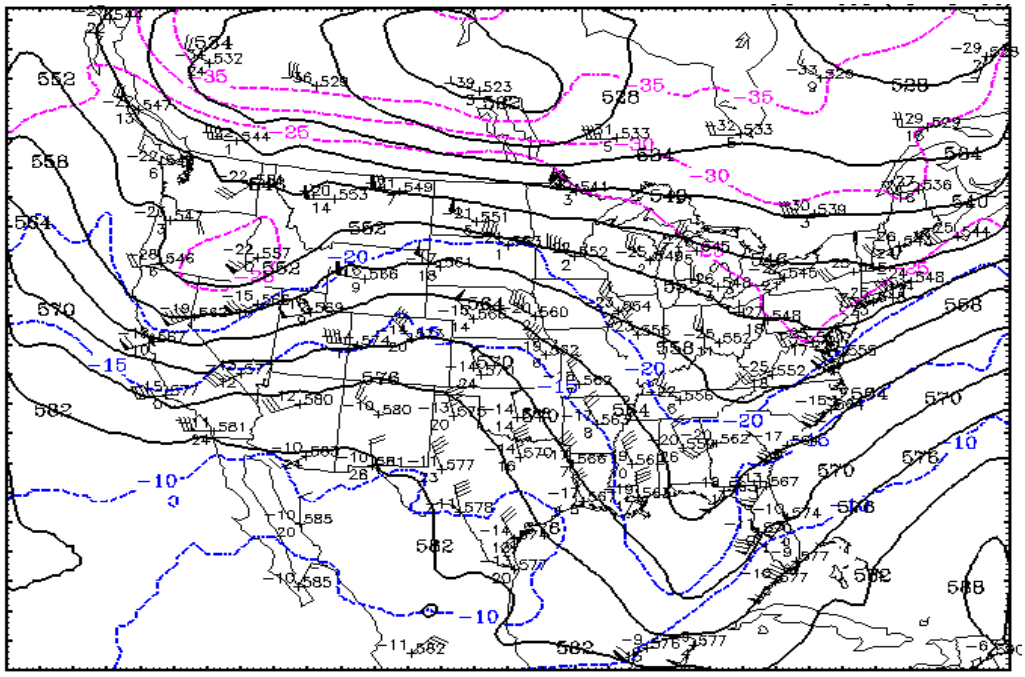

(d) RUC II simulated 500-mb temperatures (C) valid at 1800 UTC February 23, 2002, with superimposed observed 1200 UTC winds (ms^{-1}), temperatures (C), and heights (m).

Figure 16. Continued.

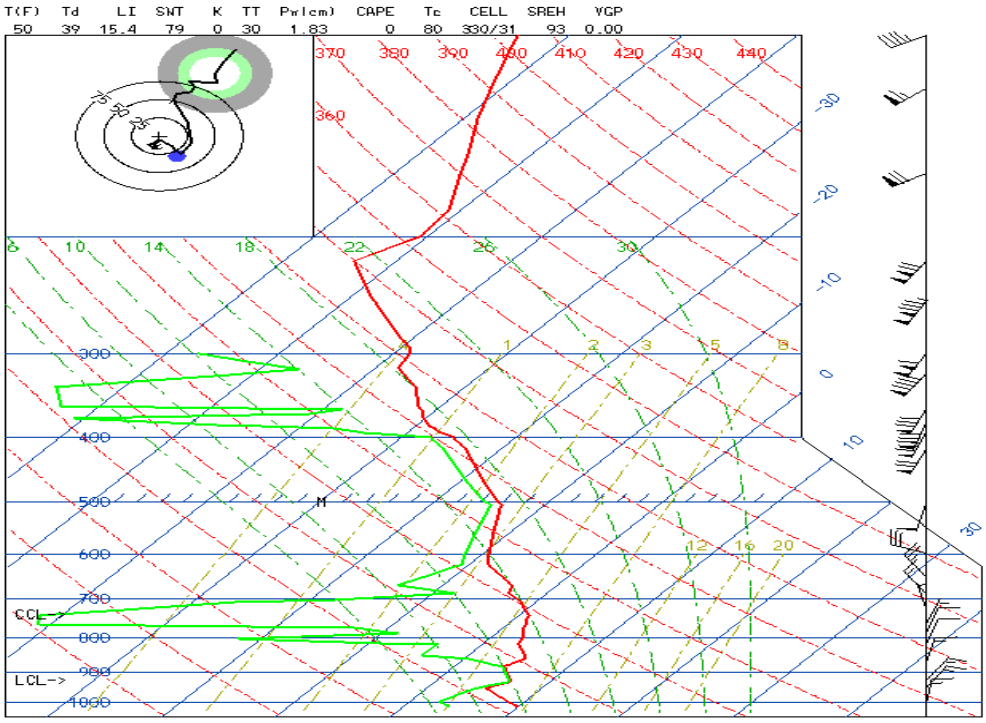

(e) Charleston, South Carolina, rawinsonde sounding valid at 0000 UTC.

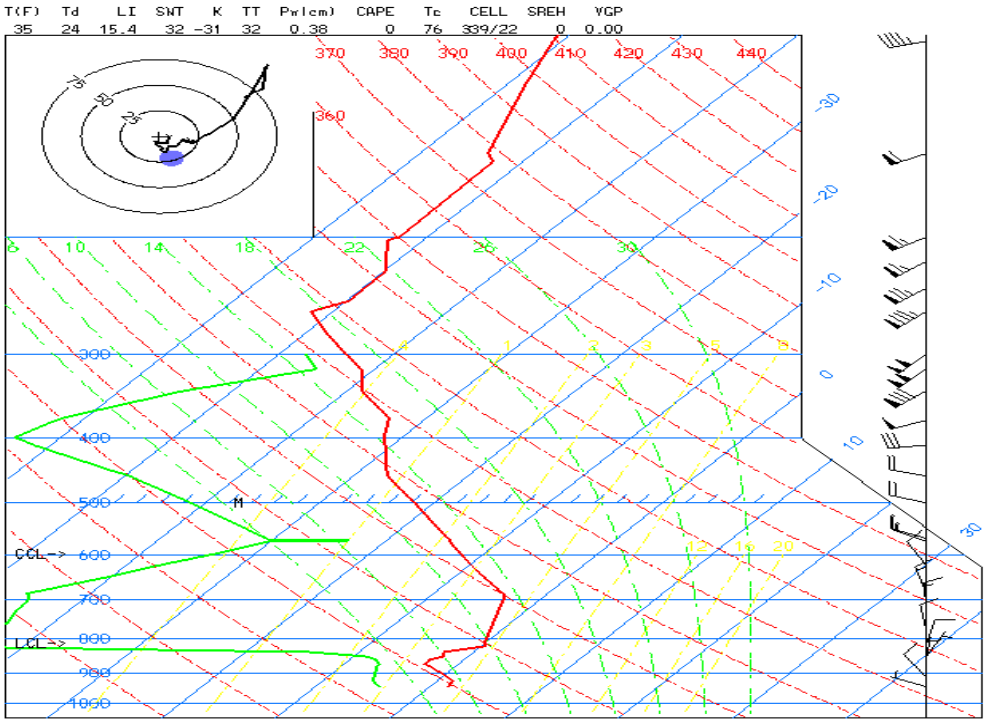

(f) Roanoke, Virginia, rawinsonde sounding valid at 0000 UTC.

Figure 16. Concluded.

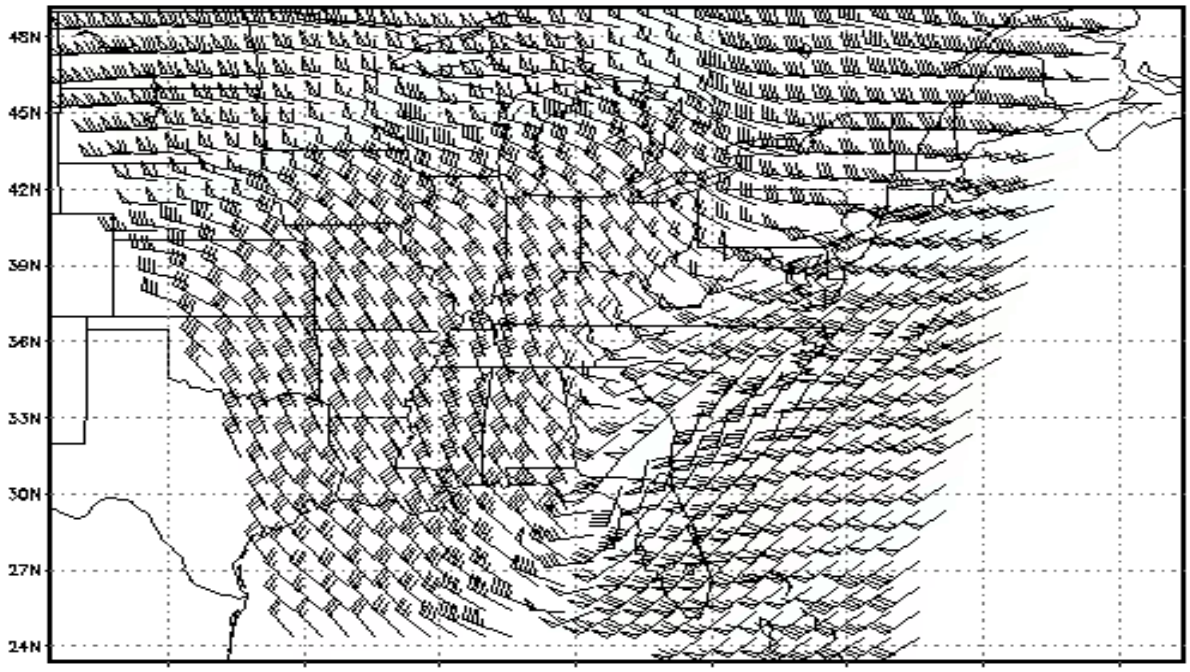

(a) RTTM fine1 simulated 22 000-ft wind isotachs and barbs (kn) valid at 2100 UTC.

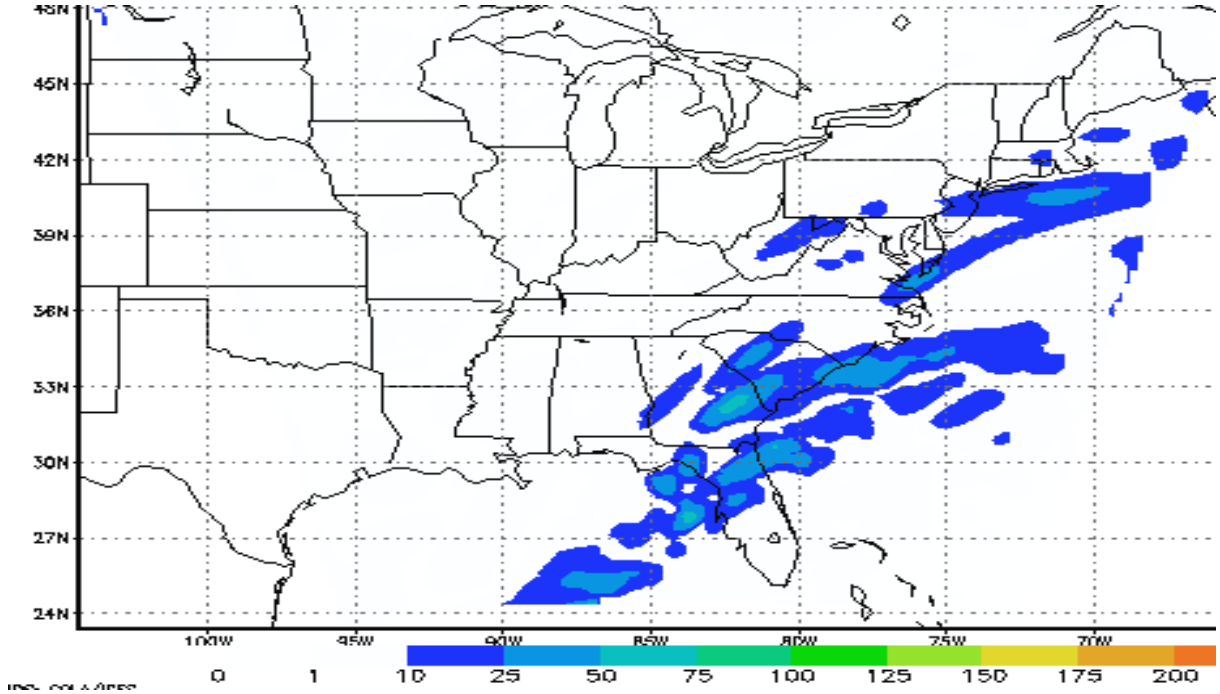

(b) RTTM fine1 simulated 22 000-ft NCSU2 index (s^{-3}) valid at 1800 UTC.

Figure 17. February 23, 2002, fine1 simulation winds, indices, precipitation, Richardson number, and sounding.

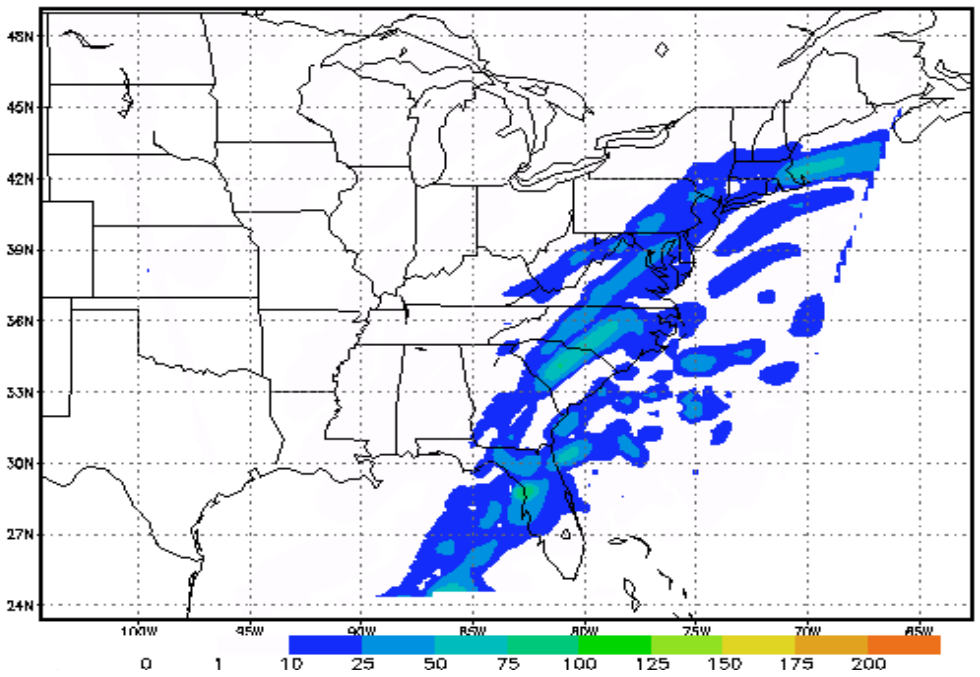

(c) RTTM fine1 simulated 24 000-ft NCSU2 index (s^{-3}) valid at 2100 UTC.

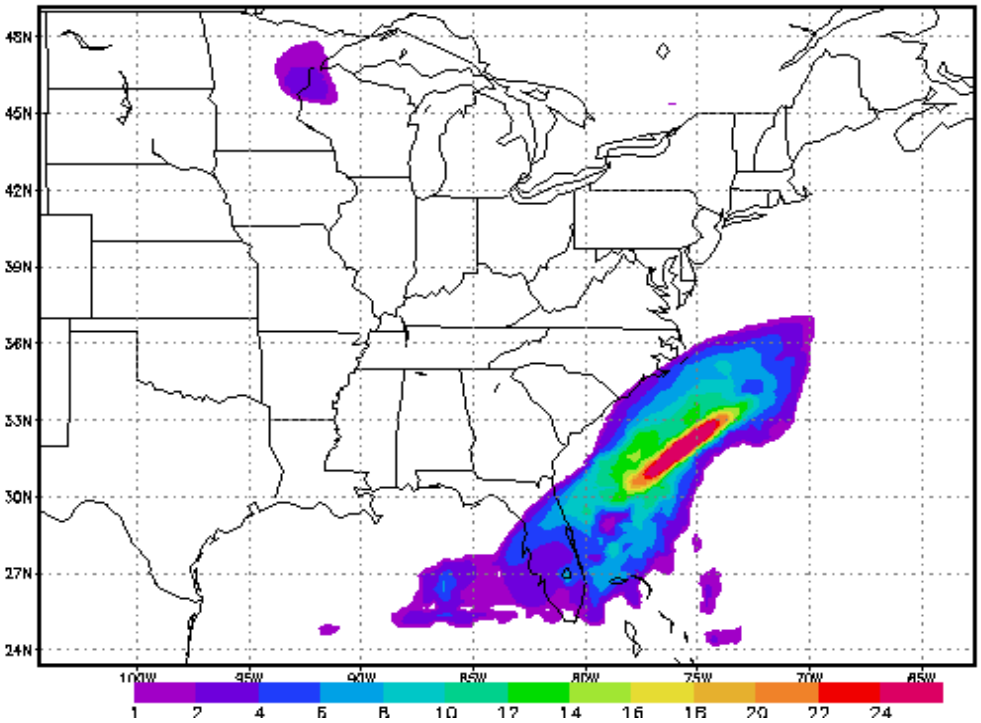

(d) RTTM fine1 simulated total precipitation (mm) valid from 1500 UTC to 1800 UTC.

Figure 17. Continued.

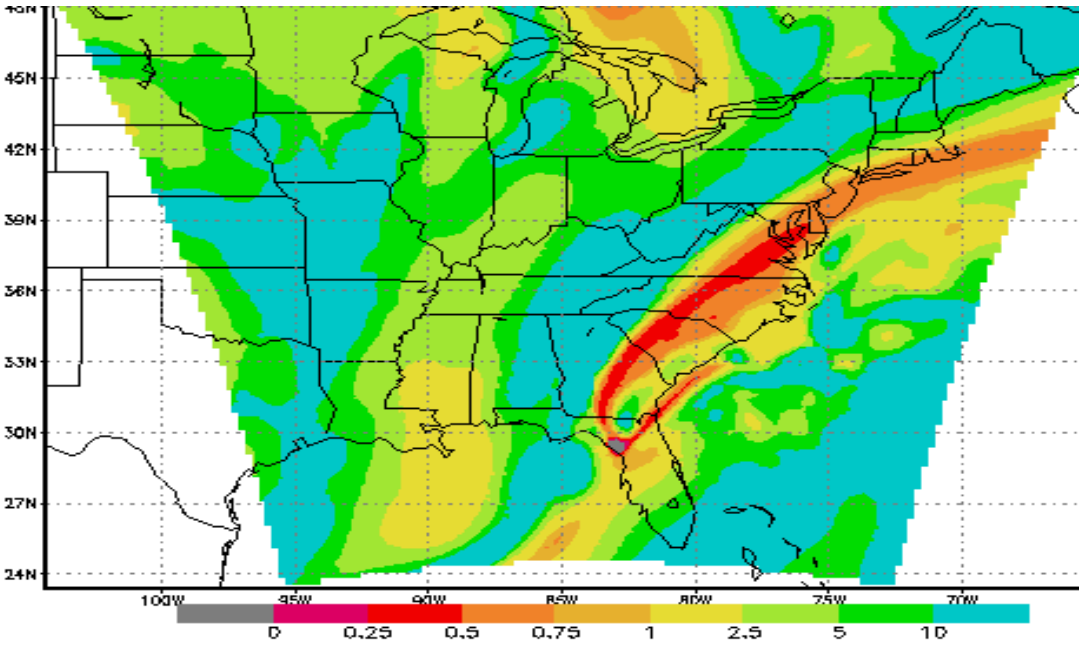

(e) RTTM fine1 simulated 22000-ft Richardson number valid at 2100 UTC.

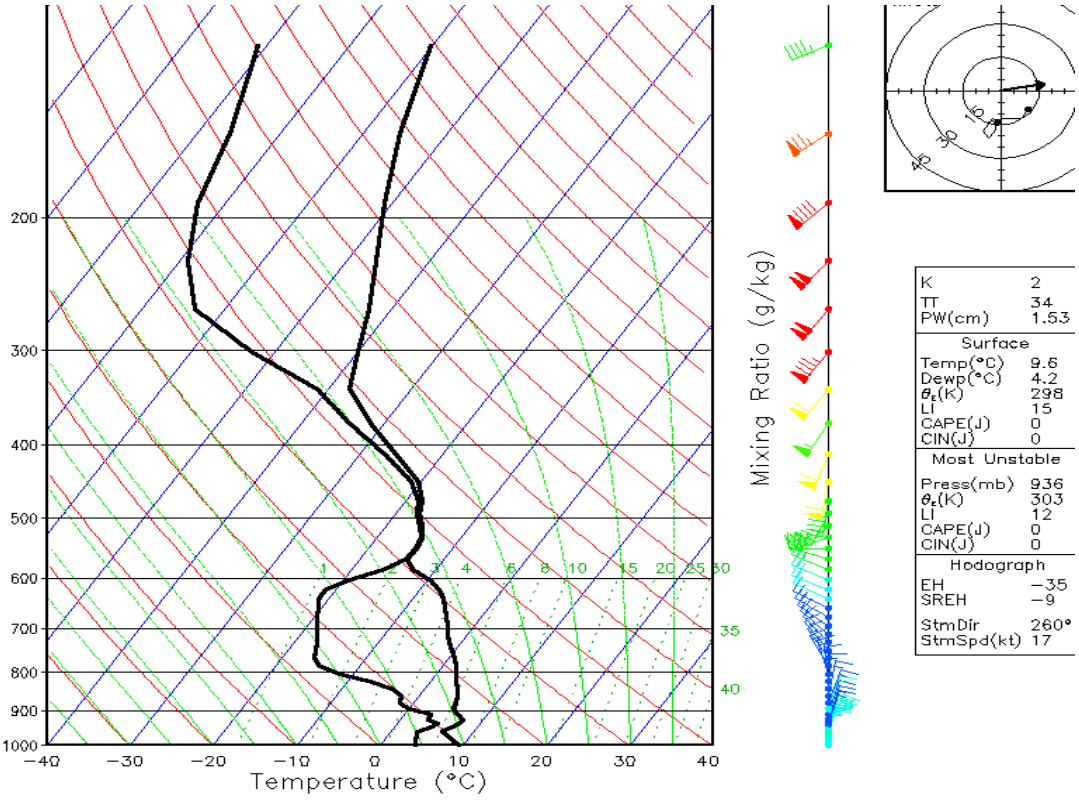

(f) RTTM fine1 simulated skew-t sounding located at Charleston, South Carolina, and valid at 0000 UTC.

Figure 17. Concluded.

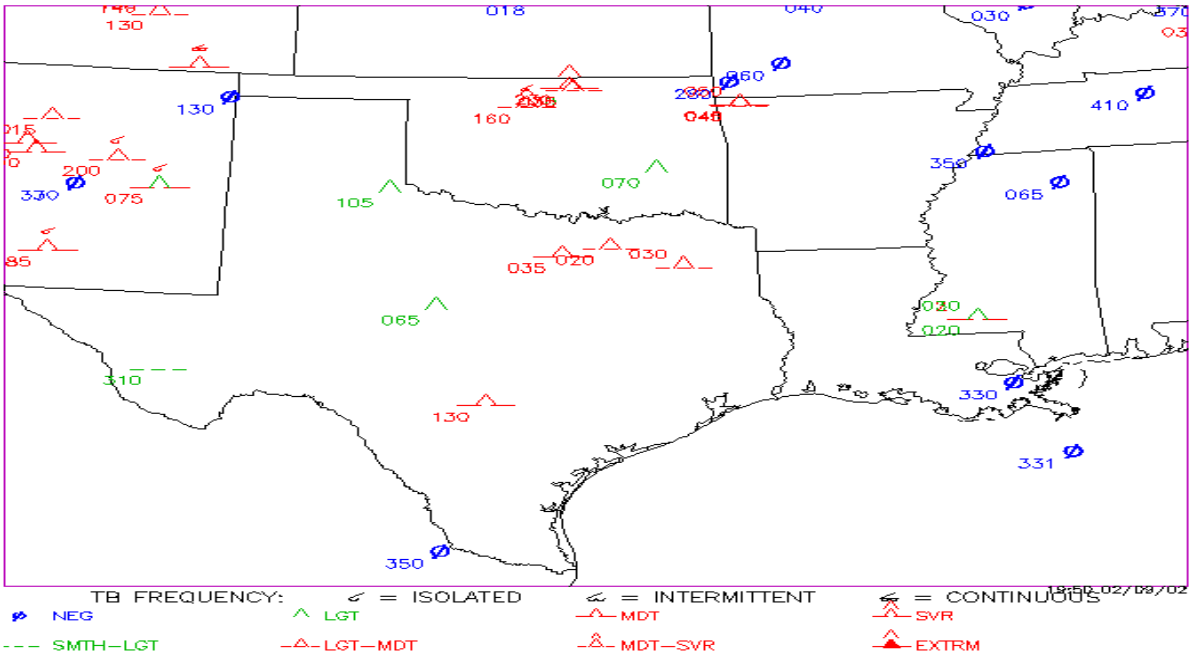

(a) Pireps from NOAA Aviation Digital Data Source valid from 1744 UTC to 1934 UTC.

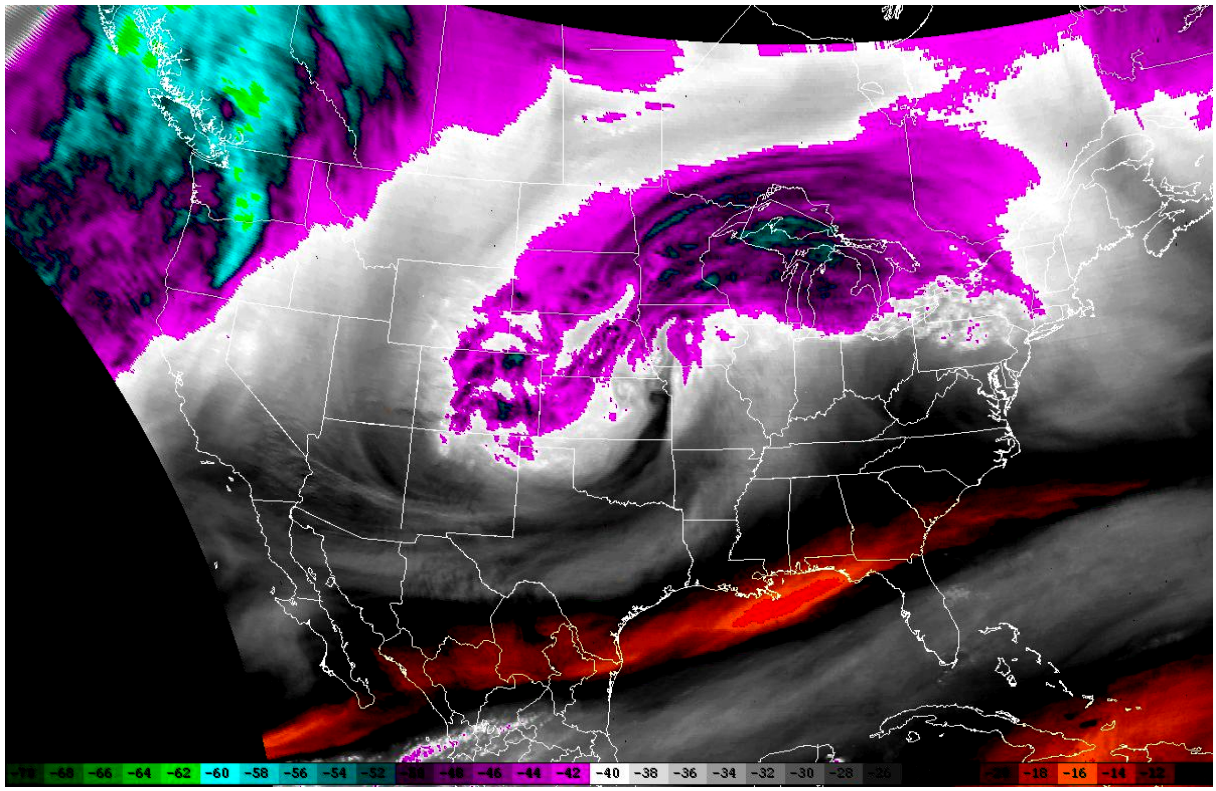

(b) Water vapor infrared satellite imagery valid at 1945 UTC.

Figure 18. February 9, 2002, pireps, water vapor imagery, RUC analyses, and rawinsonde.

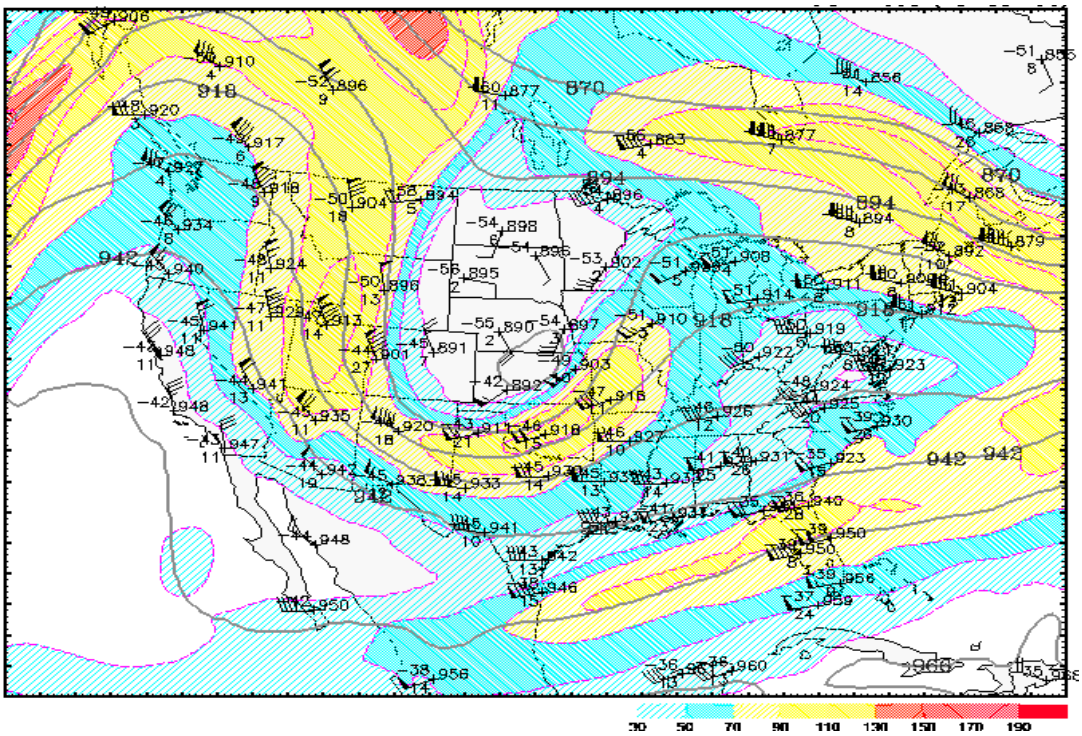

(c) RUC II simulated 300-mb winds (ms^{-1}) valid at 1800 UTC with superimposed observed 1200 UTC winds (ms^{-1}), temperatures (C), and heights (m).

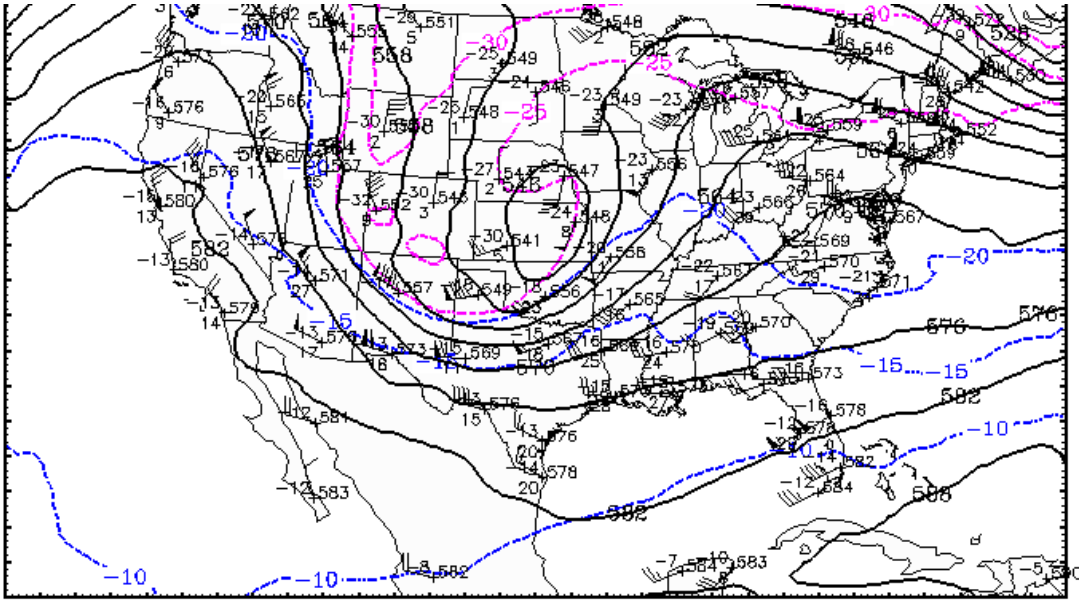

(d) RUC II simulated 500-mb temperatures (C) valid at 1800 UTC with superimposed observed 1200 UTC winds (ms^{-1}), temperatures (C), and heights (m).

Figure 18. Continued.

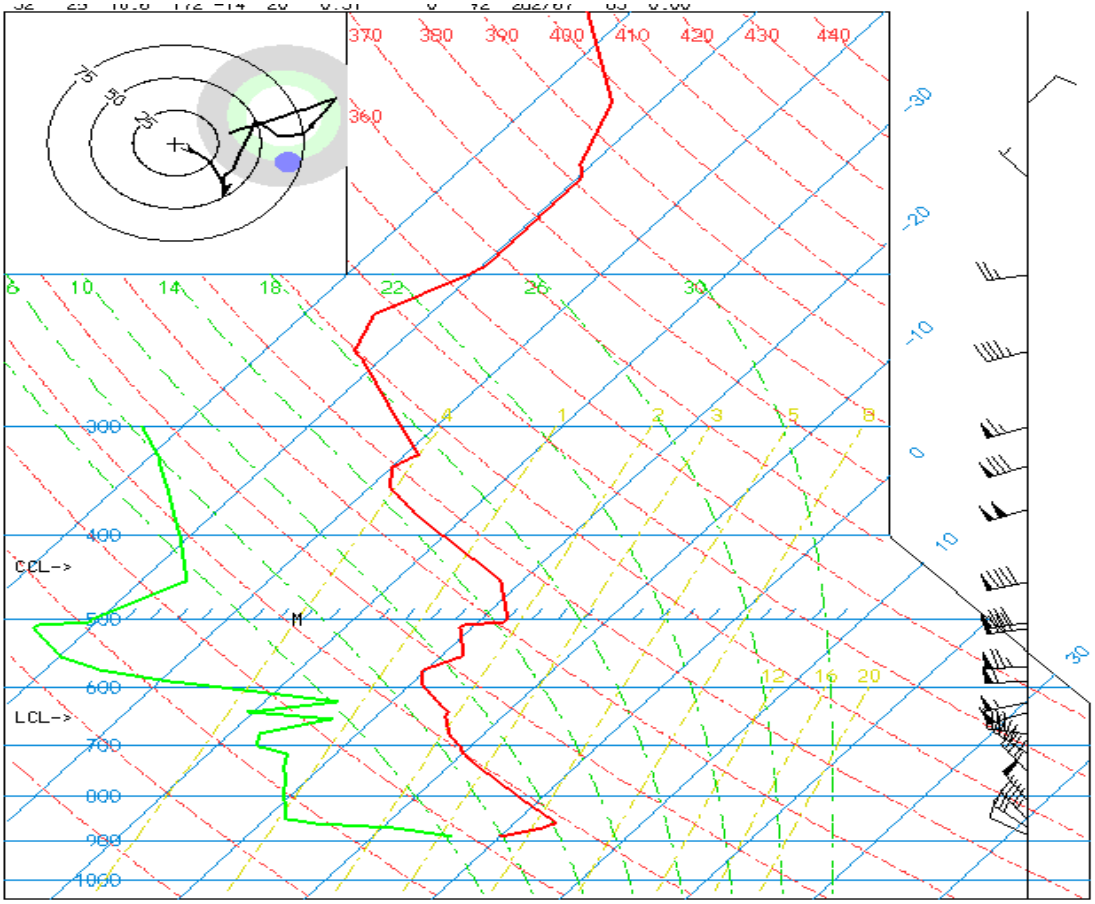

(e) Amarillo, Texas, rawinsonde sounding valid at 1200 UTC.

Figure 18. Concluded.

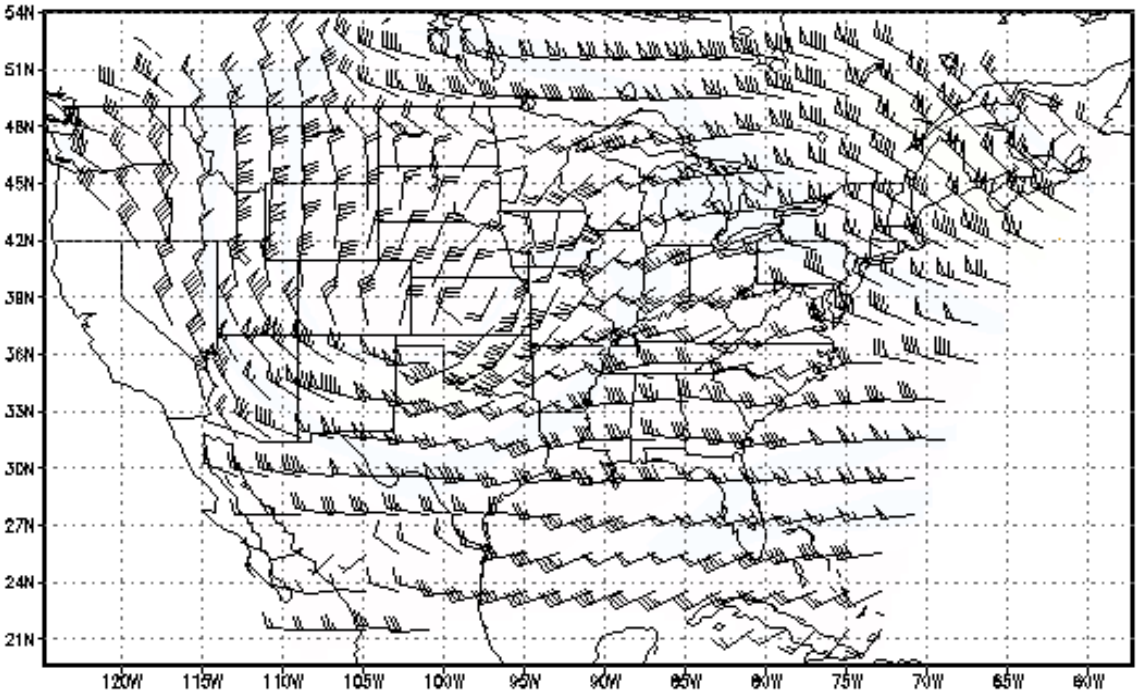

(a) RTTM coarse simulated 22 000-ft wind isotachs and barbs (kn) valid at 1800 UTC.

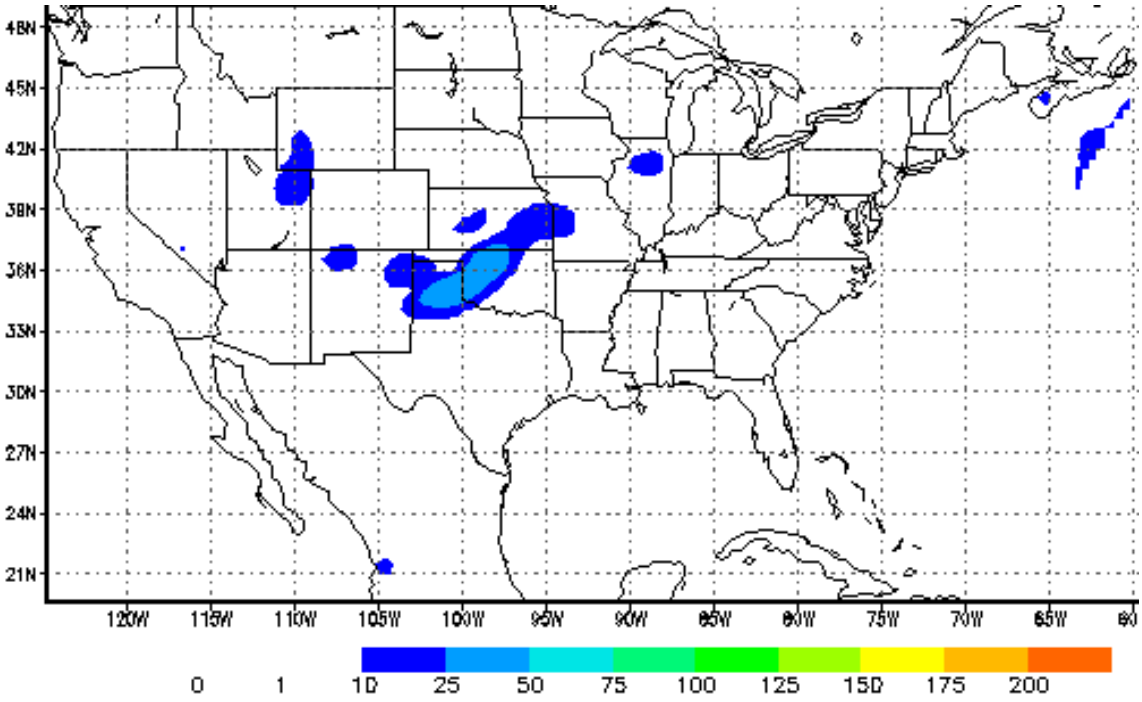

(b) RTTM coarse simulated 22 000-ft NCSU2 index valid at 1800 UTC.

Figure 19. February 9, 2002, coarse simulation winds, index, and sounding.

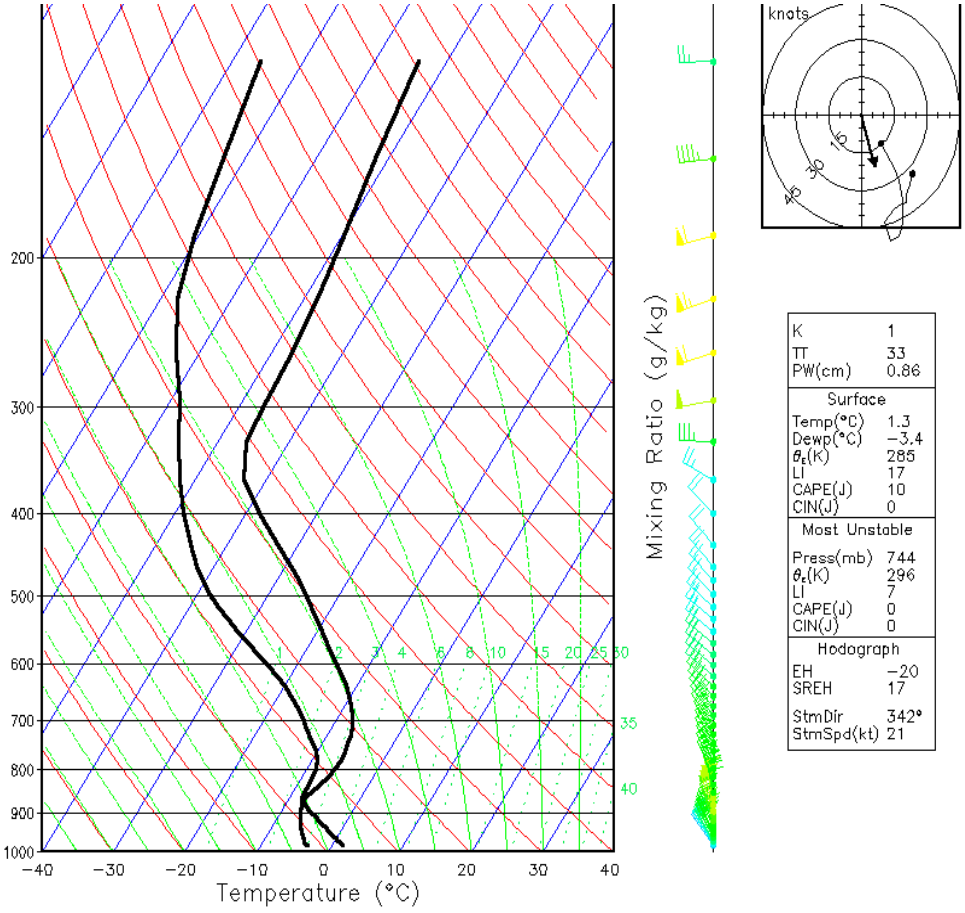

(c) RTTM coarse simulated skew-t sounding located at Oklahoma City, Oklahoma, and valid at 1800 UTC.

Figure 19. Concluded.

REPORT DOCUMENTATION PAGE

Form Approved
OMB No. 0704-0188

1. REPORT DATE *(DD-MM-YYYY)*	2. REPORT TYPE	3. DATES COVERED *(From - To)*
01- 08 - 2004	Contractor Report	

4. TITLE AND SUBTITLE

Characterizing the Severe Turbulence Environments Associated With Commercial Aviation Accidents

A Real-Time Turbulence Model (RTTM) Designed for the Operational Prediction of Hazardous Aviation Turbulence Environments

5a. CONTRACT NUMBER

5b. GRANT NUMBER

5c. PROGRAM ELEMENT NUMBER

6. AUTHOR(S)

Kaplan, Michael L.; Lux, Kevin M.; Cetola, Jeffrey D.; Huffman, Allan W.; Riordan, Allen J.; Slusser, Sarah W.; Lin, Yuh-Lang; Charney, Joseph J.; and Waight, Kenneth T.

5d. PROJECT NUMBER

5e. TASK NUMBER

5f. WORK UNIT NUMBER

23-728-40-30

7. PERFORMING ORGANIZATION NAME(S) AND ADDRESS(ES)

NASA Langley Research Center
Hampton, VA 23681-2199

8. PERFORMING ORGANIZATION REPORT NUMBER

9. SPONSORING/MONITORING AGENCY NAME(S) AND ADDRESS(ES)

National Aeronautics and Space Administration
Washington, DC 20546-0001

10. SPONSOR/MONITOR'S ACRONYM(S)

NASA

11. SPONSOR/MONITOR'S REPORT NUMBER(S)

NASA/CR-2004-213025

12. DISTRIBUTION/AVAILABILITY STATEMENT

Unclassified - Unlimited
Subject Category 03
Availability: NASA CASI (301) 621-0390 Distribution: Standard

13. SUPPLEMENTARY NOTES

Kaplan, Lux, Cetola, Huffman, Riordan, Slusser, and Lin, North Carolina State University, Raleigh, NC. Charney, USDA/Forest Serivce, North Central Research Station, East Lansing, MI. Waight, MESO, Inc., Raleigh, NC.
An electronic version can be found at http://techreports.larc.nasa.gov/ltrs/ or http://ntrs.nasa.gov Langley Technical Monitor: Fred Proctor.

14. ABSTRACT

Real-time prediction of environments predisposed to producing moderate-severe aviation turbulence is studied. We describe the numerical model and its postprocessing system designed for said prediction of environments predisposed to severe aviation turbulence as well as presenting numerous examples of its utility. The numerical model is MASS version 5.13, which is integrated over three different grid matrices in real time on a university work station in support of NASA Langley Research Center's B-757 turbulence research flight missions. The postprocessing system includes several turbulence-related products, including four turbulence forecasting indices, winds, streamlines, turbulence kinetic energy, and Richardson numbers. Additionally, there are convective products including precipitation, cloud height, cloud mass fluxes, lifted index, and K-index. Furthermore, soundings, sounding parameters, and Froude number plots are also provided. The horizontal cross-section plot products are provided from 16 000 to 46 000 ft in 2000-ft intervals. Products are available every 3 hours at the 60- and 30-km grid interval and every 1.5 hours at the 15-km grid interval. The model is initialized from the NWS ETA analyses and integrated two times a day.

15. SUBJECT TERMS

Turbulence; Convection; Vorticity; Wind shear; Jet stream

16. SECURITY CLASSIFICATION OF:			17. LIMITATION OF ABSTRACT	18. NUMBER OF PAGES	19a. NAME OF RESPONSIBLE PERSON
a. REPORT	b. ABSTRACT	c. THIS PAGE			STI Help Desk (email: help@sti.nasa.gov)
					19b. TELEPHONE NUMBER *(Include area code)*
U	U	U	UU	54	(301) 621-0390